

Comparative analysis of radar sensing waveforms for communications

Proposing time delay between radar bursts for robust
parallel sensing and communication applications


TU Delft



Comparative analysis of radar sensing waveforms for communications

Proposing time delay between radar bursts for robust parallel sensing and communication applications

By

C.J. (Joost) van Oostrum

in partial fulfilment of the requirements for the degree of

Master of Science
in Electrical Engineering

at the Delft University of Technology,
to be defended publicly on Thursday August 24, 2023, at 09:30 AM.

Student number:	1386980	
Supervisor:	Full Professor DSc. O. Yarovyj,	TU Delft
Thesis committee:	Part time Associate Professor Dr. R. Litjens MSc,	TU Delft/TNO
	Assistant Professor Dr. O. Krasnov,	TU Delft
	Dr. Ir. J.J.M. de Wit,	TNO
	Dr. W.L. van Rossum,	TNO

*This research was performed as graduation internship at TNO, the Netherlands.
This thesis is confidential and cannot be made public until September 1, 2024.*

An electronic version of this thesis is available at <http://repository.tudelft.nl/>.



Preface

“Allereest ben ik de Koninklijke Marine dankbaar dat ik de kans heb gekregen om de Master Electrical Engineering aan een van de beste universiteiten van Nederland te volgen. Om na 15 jaar weer te beginnen met een studie is zwaar. Iedereen die die ambitie heeft adviseer ik om eerst een schakeljaar te volgen. Door hard te werken (ook 's avonds en in het weekend) heb ik het wel gehaald. Het vak elektromagnetisme heb ik nu twee keer gedaan omdat de manier waarop dit vak gegeven wordt is veranderd. Gelukkig zijn de Maxwellvergelijkingen niet veranderd.

Zonder mijn vrouw Lidia en onze vier kinderen: Alina, Jonathan, Mirthe en Sophie was het niet gelukt. Ook de hulp van mijn ouders Hielke en Margreet en mijn schoonmoeder Alie was onmisbaar. Uiteindelijk heb ik met deze thesis totaal 142 studiepunten dus de norm van 120 punten ruim gehaald. Ik ben blij dat ik deze periode af kan sluiten en weer meer vrije tijd krijg.

Het was een mooie kans om mijn afstudeerstage bij TNO te kunnen doen. Helaas begon de afstudeerstage met een positieve coronatest dus kon ik pas later beginnen. Gelukkig is de coronapandemie voorbij en zijn er geen beperkingen meer. Ik hoop dat de technologie die wordt beschreven in deze thesis in de praktijk gebruikt kan worden.”

*C.J. van Oostrum
The Hague, July 2023*

Contents

Abbreviations	9
Abstract	11
Acknowledgements.....	13
1 Introduction.....	15
1.1. Motivation and goals	15
1.2. Research questions	16
1.3. Research novelty	16
1.4. Overview of the thesis structure	17
2 Background	19
2.1. Introduction	19
2.2. Setup	19
2.3. Radar assumptions	20
2.4. Radar equation	21
2.5. Waveform.....	23
2.6. Range and Doppler estimation	25
2.7. Matched filter	27
2.8. Swerling cases and detection.....	28
2.9. Communication	30
3 Literature research.....	33
3.1. Introduction	33
3.2. Radar communication integration.....	33
3.3. Comparing radar waveforms	34
3.4. Phased Attached Radar Communication.....	34
3.5. Linear Frequency Modulated Minimum Shift Keying.....	37
3.6. Sidelobes BPSK.....	38
3.7. BPSK symbol error rate.....	38
3.8. Conclusions and State-of-the-art.....	39
4 Time delay between radar bursts.....	41
4.1. Introduction	41
4.2. Time delay between radar bursts	41
4.3. Sophisticated waveforms	43
4.4. Received signals.....	45
4.5. Signal processing.....	46
4.6. Time delay estimation	49
4.7. Feasibility	50
4.8. Bit rate TDBRB	52
4.9. Error correction codes TDBRB	57
4.10. Conclusions TDBRB.....	57
5 Simulations	59
5.1. Introduction	59
5.2. MATLAB computer simulation.....	59
5.3. Results TDBRB simulations	69
5.3.1. Max function	69
5.3.2. Straddle loss.....	70
5.3.3. Number of pulses in a burst.....	71
5.3.4. Detection probabilities	73
5.3.5. Pulse duration.....	75
5.3.6. Sampling errors	76
5.3.7. Range or symbol accuracy	78
5.3.8. Swerling cases	80
5.4. Discussion and Conclusions simulations.....	82
6 Experiment and comparative analysis.....	85
6.1. Introduction	85
6.2. Variables.....	88

6.3.	Bit rate	89
6.4.	Demodulation TDBRB	89
6.5.	Regular radar performance	91
6.6.	Doubled bit rate.....	92
6.7.	BPSK experiment.....	93
6.8.	Discussion experiment	94
6.9.	Comparative analysis	96
6.10.	Conclusions experiment and comparative analysis.....	96
7	Applications	99
7.1.	Introduction	99
7.2.	Stationary primary radar scenario	99
7.3.	Automotive scenario.....	100
7.4.	Bistatic operation.....	101
7.5.	Possible problems.....	101
7.6.	Only communication application.....	102
8	Conclusions	105
8.1.	Introduction	105
8.2.	Main conclusions.....	105
8.3.	Conclusions on additional research questions.....	106
8.4.	Limitations.....	106
8.5.	Recommendations	107
	Bibliography.....	109
A.	Appendix - Unsynchronized local oscillator	113
B.	Appendix – Figures BER and SER rates.....	117

Abbreviations

AoA - Angle of arrival
ARQ - Automatic repeat request
AWG - Arbitrary waveform generator

BCD - Binary-coded decimal
BER - Bit error rate
BPSK - Binary phase shift keying
BRGC - Binary reflected Gray code

DC - Direct current
DFRC Dual-function radar and communication

EM - Electromagnetic

FEC - Forward error correction
FFT - Fast Fourier transform

GLRT - Generalized likelihood ratio test
GPS - Global positioning system
GSM - Global system for mobile communications

HF - High frequency

IF - Intermediate frequency
IoT - Internet of things
ISAC - Integrated sensing and communications

JCAS - Joint communication and radio/radar sensing
JCR - Joint communication and radar
JRC - Joint radar and communication

LFM - Linear frequency modulated
LFM-MSK - Linear frequency modulated – minimum shift keying
LNA - Low noise amplifier
LO - Local oscillator
LOS - Line-of-sight
LTE - Long term evolution

MIMO - Multiple-input and multiple-output
MTI - Moving target indicator

NLOS - Non-line-of-sight

OOI - Object-of-interest
OFDM - Orthogonal frequency division multiplexing

PARC - Phase attached radar communication
PC FMCW - Phase coded frequency modulated continuous wave
PRF - Pulse repetition frequency
PRI - Pulse repetition interval

RadCom - Radar Communication
RCC - Radar communication co-existence
RCSS - Radar and communication shared spectrum
RF - Radio frequency
RFID - Radio frequency identification
RX - Receiver

SATCOM - Satellite communication
SBCD - Simple binary-coded decimal
SER - Symbol error rate
SINR - Signal-to-noise-and-interference ratio
SNR - Signal-to-noise ratio
SS - Spread-spectrum

TDBRB - Time delay between radar bursts
T/R - Transmit/receive
TX - Transmitter

UHF - Ultra high frequency

VHF - Very high frequency

Wi-Fi - Wireless fidelity

ZWGN - Zero-mean white Gaussian noise

Abstract

A novel new waveform is compared with two other existing waveforms to create a radar network. In this radar network one primary radar transmits a waveform for sensing and communication and one or multiple radars receive these waveforms. The constraint for the radars is that all radars can build up a radar picture and situation awareness. What also means that the performance of the primary radar does not degrade. This new radar type is called cooperative hitchhiker with communications. In this radar network the main task is sensing, therefore additional communication signals are used to increase the performance of the sensing task. The advantages of parallel sensing and communications are reducing interference, dual use of the scarce electromagnetic (EM) spectrum in a congested EM environment and it is possible in a bistatic configuration to detect a bistatic scattering object.

The three waveforms which are compared are phase coded frequency modulated continuous wave (PC FMCW) linear frequency modulated – minimum shift keying (LFM-MSK) and a new waveform time delay between radar bursts (TDBRB). TDBRB is a simple but effective communication method on top of the sensing waveform and can be used with staggered waveforms. Where the first two waveforms make use of binary phase shift keying (BPSK), TDBRB uses a time modulation with the inserted time delay between two successive radar bursts. To distinguish the two radar bursts the first burst has a linear frequency modulated (LFM) upchirp and the successive burst, after the inserted time delay, has an LFM downchirp. PC FMCW and LFM-MSK data are compared with simulations and an experiment of the TDBRB waveform.

The conclusions are that PC FMCW has the highest data rate, followed by LFM-MSK, and TDBRB has the lowest data rate for line-of-sight connections. The first two make use of the information in one pulse, or FMCW chirp. This results in a lower signal-to-noise ratio (SNR) and is therefore only suited for line-of-sight connections. With a matched filter and coherent integration of the TDBRB signals, this waveform is most suited for non-line-of-sight connections and communication over an object-of-interest at the cost of a lower bit rate. TDBRB has a similar performance for the different Swerling cases as the detection probability of a regular radar. The degradation in performance with the TDBRB waveform is only a fraction of the burst time because the time delay is added to an original radar burst. These results make TDBRB most suited for non-line-of-sight communication and for communications with a low signal-to-noise ratio.

Acknowledgements

Firstly, I want to thank Jacco de Wit and Wim van Rossum and TNO for giving me the opportunity to do this research and for their useful feedback. It started with my idea of a passive radar which is helped by another radar with additional information without degrading the performance of the other radar. It was great to be able to do research on my own idea. Secondly, I want to thank my supervisor at TU Delft Oleg Krasnov who asked good questions and challenged me to improve my work during the project and the other members of the thesis committee Olexander Yarovy and Remco Litjens for the final part of my thesis. And finally, I want to thank Bas Jacobs and Faruk Uysal who gave me fruitful feedback during the project meetings and for the report and Jasper Schneijdenberg who helped me with the experiment.

1 Introduction

1.1. Motivation and goals

Since, first communication systems were designed just before the end of the 19th century, followed by the development of radar in the beginning of the 20th century, there have been ideas to combine those users of the same electromagnetic (EM) spectrum in the 20th and 21st century. Because communication and radar sensing use the same EM spectrum, interference is introduced. The EM spectrum is divided between communication and radar applications by radiocommunication agencies, and frequencies are assigned to both applications. This EM spectrum is scarce and congested and therefore a need of combining those, to make optimal use of the spectrum, occurred. The sense of urgency to do this research now is congestion due to wireless fidelity (Wi-Fi), internet of things (IoT) and mobile phones. The interference is reduced when the different applications are matched to each other. In literature like the book of Blunt [1-01] this is named co-existence.

The main goal of this thesis is to design a radar network, where one radar transmits and receives, and another radar only receives, for both radars to build up a situation awareness radar picture. To reach this goal the active (monostatic or primary) radar will transfer information to the receiving radar. The transmitting radar has two tasks. Firstly, it will provide situational awareness to its own platform without degradation of its performance when using radar waveforms to communicate. Secondly, it will communicate to the receiving radar additional information, which can be used at the receiving radar to build up its own situation awareness radar picture. Simply put, the active radar has a 1-way communication line (simplex) through its radar signal to the receiving radar to achieve situational awareness at both radars.

This system setup is related to bistatic radar as described in the book of Willis [1-02]. However, a bistatic closed combined radar system, with transmitter and receiver separated from each other, is different from the two separated systems which are proposed here. With bistatic passive radar it is possible to use the communication signals for radar purposes. Here both applications are combined without causing any interference. In this case the passive radar must work with the signal which is available at that moment and cannot be modified to improve the radar signal. Radar waveforms are designed to retrieve the distance to an object-of-interest and estimating its Doppler frequency, while communication waveforms or modulation schemes are specified to transfer data with a reliable connection. The receive radar in the proposed radar network works similarly as passive radar, although it uses radar signals which are enriched with information to build up its own situation awareness radar picture. When a radar operates only with received radar signals of another radar it is called a bistatic hitchhiking radar as described in Overrein et al. [1-03]. The proposed system is a with-communication-enhanced bistatic hitchhiking radar.

The characteristics of the transmitting radar must be known at the receive radar to make use of bistatic or multistatic radar data. These characteristics include data like transmission time, position of the transmitter, speed of the transmitter, modulation, waveform, direction of transmission. These data can be sent using a separate communication channel in the radar. Or they can be sent by separate radiocommunications like high frequency (HF), very high frequency (VHF), ultra high frequency (UHF), telephony systems like global system for mobile communications (GSM), long term evolution (LTE) or satellite communications (SATCOM). Another way is to modulate this information on the radar waveform. In that way the transmitting radar will send its data in the transmitted pulses or chirps. Communication between radars by making use of information in the radar waveform to another radar will be faster as with radiocommunications because the information will be present in the radar system. Extra steps from radar to communication systems and vice versa are prevented.

More communication systems and radars are introduced due to the development in technique and reduced costs of those systems. The motivation of the research presented in this thesis is to limit interference between systems, to limit the use of EM spectrum, and to limit transmitted power. For instance, this can be useful in automotive scenarios. Interference will occur when automotive vehicles, equipped with radars, are moving around. This interference can be limited when it is possible for one radar to make use of the transmissions of another radar. In this case both vehicles connect to a radar network of opportunity. Less transmissions automatically reduces the usage of EM spectrum. Power is saved when one radar turns off or does not use its transmitter. Another advantage is the possibility of detecting objects with bistatic scattering. The receiving radar can benefit from it, although the primary radar cannot benefit of this bistatic scatter. Another advantage can be communications with the radar system, while there is no line-of-sight connection between the radars. This will happen in case the communication signal of the primary radar is reflected by an

object-of-interest and is received at the receiving radar. Besides the automotive domain, there can be applications for the proposed radar network and techniques in other domains.

To achieve the design of a radar network where two or maybe more radars can benefit from each other, the following research of techniques which are able to transfer information with a radar waveform is necessary. Firstly, the active radar must modulate information on its waveform to communicate to the receiving radar. Secondly, the waveform should not degrade the performance of the active radar. In the following section the research questions are stated.

1.2. Research questions

The main research questions are written below as follows:

1. What techniques can be used to build a radar network, where one radar transmits and another radar only receives, for both radars to build up situation awareness with minimal adjustments to the primary radar task?
2. What radar waveform is suited of performing both radar sensing and communications in low signal-to-noise ratio environments for both radar as communication tasks, and what is the performance of the waveform?

Additional questions follow from the main questions, are as follows:

- a) What are necessary assumptions for a radar network of opportunity?
- b) What method of information transfer is possible with and without a line-of-sight connection?
- c) What are relevant measures to determine which waveform is suited for the different scenarios?
- d) What are the results of the simulations and experiment with the proposed waveforms for the different scenarios?
- e) How robust are the different methods of transferring information with radar?
- f) How is the probability of detection influenced by the proposed waveform?

1.3. Research novelty

The novelty of this thesis is the new proposed system design of two radars working together. One radar transmits its radar signal with communications and has no degradation of its own performance. While the other radar is not transmitting. This receiving radar works as a passive radar and will be able to detect the communications sent by the transmitting radar. Another novelty is the proposed technique, time delay between radar bursts, which can communicate without a line-of-sight connection over an object-of-interest. This technique works by inserting a time delay between an upchirp burst and a downchirp burst of radar pulses. This principle is shown in Figure 1. With TDBRB it is possible to transmit and receive different communication symbols each radar burst. The number of communication symbols and the related symbol or bit rate is determined by the pulse repetition interval (PRI), number of range cells (related to the bandwidth) and number of pulses in a burst. For the primary radar the transmitted signal is known, and it is possible to perform the regular radar operation to determine the distance to the object-of-interest. The receive radar will receive only the reflected bistatic signals and does not know when the upchirp is transmitted. It is not possible to determine when the signals are transmitted at the receive side. However, it is possible to determine the inserted time delay by performing a cross-correlation of the upchirp burst with the downchirp burst.

This method to transmit data with radar waveforms, and in a radar way (transmitting, receiving, detection and estimation) has potential for other communication purposes. By executing communication in a radar way, the benefits of detection with a low signal-to-noise ratio (SNR) and coherent integration of a radar system are used. With coherent integration all received pulses of a burst are added up to receive more signal power and detect an object-of-interest. By making use of both radar principles to communicate, communications can be more reliable and performed without a line-of-sight connection.

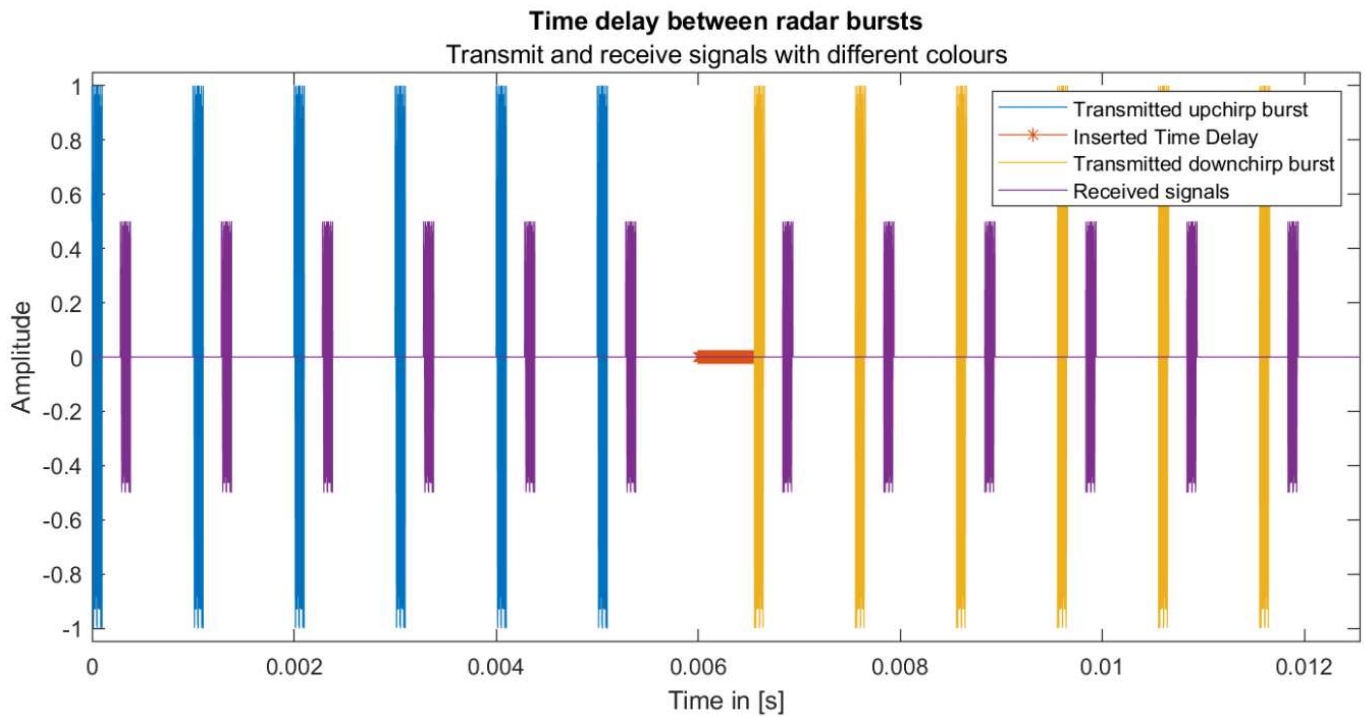


Figure 1 Principle of time delay between radar bursts

1.4. Overview of the thesis structure

The structure of this thesis is as follows. In chapter 2 the background on radar and communications is presented. In chapter 3 the literature research of this thesis is stated with special attention to two other radar and sensing waveforms and the state-of-the-art is described. The novel time delay between radar bursts waveform is explained in more detail in chapter 4. Chapter 5 explains the working of the used MATLAB simulation programs and presents the results of the simulations. The experiment of the suggested new technique compared to binary phase shift keying is described and reported in chapter 6 where also the comparative analysis of the novel waveform to the two other sensing and communication waveforms is stated. Possible applications and scenarios where time delay between radar bursts can be used are described in chapter 7. This report concludes with the conclusions and recommendations in chapter 8.

2 Background

2.1. Introduction

In this chapter the background for communication and radar systems is presented. It starts with the bistatic system setup which describes the radar setup followed by the background for radar systems and the background for communication systems.

2.2. Setup

In this section the bistatic radar setup, while only one radar is transmitting, and one radar is receiving is described. In this thesis two radars are described, although in general there can be more than one receiving radar. The first radar is called the primary radar which uses its transmitter (TX) and receiver (RX), and the other is called the receive radar, which only uses its RX. The primary radar has no degradation of its own radar operation when only radar waveforms are used. Two scenarios are introduced where the main difference is with or without line-of-sight. In Figure 2 the radar setup is shown where a primary regular radar system is an active system which is used to build up its own situation awareness radar picture. The receive radar only detects the signals, which are transmitted by the primary radar. Scattered by the object-of-interest and by means of a line-of-sight connection. To test the performance of different radar with integrated communications techniques, the two cases line-of-sight (LOS) and non-line-of-sight (NLOS) are introduced.

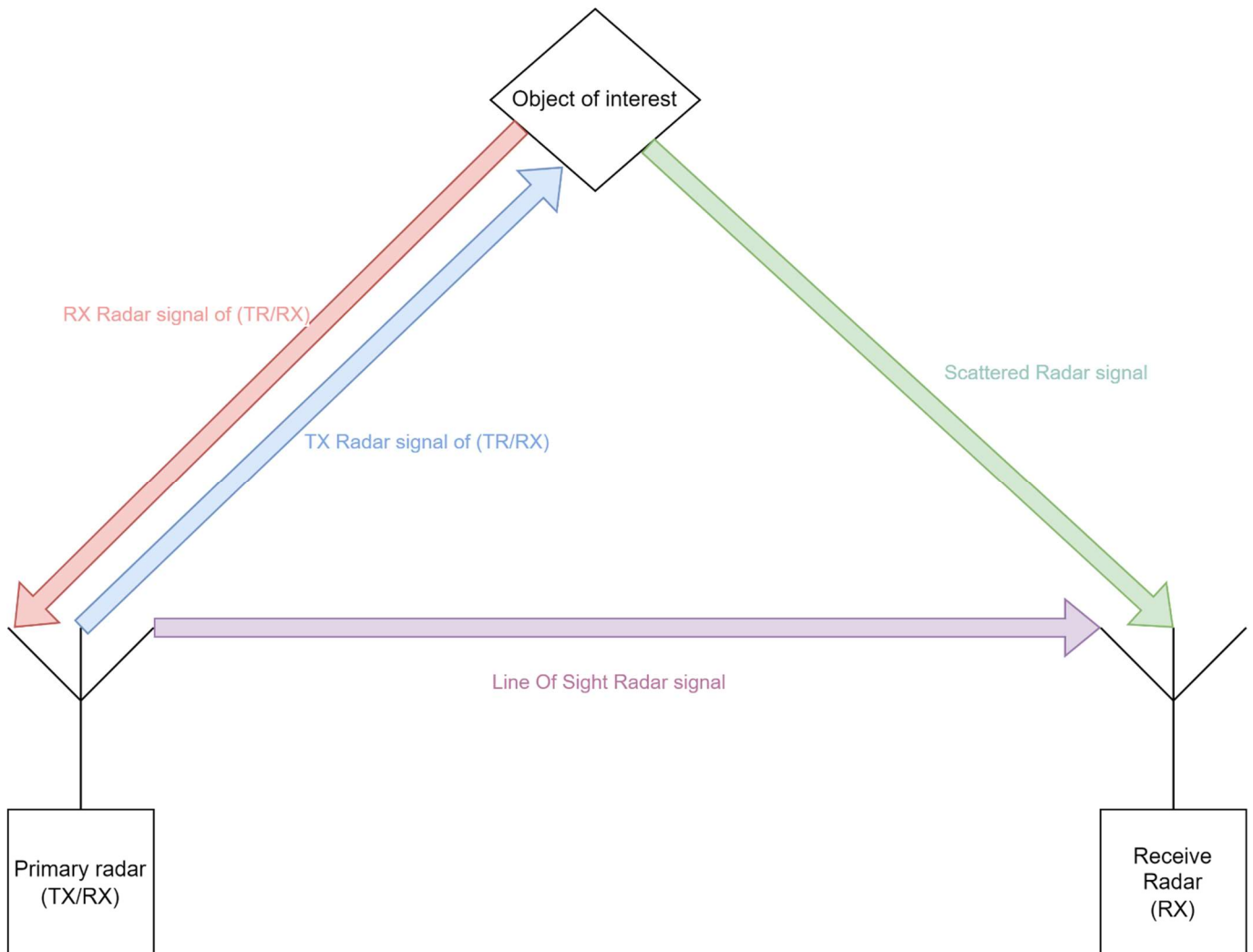


Figure 2 Radar setup with one TR/RX radar which can build up its own situation awareness radar picture and one receive (RX) radar which receives signals through a line-of-Sight connection and the scattering of an object.

In Figure 3 the line-of-sight connection between the primary radar and the receive radar is shown. The scenario in which the receive radar does not have a line-of-sight connection with the primary radar is shown in Figure 4.

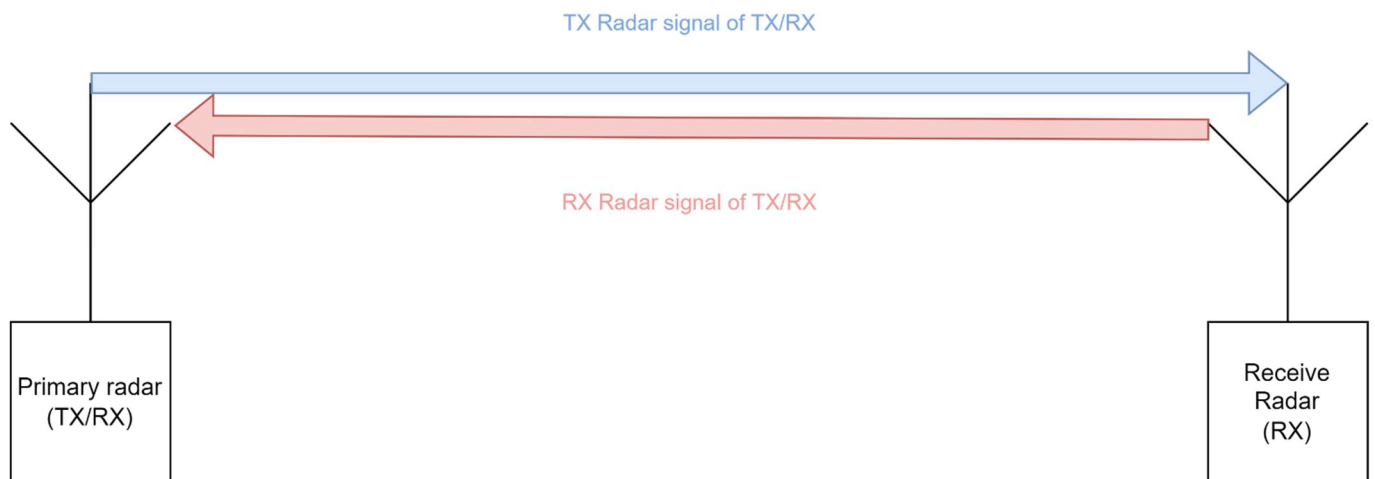


Figure 3 Line-of-sight scenario between primary radar and receive radar.

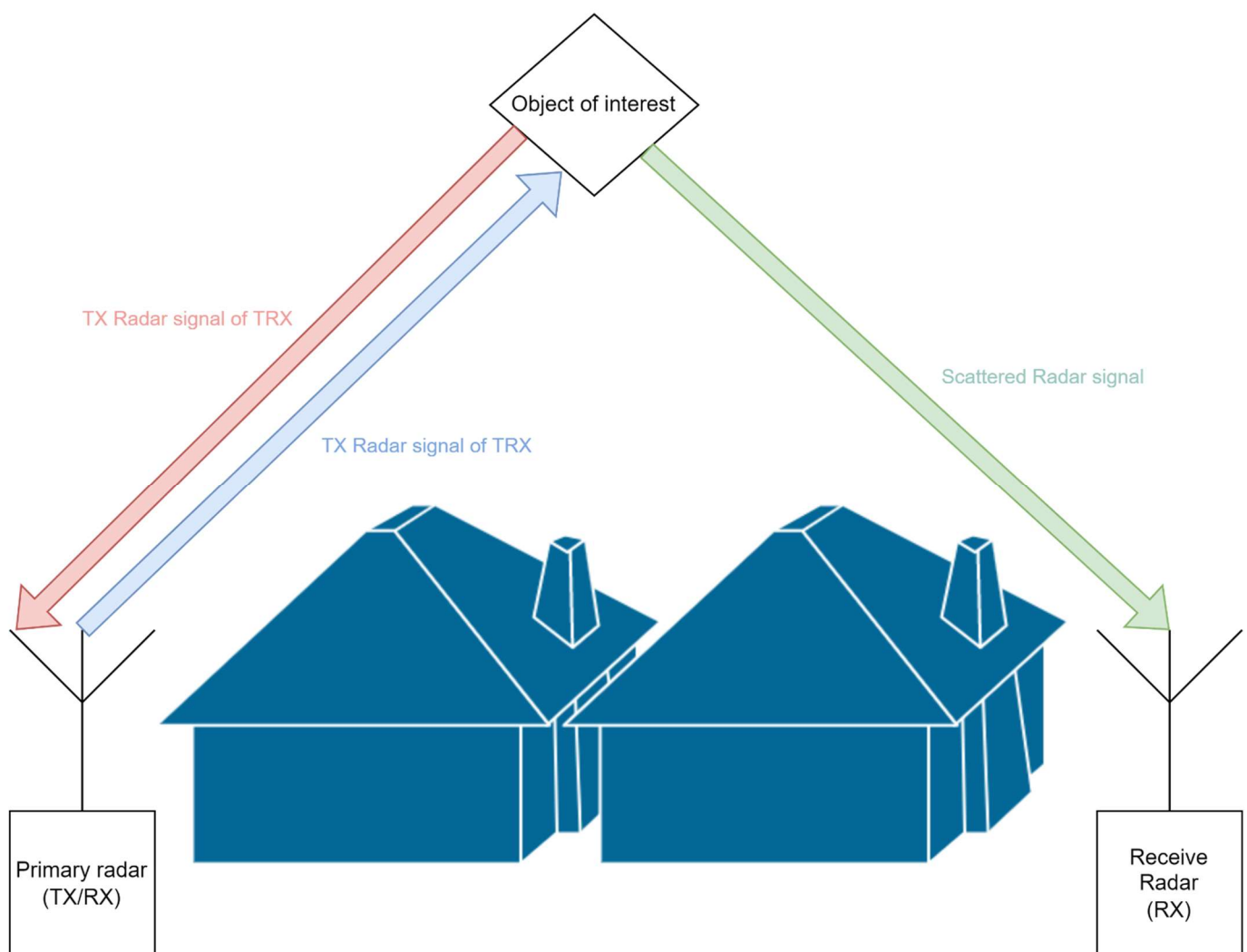


Figure 4 Non-line-of-sight scenario connection.

2.3. Radar assumptions

The main assumptions regarding to the radar systems are two similar radars. In that case each radar can be used as primary radar or switched to receive only mode. The radars must be multichannel radar

systems like phased array or multiple-input and multiple-output (MIMO) radar systems. The antennas should have a high directionality. This means the sidelobes are assumed to be neglectable and the main lobe is narrow to obtain a high angular resolution. Multichannel radars can detect signals from different directions, at the same time, to process them and determine the direction of arrival of the signals. The radars are similar and can perform signal processing of radar signals, send by each other. Although the receive radar does not use its transmitter, it detects and processes only the signals transmitted by the primary radar.

In Figure 5 a block scheme is shown of a simplified pulsed radar system, constructed with information from the books of Skolnik [2-01], Edde [2-02] and Richards et al. [2-03]. On the left an antenna is mounted with a duplexer or transmit/receive (T/R) switch, which in combination with a limiter prevents the receiver to receive too much power. The path of the transmitter can include the local oscillator (LO), although in this figure it is not counted to the receive or transmit path, because it is used by both operations. The pulses are modulated by the pulse modulator and upconverted by the LO to the carrier frequency. In the pulse modulator the signal pulses are intermitted with time slots which are recognized in the receiver as listening time. After this operation the power amplifier will amplify the signal for the radar to have more transmit power. After the transmission of each pulse, monostatic scattered pulses are received in the radar at the receive part. First the low power signals are amplified with the low noise amplifier (LNA). The LNA has a direct impact on the noise figure of the radar. This LNA is sensitive to prevent additional noise to the received signals. With the local oscillator reference signal, the received signal is down converted. The analogue received signal will be converted to a digital signal in the A/D converter, from where it continues in the signal processing and data processing steps to produce plots and the situation awareness radar picture.

To make use of the benefits of a matched filter, a synchronized local oscillator is essential. The benefits of the matched filter or other correlation techniques are the coherent integration what results in a processing gain. In a regular radar system, there is only one local oscillator, which is used to generate the transmit signal and to down convert the received signal. There are ways to synchronize the local oscillators or precisely determine the reference signal. In this thesis is assumed that the two LOs of the primary and receive radars are synchronized.

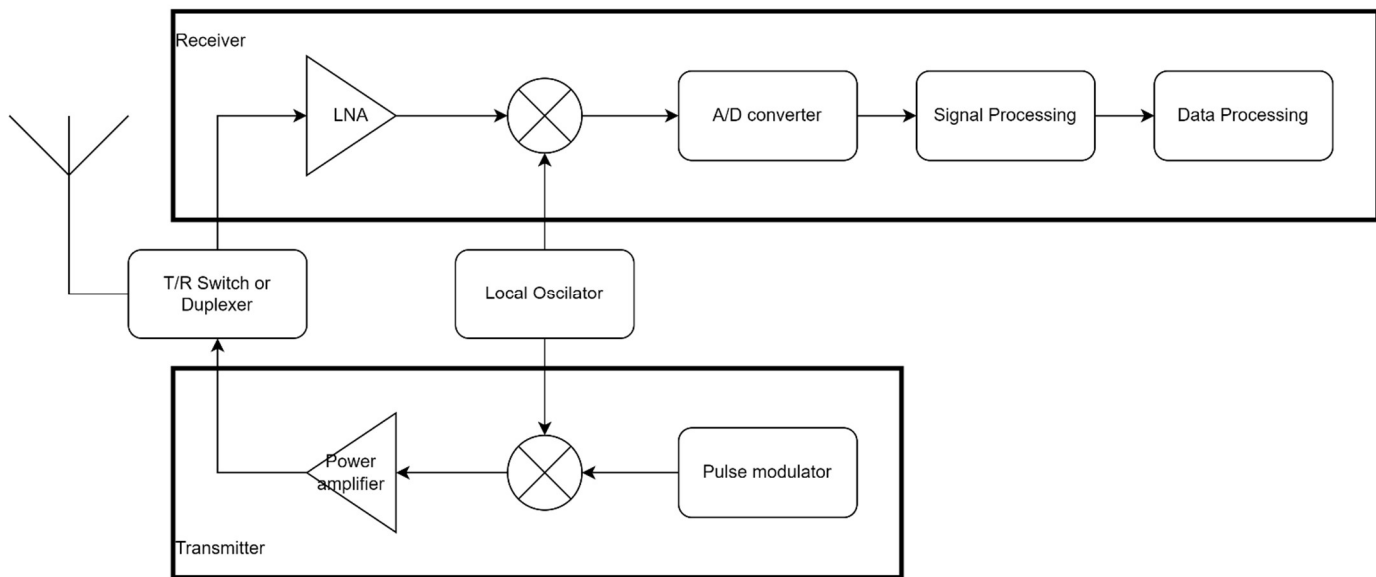


Figure 5 Simplified pulsed radar block scheme.

2.4. Radar equation

In this section the radar equations are presented. The radar equation is given in different books [2-01-203]. For the primary radar this is the well known one given below. Where the input signal-to-noise ratio SNR (dimensionless often calculated in dB) is calculated as follows:

$$SNR = \frac{P_t \cdot G_t \cdot G_r \cdot \lambda_c^2 \cdot \sigma_{op}}{(4\pi)^3 \cdot R^4 \cdot k \cdot T_0 \cdot F \cdot B} \quad (1)$$

Where in this expression: P_t is the transmitted power in [W], G_t is the gain of the transmit antenna, G_r is the gain of the receive antenna, λ_c is wavelength of the carrier in [m], σ_{op} is the radar cross section from the object-of-interest towards the primary radar in [m²], R is the range from the radar to the object-of-interest in [m], k is Boltzmann's constant (1.38×10^{-23} W/K/Hz), T_0 is the standard temperature (290 K), B is the bandwidth in [Hz] and F is the noise figure of the receiver (dimensionless).

The next step is to introduce the bistatic configuration. First a schematic figure of the bistatic situation is shown in Figure 6. This figure corresponds to Willis's book [1-02] about bistatic radar. Where the 2-dimensional bistatic configuration is described with N as the North orientation and R_L as baseline between the two radars. The range R_0 and R_1 are the distances to the object-of-interest. The ellipse has two focus points at the position of the primary radar and receive radar. The ellipse corresponds to the isorange contours of R_0 plus R_1 . In passive radar the isorange contours are the possible range positions of the object-of-interest. In this simplified scheme the primary and receive radar are stationary and only two dimensions are used. The velocity vector of the object-of-interest is v_o . This velocity is translated to a radial velocity towards both receivers. For the primary radar this is the radial velocity of the object-of-interest towards it v_{rop} . And successively v_{ror} is the radial velocity of the object-of-interest towards the receive radar.

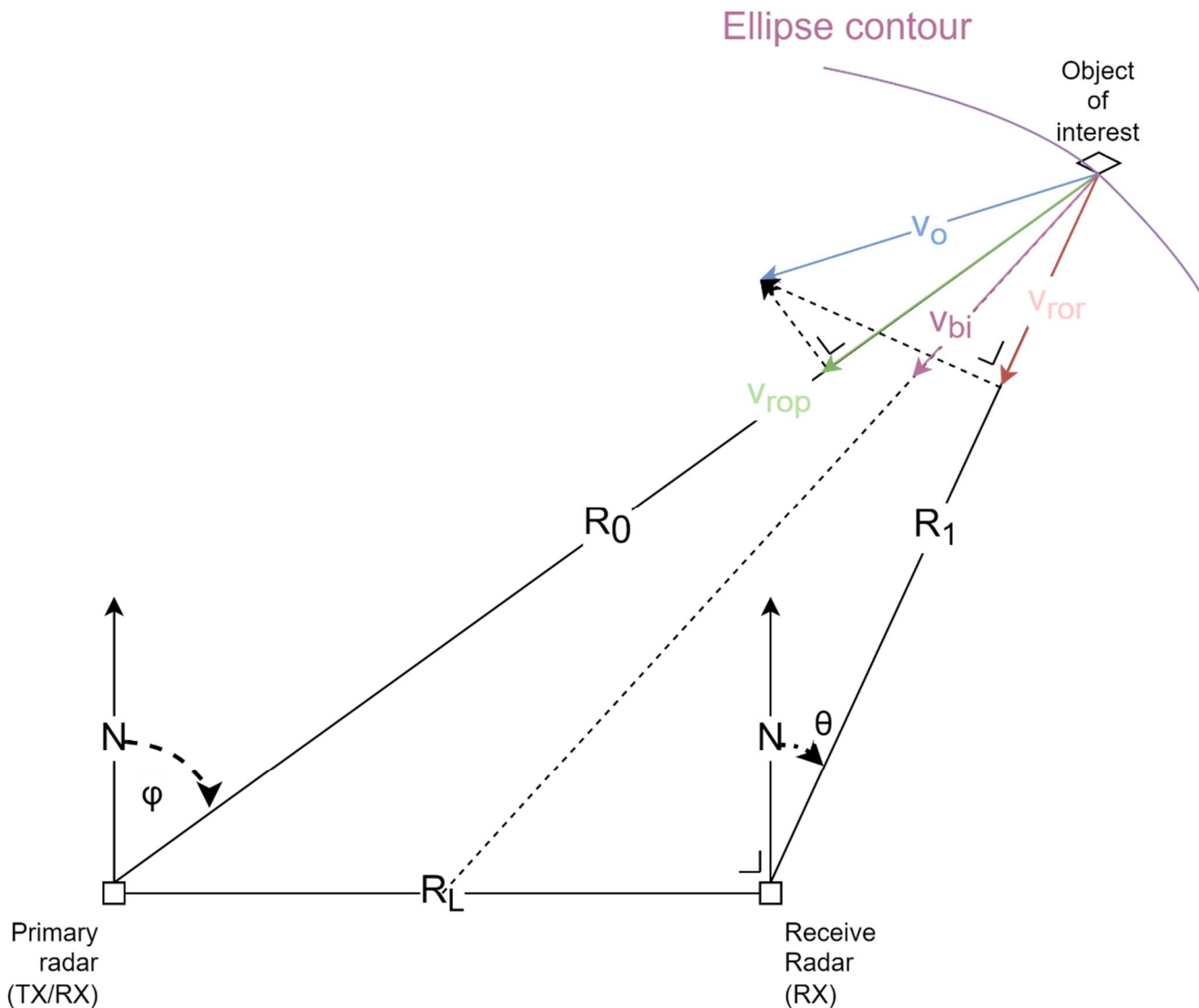


Figure 6 Schematic bistatic situation.

Without changing the variables as mentioned before the bistatic radar equation will become:

$$SNR_{bi} = \frac{P_t \cdot G_t \cdot G_r \cdot \lambda_c^2 \cdot \sigma_{bi}}{(4\pi)^3 \cdot R_0^2 \cdot R_1^2 \cdot k \cdot T_0 \cdot F \cdot B} \tag{2}$$

Where SNR_{bi} is the bistatic signal-to-noise ratio, R_0 the distance from the primary radar to the object-of-interest in [m] and R_1 the distance from the object-of-interest to the receive radar in [m], σ_{bi} is the bistatic radar cross section in [m²].

With only a line-of-sight connection the radar range equation (1) is simplified to a quadratic function of the range.

$$SNR_{LOS} = \frac{P_t \cdot G_t \cdot G_r \cdot \lambda_c^2}{(4\pi)^2 \cdot R_L^2 \cdot k \cdot T_0 \cdot F \cdot B} \quad (3)$$

Where R_L is the range of the baseline between the primary radar and the receive radar and $R_L \leq R_0 + R_1$. Thus in this case (a line-of-sight situation) $R_L = R_0 + R_1$. And for a coherent burst of K pulses:

$$SNR_{LOS,c} = \frac{P_t \cdot G_t \cdot G_r \cdot \lambda_c^2 \cdot K}{(4\pi)^2 \cdot R_L^2 \cdot k \cdot T_0 \cdot F \cdot B} \quad (4)$$

The first thing what stands out when there is a line-of-sight connection is that the theoretical received SNR is higher. R_L is always a shorter distance as $R_0 + R_1$ and it decreases in a quadratic way as function of range while in case there is a reflection it decreases to the power 4.

The SNR will increase with the number of pulses (K) times the SNR of a single pulse when the coherent integration can be performed. This is as expected from the theory that the processing gain is increasing with the number of pulses K in white noise as showed in the next equation from Richards et al. [2-03]:

$$SNR(K) = K \cdot SNR(1) \quad (5)$$

Equation (1) will change into to the coherent the signal-to-noise ratio SNR_c this is calculated as follows according to Richards [2-03]:

$$SNR_c = \frac{P_t \cdot G_t \cdot G_r \cdot \lambda_c^2 \cdot \sigma_{op} \cdot K}{(4\pi)^3 \cdot R^4 \cdot k \cdot T_0 \cdot F \cdot B} \quad (6)$$

The next step is to use the pulse compression or processing gain in the radar equation. Therefore, the bandwidth pulse duration product ($B \cdot T_p$) will be multiplied with the coherent SNR. The coherent matched filtered is signal-to-noise ratio $SNR_{c,MF}$ is defined into the following equation:

$$SNR_{c,MF} = \frac{P_t \cdot G_t \cdot G_r \cdot \lambda_c^2 \cdot \sigma_{op} \cdot K \cdot T_p}{(4\pi)^3 \cdot R^4 \cdot k \cdot T_0 \cdot F} \quad (7)$$

Where T_p is the pulse duration in [s]. The bandwidth in the denominator is cancelled by bandwidth in the numerator in (6) therefore only the pulse duration remains. The bistatic radar equation can also be expressed in this way:

$$SNR_{bi,c,MF} = \frac{P_t \cdot G_t \cdot G_r \cdot \lambda_c^2 \cdot \sigma_{bi} \cdot K \cdot T_p}{(4\pi)^3 \cdot R_0^2 \cdot R_1^2 \cdot k \cdot T_0 \cdot F} \quad (8)$$

2.5. Waveform

To measure the distance accurate and determine the Doppler frequency a linear frequency modulated (LFM) waveform is a useful waveform for radar systems. A radar determines the time between the transmission of a signal and the arrival of a received signal with great precision. The main limitation to detect objects-of-interest is the received signal-to-noise-ratio (SNR). The problem here is the received signal which can be below the noise level. In case multiple communication systems operates in the same electromagnetic

spectrum, there is also interference which is added to the noise. This will lead to the signal-to-noise-and-interference ratio (SINR). At one side the transmit power can be increased or the antenna gain can be improved. Another way of coping with this problem is to send a radar burst. These radar bursts consist of multiple pulses to detect signals. A pulsed radar with LFM waveform is modelled in this section.

The mathematical expression for the signal as function of time $s_{pulse}(t)$ with one pulse and direct current (DC) amplitude A is as follows:

$$s_{pulse}(t) = A \cdot (u(t) - u(t - T_p)) \tag{9}$$

Where $u(x)$ is the Heaviside function, and t the time in [s].

The transmit signal will be extended with a frequency sweep. The LFM upchirp pulse $s_U(t)$ is expressed as follows:

$$s_U(t) = e^{j\pi\gamma t^2} \tag{10}$$

Where j the complex number notation, and γ the chirp rate in [Hz/s] which can be expressed as:

$$\gamma = \frac{B_{LFM}}{T_p} \tag{11}$$

To process the signal correctly the bandwidth must be sampled with a frequency which is at least 2 times the bandwidth. This is according to the Nyquist–Shannon sampling theorem described in Couch [2-04]. Therefore, the sampling frequency f_s becomes:

$$f_s = 2 \cdot B_{LFM} \tag{12}$$

The LFM upchirp signal is presented in the time domain in Figure 7.

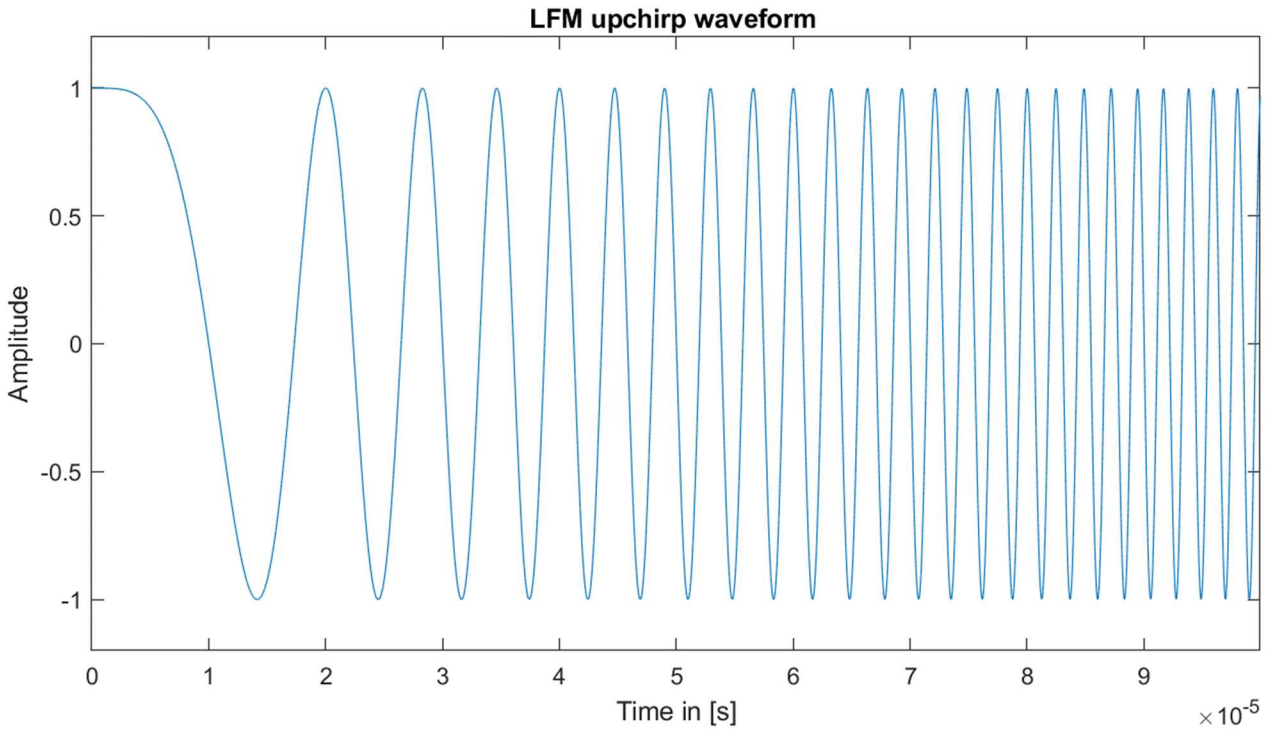


Figure 7 LFM upchirp waveform

The LFM envelope of the upchirp signal can be multiplied with (9) which will lead to:

$$s_{PU}(t) = e^{j\pi\gamma t^2} \cdot s_{pulse}(t) \quad (13)$$

This signal can be transmitted in a burst $s_{BU}(t)$ which will lead to:

$$s_{BU}(t) = \sum_{k=0}^{K-1} s_{PU}(t - k \cdot T_{PRI}) \quad (14)$$

Where K is the number of pulses in a burst. The next step is to modulate this signal on a carrier frequency f_c :

$$s_{BULFM}(t) = e^{j2\pi f_c t} \cdot s_{BU}(t)$$

The pulse repetition frequency (PRF) is the inverse of the PRI and determines the unambiguous range of a radar. With a staggered PRF the unambiguous range can be extended. Therefore, the PRF is changed for the different bursts. An example of a staggered radar waveform is presented in Figure 8. The staggered PRF can also be used to avoid blind speeds which occur at the primary radar because of the use of a moving target indicator (MTI) according to Richards [2-03].

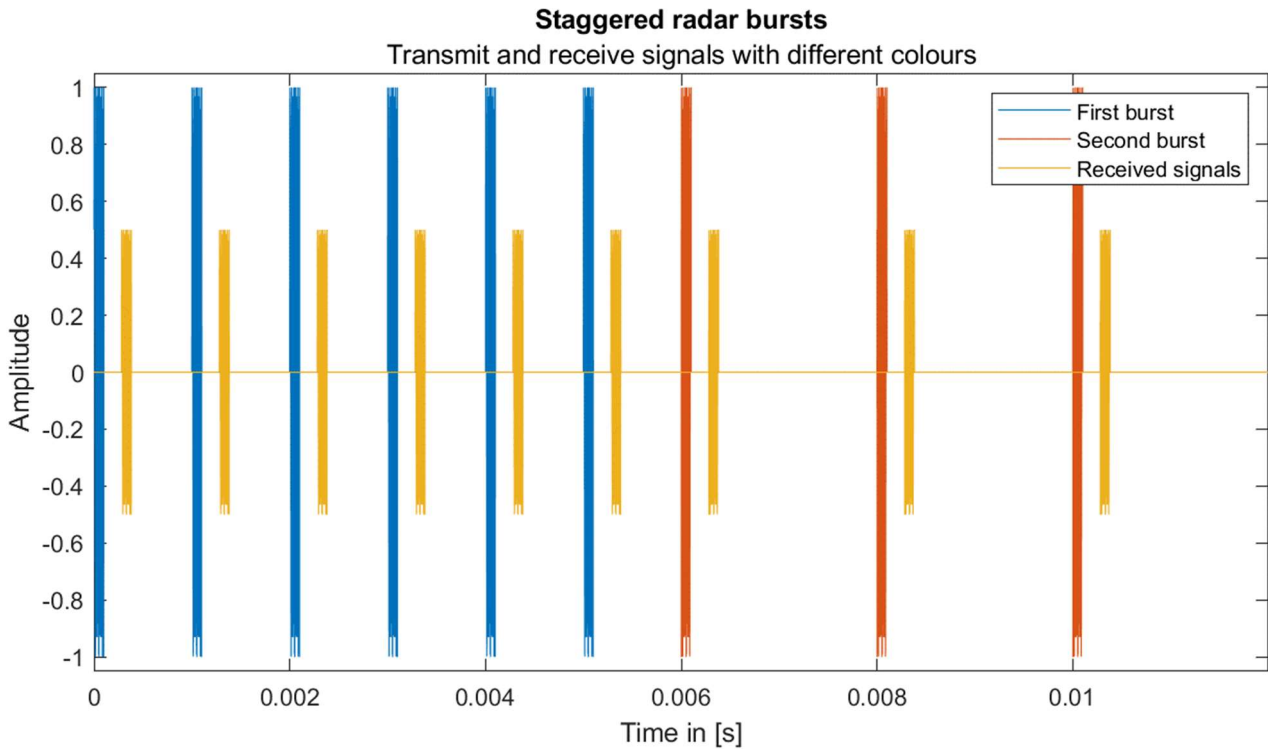


Figure 8 Example of a staggered waveform with a PRF of 1000 Hz and a PRF of 500 Hz.

2.6. Range and Doppler estimation

The main variable which can be measured with radar is range. The other important variable which can be measured is the Doppler frequency which is related to the radial velocity. The primary radar is capable of determine the distance from the object-of-interest to the radar. First the round-trip delay time from the primary radar to the object-of-interest is calculated followed by the distance:

$$\tau_p(t) = \frac{2(R_0 + v_{rop}t)}{c} \quad (15)$$

Where v_{rop} is the radial velocity of the object-of-interest towards the primary radar in [m/s].

In the bistatic configuration the time delay at the receive radar becomes:

$$\tau_r = \frac{(R_0 + R_1 + (v_{rop} + v_{ror}) \cdot t)}{c} \quad (16)$$

It is impossible to determine the distances R_0 and R_1 at the receive side without the knowledge of the exact moment when the burst is transmitted.

The number of range cells for a pulse compressed radar signal can be derived with the equation for the range resolution δR and the unambiguous range R_{un} . The equation for the range resolution is as follows:

$$\delta R = \frac{c}{2 \cdot B_{LFM}} \quad (17)$$

Where B_{LFM} is the bandwidth of the LFM sweep in [Hz] and c the speed of light in free space (299 792 458 m/s). The equation for the unambiguous range is as follows:

$$R_{un} = \frac{c \cdot T_{PRI}}{2} \quad (18)$$

With T_{PRI} the PRI in [s]. The number of range cells N_{RC} is calculated as follows:

$$N_{RC} = \frac{R_{un}}{\delta R} = \frac{c \cdot T_{PRI}}{2} \cdot \frac{2 \cdot B_{LFM}}{c} = T_{PRI} \cdot B_{LFM} \quad (19)$$

The accuracy of the range measurement depends on the SNR. According to Richards [2-03] accuracy of the range resolution can be calculated with the lower limit of the Cramér-Roa bound. The standard deviation of the range measurement σ_R becomes:

$$\sigma_R = \frac{c}{4\pi \cdot B_{LFM,RMS}} \frac{1}{\sqrt{SNR}} \quad (20)$$

Where $B_{LFM,RMS}$ the root mean squared bandwidth of the LFM pulse is. The variance of the range accuracy depends on the inverse of the square root of the SNR.

The other main variable what can be measured with radar is the Doppler frequency which is related to the radial velocity of an object-of-interest. In Richards [2-05] the Doppler shift f_d is approximated by ignoring the second order and higher terms and therefore:

$$f_d = + \frac{2v}{c} f_c = + \frac{2v}{\lambda_c} \quad (21)$$

Where the increase of the Doppler frequency is defined as a positive velocity. So, an approaching target has a positive velocity. The Doppler resolution Δf_d depends on the time on target as expressed in the following equation:

$$\Delta f_d = \frac{1}{T_{ot}} \quad (22)$$

Where T_{ot} is the time on target. The Doppler shift can be calculated with a fast Fourier transform (FFT).

2.7. Matched filter

The matched filter starts with the received delayed signal $s_r(t) = s(t - \tau)$ for a single object-of-interest with delay τ as described in the book of Harrison [2-06]. Presented as a block diagram in Figure 9.

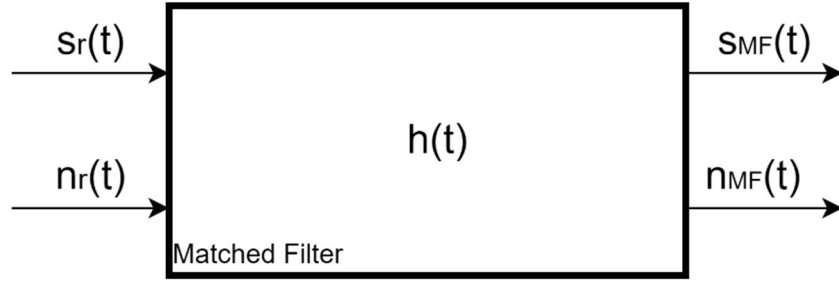


Figure 9 Matched filter block diagram.

The received signal $s_r(t)$ and the noise $n_r(t)$ are the inputs for the matched filter. The total signal is the reflected waveform and the noise. Therefore, the input for the matched filter $z_i(t)$ stated in an equation as follows:

$$z_i(t) = s_r(t) + n_r(t) = s(t - \tau) + n_r(t) \quad (23)$$

And the output signal is convoluted with the filter $h(t)$.

$$z_{MF}(t) = s_{MF}(t) + n_{MF}(t) = s(t - \tau) * h(t) + n_r * h(t) \quad (24)$$

With matched filter $h(t)$, filtered signal $s_{MF}(t)$, filtered noise $n_{MF}(t)$, original signal $s(t)$ time delay τ and the received noise n_r .

With zero-mean white Gaussian noise the calculation of the noise power is easy. The expected value is the variance of the noise. The power of the matched-filtered signal is the squared root mean squared signal. This leads to the signal-to-noise ratio:

$$SNR = \frac{P_{MF \text{ signal}}}{P_{noise}} = \frac{|s_{MF}(t_0)|^2}{E\{|n_{MF}(t)|^2\}} \quad (25)$$

With $E\{x\}$ as the expected value of x . It is possible to deconvolute the signal if the practical applications this allows. In that case the convolution of the received signal time domain signal with a time reversed version of the transmitted waveform will form the basis of the matched filter. This convoluted signal must be normalized to the signal power of the transmitted signal. The other way to conduct a matched filter is with a filter in the frequency domain. In that case the convolution will simplify to a multiplication. The generalized likelihood ratio test (GLRT) matched filter can be derived from Robey [2-07]. Mathematical the matched filter with LFM envelope $s_{LFM}(t)$ as defined in (10) as upchirp however $s_{LFM}(t)$ can also be a downchirp. The matched filter output is of the following form:

$$z_{MF}(t) = \frac{s_{LFM}(-t)^H * z_i(t)}{s_{LFM}(t) \cdot s_{LFM}(t)^T} \quad (26)$$

The autocorrelation of the envelope $s_{LFM}(t)$ as defined in (10) is presented in Figure 10. The main lobe is narrow what will contribute to the range resolution. Another advantage of the matched filter is the processing gain which are included in the SNR calculations in (7) and (8).

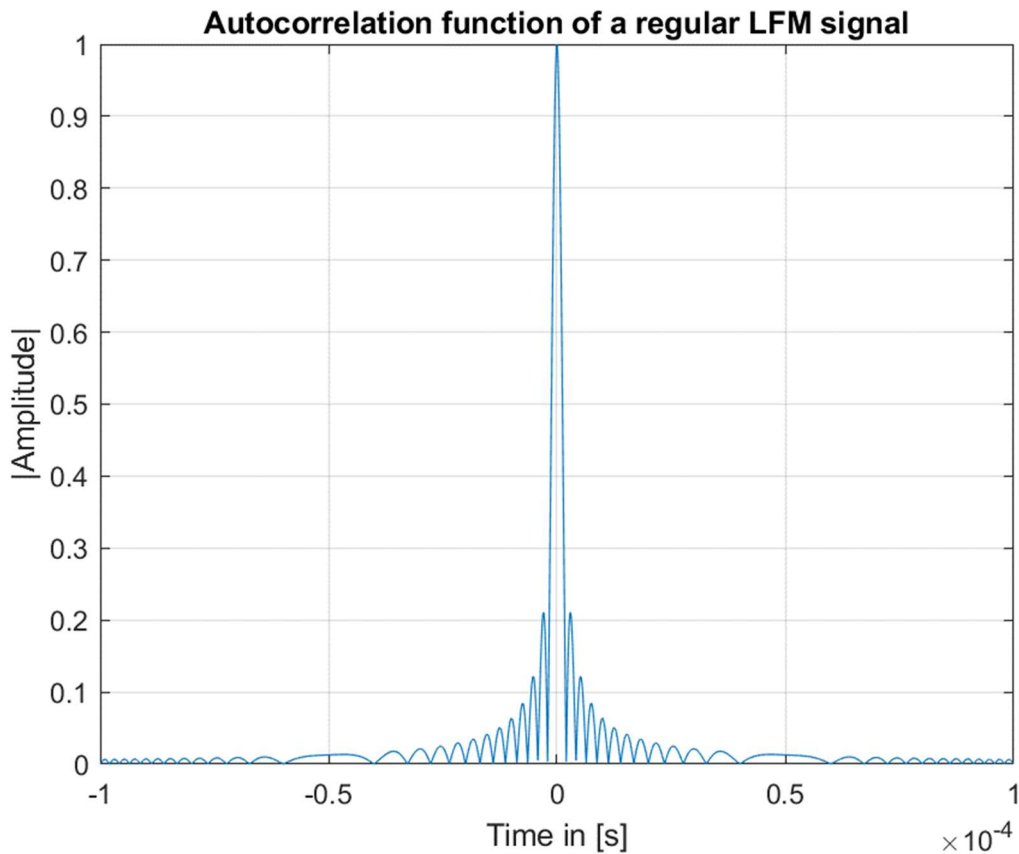


Figure 10 Autocorrelation function of a regular LFM sweep.

2.8. Swerling cases and detection

The geometry of the object-of-interest determines its RCS. The simplest form is a sphere. However, a sphere is not likely for the different scenarios so it should be modelled in another way. Therefore, the Swerling case model can be used. The 5 Swerling cases as identified by Swerling [2-08] are as follows. The first Swerling case 0 (also known as 5) is a stationary object where no fluctuations in RCS occur. The other Swerling cases depend on their probability density function (exponential or chi squared with 4 degrees of freedom) and if they fluctuate on a pulse-to-pulse or scan-to-scan basis. This is presented clearly in Table 1 from Richards [2-03]:

Probability density function of RCS	Decorrelation	
	Scan-to-scan	Pulse-to-pulse
Exponential	Case 1	Case 2
Chi-square, degree 4	Case 3	Case 4

Table 1 Swerling Models.

The different Swerling cases together with the noise determine the probability of detection. The hypothesis signal with noise model will be introduced. This is shown in Table 2.

Hypothesis	Received signal
$H_0(\text{Noise})$:	$z(t) = n(t)$
$H_1(\text{Signal} + \text{Noise})$:	$z(t) = s_{TDLFEMUD}(t) + n(t)$

Table 2 Hypothesis signal and noise model

Where $z(t)$ is the received signal, $n(t)$ the noise with the main assumption that it is zero-mean white Gaussian noise (ZWGN) $\sim N(0, \sigma_n^2)$ and σ_n^2 is the variance of the noise.

In Figure 11 two different kinds of detectors are shown which can be used for the primary radar operation. These detectors are described in the book of Harrison [2-06]. In this figure the variable for the threshold is T . The hypothesis H_0 is accepted when the measured value is below the threshold. The hypothesis H_1 is accepted when the measured value is above the threshold.

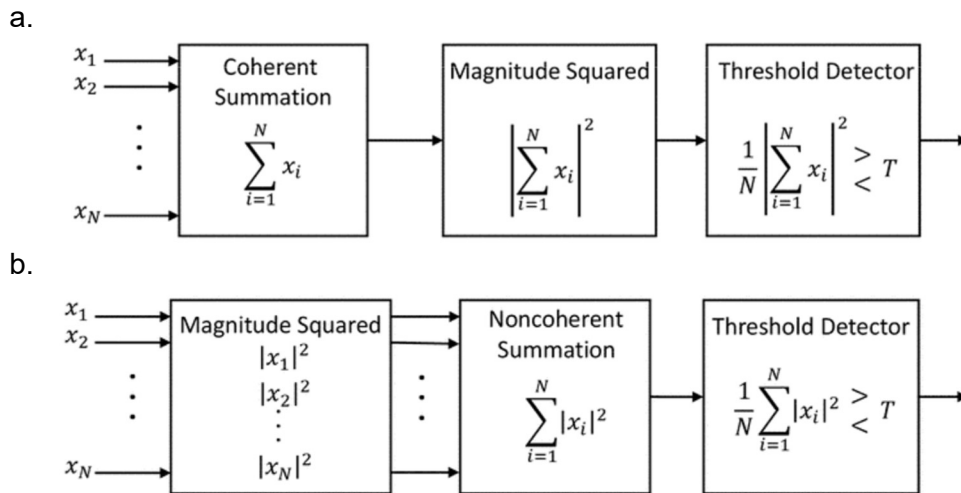


Figure 11 Detectors described in the book of Harrison [2-06]: a. Coherent detection b. Noncoherent detection.

It is possible that mistakes are made by accepting or rejecting a hypothesis. The threshold determines the probability of detection and probability of false alarm. The following scheme stated in Table 3 is used to determine the probabilities of detection P_D , of false alarm P_{fa} , of missed detection P_M and (correct) no detection P_{ND} of a regular radar.

Hypothesis	Signal is transmitted	Signal is not transmitted
$H_1(\text{Signal} + \text{Noise}):$	P_D	P_{fa}
$H_0(\text{Noise}):$	P_M	P_{ND}

Table 3 Hypothesis and probabilities scheme regular (primary) radar.

With the theory mentioned above the probability of detection can be estimated as function of the SNR for the different Swerling cases. This is shown in Figure 12 which is a graph from the book of Harrison [2-06]. Harrison used in his graph noncoherent integration over 10 pulses with a false alarm rate of 1×10^{-6} . The threshold of a regular radar is 13 dB to create a probability of detection of 0.9 and a probability of false alarms of 1×10^{-6} .

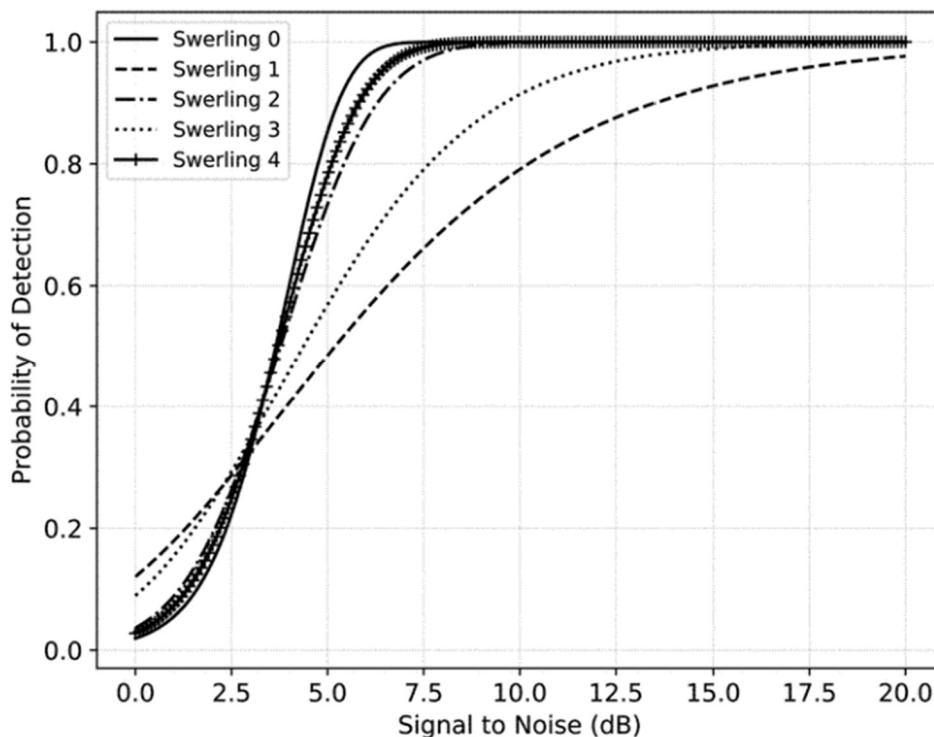


Figure 12 Influence probability of detection on the SNR. Graph from Harrison [2-06].

The performance of a radar is also influenced by its duty cycle. The duty cycle dc is defined in Richards [2-03] as the fraction of total time that the transmitter is on. The average power P_{av} in W of a pulsed radar is defined as:

$$P_{av} = P_p \cdot T_p \cdot PRF = P_p \cdot dc \quad (27)$$

With peak power P_p . With this equation the influence of the average power and duty cycle on the SNR and detection probability becomes visible. This relation is when the duty cycle is decreased the average power decreases and subsequently the SNR will decrease, and probability of detection will drop.

2.9. Communication

The radar performance is influenced when communication modulation schemes like binary phase shift keying (BPSK) are used. Communications and sensing waveforms are optimized for their purposes. Where radar uses the radar equation as base for the radar sensing applications in communications this is the Friis equation which can be presented as signal-to-noise ratio SNR_{Comms} which is equal to the SNR_{LOS} earlier defined in (3):

$$SNR_{Comms} = \frac{P_t \cdot G_t \cdot G_r \cdot \lambda_c^2}{(4\pi)^2 \cdot R_L^2 \cdot k \cdot T_0 \cdot F \cdot B} \quad (28)$$

Wireless communication applications measure their performance in bit rate and bit error rate. The baud or symbol rate is defined in Couch [2-04] with a fixed duration of the transmitted symbol as follows:

$$D = \frac{N_S}{T_S} \quad (29)$$

Where D is the baud in [symbols/s], T_S the time of one symbol in [s] and N_S is the number of different symbols. The bit rate R_B is the number of bits per second in [bit/s] and given in Couch [2-04]:

$$R_B = \frac{N_{bit}}{T_S} \quad (30)$$

Where N_{bit} is the number of bits sent in the T_S . In a binary signal the baud is equal to the bit rate.

The bit error rate (BER) or symbol error rate (SER) determines the performance of a communication system. It depends on the energy per bit or symbol. The BER is calculated as follows:

$$BER = \frac{\#Errors}{\#Bits} \quad (31)$$

The SER is calculated as follows:

$$SER = \frac{\#Errors}{\#Symbols} \quad (32)$$

These error rates can be transferred to probability of error which will be simulated in the chapter Simulations.

In 2-way (duplex) wireless communication systems it is common to use an automatic repeat request (ARQ) if the data is not correct received. The other main method for error correction codes is forward error correction (FEC) Couch [2-04] which is useful in simplex communication systems. The downside of FEC is that the more bits are needed for redundancy. Successively the data rate increases or put in a different way the information rate decreases.

Bit synchronization must be performed with BPSK. With a radar network of opportunity without a fixed synchronization protocol the bit synchronization is hard to implement. In data communications a prefix for a packet of data is used. The maximal bit rate of BPSK is high and can be calculated as follows:

$$R_{B,BPSK} = \frac{1}{T} \quad (33)$$

The bit rate is the inverse of the bit duration T .

Although multiple modulation and communication methods are known, in this thesis the focus is on BPSK. This is a commonly used modulation scheme which can be combined with a sensing waveform. The waveform shall be introduced on the end of the literature research in the next chapter.

3 Literature research

3.1. Introduction

In literature the combination of radar with communications is named differently according to its purpose. For instance, radar and communication shared spectrum (RCSS) Guerci et al. [3-01] and Hayvaci et al. [3-02], radar communication co-existence (RCC) Zheng et al. [3-03]. Further RadCom is mentioned [3-04] which is also the name of the magazine of the Radio Society of Great Britain [3-05], joint communication and radar (JCR) (Zhang et al. [3-06], Zang et al. [3-07] and Paul et al. [3-08]) and the reciprocal joint radar and communication (JRC) (Feng et al. [3-09], Liu et al. [3-10], Sturm et al. [3-11]), dual-function radar and communication (DFRC) (Hassanien et al. [3-12,3-13] and Euziere et al. [3-14]) are also familiar terms. And lately joint communication and radio/radar sensing (JCAS) [3-09] and Wild [3-15], and integrated sensing and communications (ISAC) for beyond 5G and 6G systems are added to this list Liu et al. [3-16] Yuan et al. [3-17]. The focus of this thesis is on the radar domain with a radar application which benefits from additional communication methods.

In Richards et al. [3-18] a figure of the taxonomy of radars is stated for bistatic radar. This figure is shown in Figure 13 as white boxes. The blue text box is the new proposed radar application. Where the primary radar (cooperative transmitter) can perform its own monostatic radar operation. This is pictured by the blue arrow of the monostatic radar to the cooperative transmitter. The primary radar can, in parallel with its monostatic operation, provide the cooperative hitchhiker additional information with communications. To the best of the authors knowledge, a similar system is not found in literature.

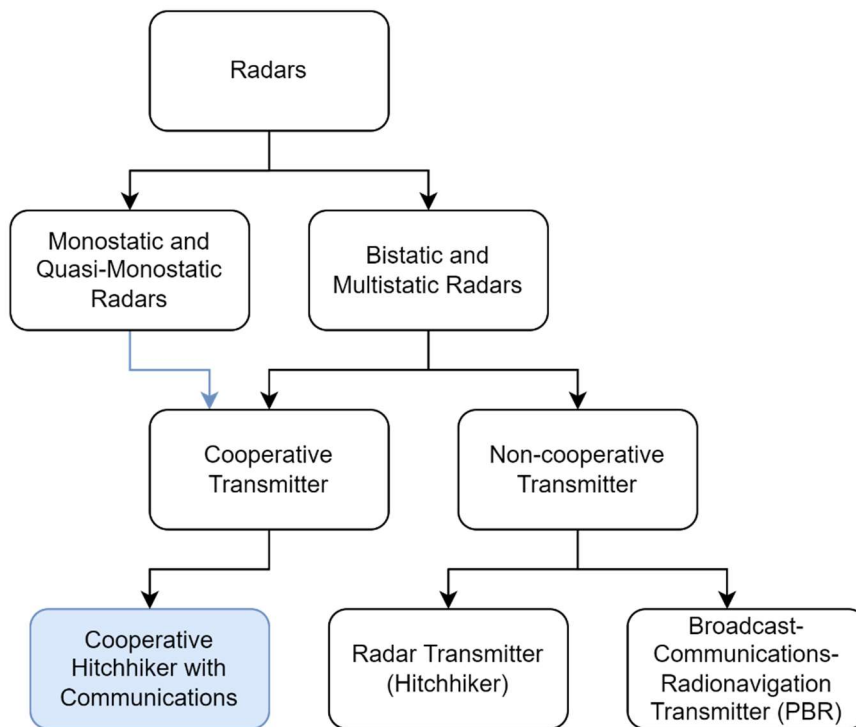


Figure 13 Bistatic radar taxonomy.

3.2. Radar communication integration

In Quan et al. [3-19] an overview of radar and communication integration is given. In this paper the main approaches are time-sharing, sub-beams and signal-sharing. Time-sharing is made possible with a strobe switch where a radar signal processor and a communication modem are connected to. Sub-beams are used in phased array systems and nowadays in MIMO as described by techniques systems Liu [3-20]. The last approach is signal-sharing where communications are mixed on the same waveform. Examples of signal-sharing are orthogonal frequency division multiplexing (OFDM), frequency division multi-carrier and spread-spectrum (SS). A newer signal sharing SS technique is chaos based frequency modulation waveforms as proposed in Pappu et al. [3-21] for bistatic imaging systems. In this bistatic operation the transmitter and

receiver have a line-of-sight connection. This thesis focusses on the signal sharing perspective with minimal degradation of the performance of primary radar and a possibility to communicate over an object-of-interest. In Garmatyuk et al. [3-22] randomized OFDM waveforms are proposed to covertly communicate over an object-of-interest. This method uses an on-off-keying modulation and retransmissions of the signal to get a better bit error rate.

In this thesis a joint waveform design is proposed to prevent degradation of the primary radar. In Xiong et al. [3-23] an overview of ISAC waveforms is given. The proposed application in this thesis should fit in “Tightly coupled radar waveform based traditional radar waveforms” as described by Xiong. Another method in the tightly coupled radar waveform section is index modulation. Index modulation divides the data into two methods to transfer these data. The first part is to transfer information with the index of the assigned resources like: antennas, subcarriers, or SS. The second part modulates the remaining bits with a regular communication modulation form like amplitude or phase modulation. In Ciunzo et al. [3-24] and Blunt et al. [3-25] communication signals are added to the radar pulse in a radio frequency (RF) tag or RF transponder. In that case the original radar signal remains the same until its scatterers. As a scattering surface a semi-passive reflector or a radio frequency identification (RFID) surface can be used. At that surface the communication modulation is embedded.

3.3. Comparing radar waveforms

The scope of this research is into pulsed radar with an LFM sweep. FMCW is a comparable technique which uses similar LFM waveforms although applications might differ from pulsed radar. One of the state-of-the-art techniques is phase coded FMCW as described in Kumbul et al. [3-26]. Another technique is Linear Frequency Modulated – Minimum shift keying (LFM-MSK) which is described by Dong et al. [3-27] and uses pulsed radar. Both papers will be described in the following subsections. In this thesis both techniques will be compared to a novel TDBRB waveform which uses also pulsed radar with an LFM sweep.

In the paper of Kumbul et al. it is assumed that the LFM signal is synchronized by using GPS. With a synchronized signal it is possible to dechirp the FMCW chirp. After downmixing the phase coded signal remains. In automotive scenarios phase coding can be used to reduce the interference. The interference is reduced when different vehicles use different phase codes. It is also possible to use these phase codes to transfer information. The phase coded signal is a BPSK signal which will lead to a data transfer of 1 Mbit/s at 100 m as determined by Kumbul et al. [3-26]. The own radar (in this thesis the primary radar) is degraded by the communication signal due to the sidelobes. Further, the communication signal at the receive side is not used for radar processing what is intended in this thesis. Another disadvantage is that methods based on BPSK require a higher energy per bit or signal-to-noise level for a sufficient bit error rate.

The paper of Dong et al. [3-27] describes an integrated waveform for communication and sensing. The focus is on bistatic radar although the communication signal is placed in two successive pulses in a burst. This is due to the MSK coding. The advantage is that the information is repeated. Because of the MSK the signals can be multiplied by each other to get the original LFM pulse back. A burst of these LFM pulses can be used to perform the radar operation at the primary radar and the receive radar. This technique can be useful for the setup in this thesis, however the communication signals which are based on BPSK rely on the signal-to-noise level of one (or two due to the MSK) pulses. The paper suggests a bit rate which is larger as 25 kbit/s when 128 pulses are used with a pulse repetition frequency of 1000 Hz and 50 bits per pulse. Another disadvantage of this technique is that the coherent integration gain is halved because only 64 pulses can be used for processing and the required bandwidth is doubled due to the MSK.

The next sections describe the techniques which are described in the papers of Kumbul [3-26] and Dong [3-27]. It starts with phase attached radar communication (PARC) which is the technique used for PC FMCW followed by the principle of LFM-MSK.

3.4. Phased Attached Radar Communication

In this section the mathematical framework for PARC is derived from literature. In an article of Uysal [3-28] a phase attached radar communication system for an automotive frequency modulated continuous wave radar is described. This PARC has a similar way of communication as PC FMCW of Kumbul [3-26]. Figure 14 shows the transmitted and received signals in the frequency and phase domain (pictured as positive or negative amplitude). The positive or negative amplitude or 180° phase shift corresponds to BPSK. Figure 15 shows the time domain signal of this BPSK-modulated signal for an actual linear frequency modulated (LFM) signal in the time domain.

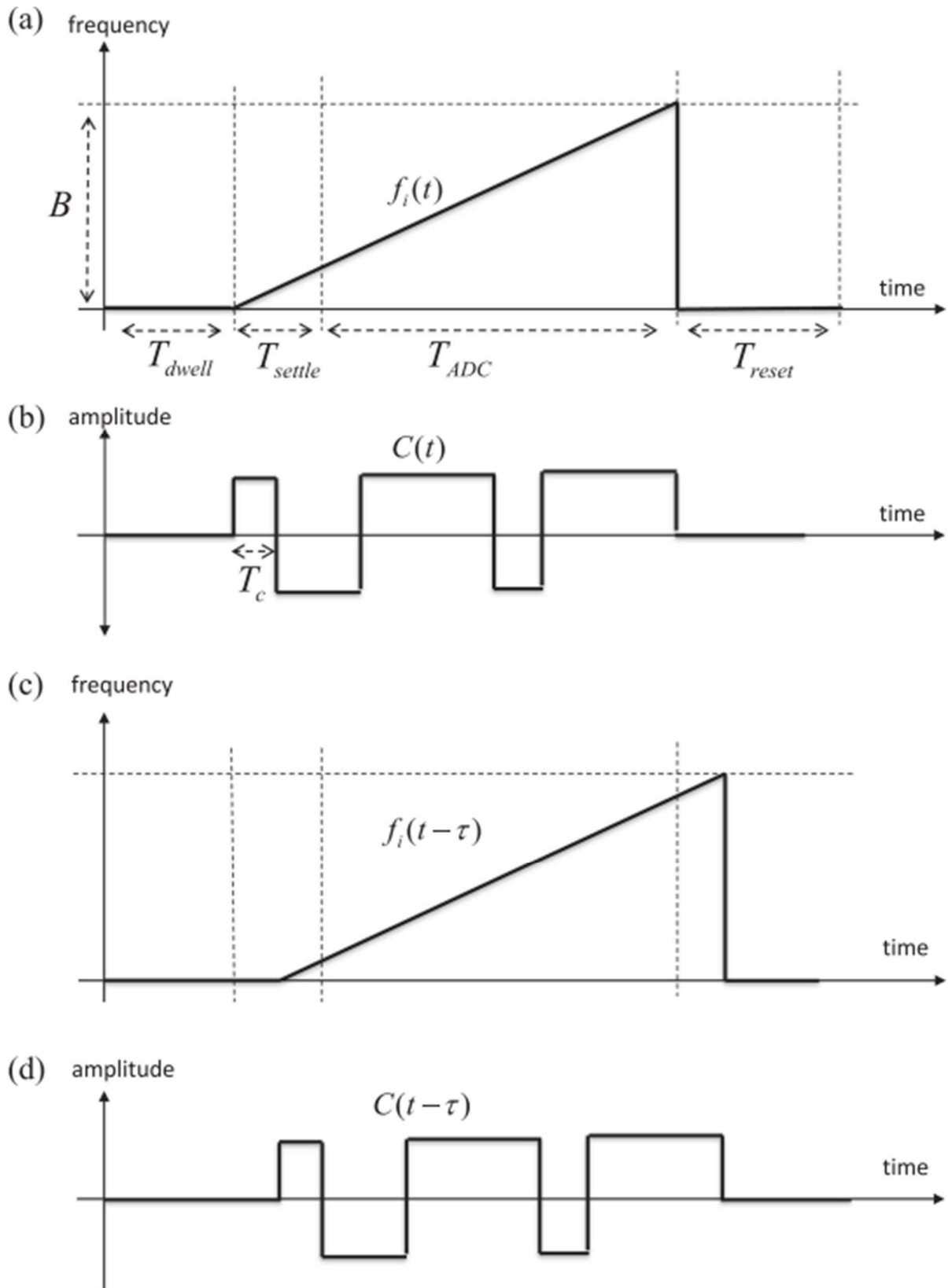


Figure 14 "Illustration of typical transmitted and received signal with their envelopes. a. The instantaneous frequency of the transmitted signal. b. The envelope of transmitted signal as bipolar binary coding. c. The instantaneous frequency of the received signal. d. The envelope of the received signal as bipolar binary coding." [3-28] Uysal PARC waveform for FMCW with permission for using this figure.

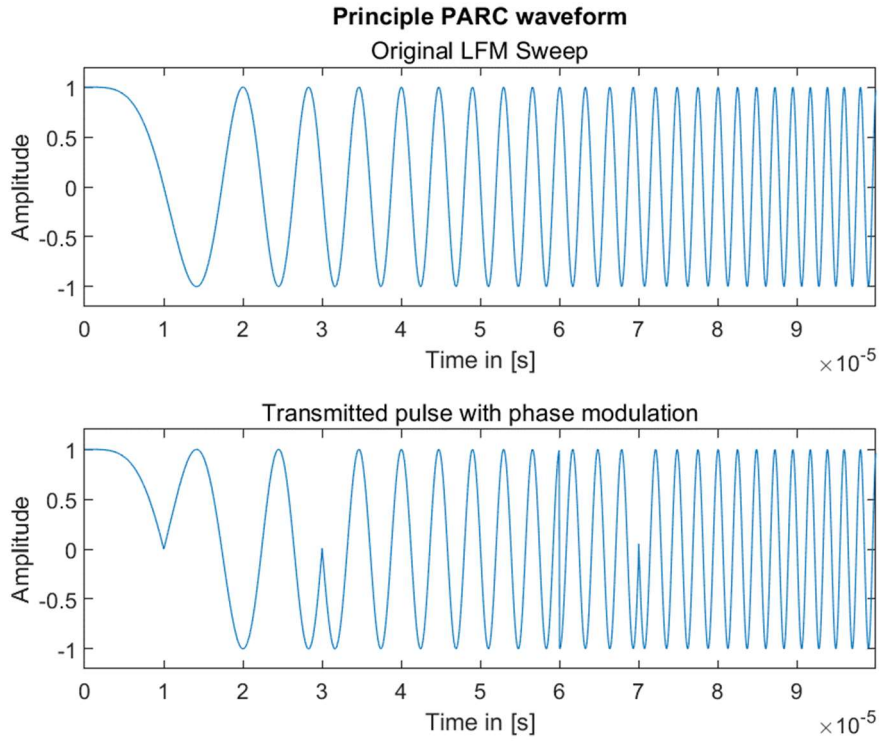


Figure 15 FMCW chirp as in previous figure with binary phase shift keying in the time domain.

In essence the LFM sweep of the FMCW chirp has the same properties as the LFM pulse in the pulsed radar. Therefore (10) can be used. The bandwidth of the LFM sweep of the pulse is the chirp bandwidth and the chirp duration corresponds to the pulse duration.

$$s_{LFM}(t) = a(t) \cdot e^{j(2\pi f_c t + \pi \gamma_c t^2)} \quad (34)$$

Where f_c is the carrier frequency of the FMCW radar, and γ_c the FMCW chirp rate in Hz/s which can be expressed as:

$$\gamma_c = \frac{B_C}{T_C} \quad (35)$$

With B_C as bandwidth of the FMCW LFM sweep and T_C as the pulse or chirp duration. At this point the pulsed coding can be introduced. The most used form is binary phased shift keying.

For the sequence $\alpha_1, \alpha_2, \alpha_3, \dots, \alpha_{L_C}$ with $\alpha_n \in \{-1, +1\}$ the phase corresponds to $\varphi_n \in \{0, \pi\}$. For L_C bits in one pulse interval Uysal [3-28] represents this code as:

$$C(t) = \sum_{n=1}^{L_C} e^{j\varphi_n} \cdot \left(\text{rect} \left(\frac{t - (n - \frac{1}{2}) \cdot T_B}{T_B} \right) \right) \quad (36)$$

Where $\text{rect}(x)$ is a rectangular function of a block pulse with a length and height 1 on the interval -0.5 to +0.5 and T_B corresponds to the duration of one bit. Translated to a Heaviside function this results in:

$$C(t) = \sum_{n=1}^{L_C} e^{j\varphi_n} \cdot (u(t - (n - 1) \cdot T_B) - u(t - n \cdot T_B)) \quad (37)$$

Although the application is mainly in FMCW radar, the signal can be used in pulsed radar systems. The phased coded signal can be sent in a burst of equal pulses. After the matched filter these bursts can be used to coherently integrate the signals.

The data modulated on PARC signals with BPSK depends on the code length L_C . Therefore, L_C bits can be transmitted. The code length can be adjusted to make a transmission more reliable. Although this must be known by the receive radar on forehand.

3.5. Linear Frequency Modulated Minimum Shift Keying

In this section the mathematical framework for is given as presented in Dong [3-27]. The principle works with two successive MSK modulated pulses which will return a LFM signal when both pulses are multiplied with each other. This principle is shown in Figure 16. The starting point for one LFM-MSK pulse is the phase code signal as in (37).

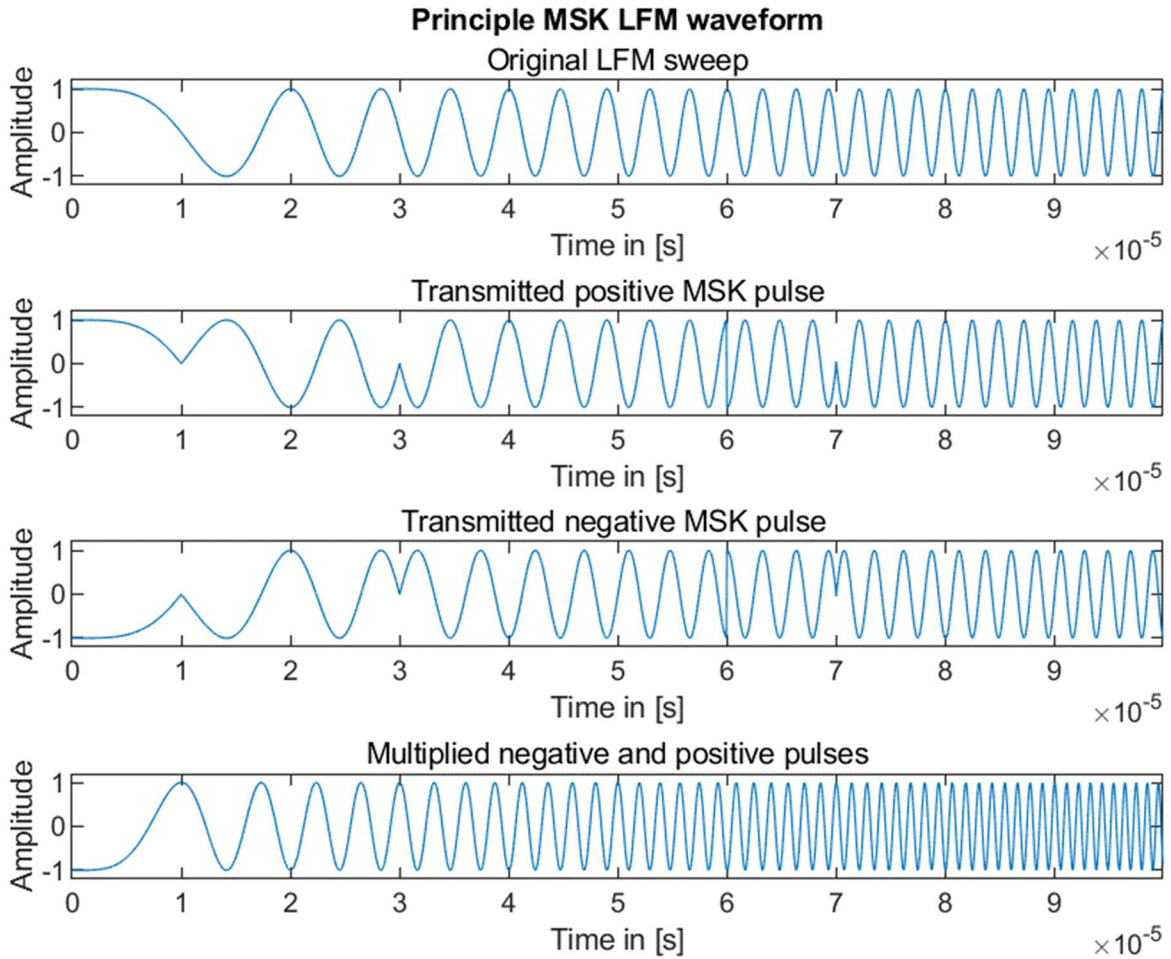


Figure 16 Two successive LFM-MSK pulses (positive and negative) followed by the multiplication of both (the resulting LFM sweep).

The difference in the positive and negative MSK pulse is a phase shift of 180° or multiplication with $e^{j\pi}$. Mathematical this has the following characteristics:

$$C^+(t) = \sum_{n=1}^{L_C} e^{j\varphi_n} \cdot (u(t - (n - 1) \cdot T_B) - u(t - n \cdot T_B))$$

$$C^-(t) = e^{j\pi} \cdot \sum_{n=1}^{L_C} e^{j\varphi_n} \cdot (u(t - (n - 1) \cdot T_B) - u(t - n \cdot T_B))$$

(38)

Both codes can be decoded separately, and the modulated information can be recovered. Only one MSK pulse is needed to decode the information. The result of the multiplication of codes with their LFM envelopes which is similar as the upchirp signal defined in (10) is as follows:

$$s_{MSK LFM}(t) = C^+(t) \cdot s_U(t) \cdot C^-(t) \cdot s_U(t) = e^{j\pi} \cdot e^{j2\pi\gamma t^2} = -e^{j2\pi\gamma t^2} \quad (39)$$

This result is an LFM signal with a doubled chirp rate. This is also visible in the bottom image in Figure 16. In this way the matched filter for a burst of LFM pulses can be used to perform radar operations.

3.6. Sidelobes BPSK

The major downside of using BPSK is the increased sidelobes with respect to the regular LFM signal. For the original LFM sweep and the BPSK signal of Figure 15 the autocorrelation function is presented in Figure 17. The sidelobes for BPSK are larger as is clearly visible in this figure. In PC FMCW therefore also Gaussian MSK is used which suppresses the sidelobes however there is always a degradation of the radar performance when these modulation schemes are used.

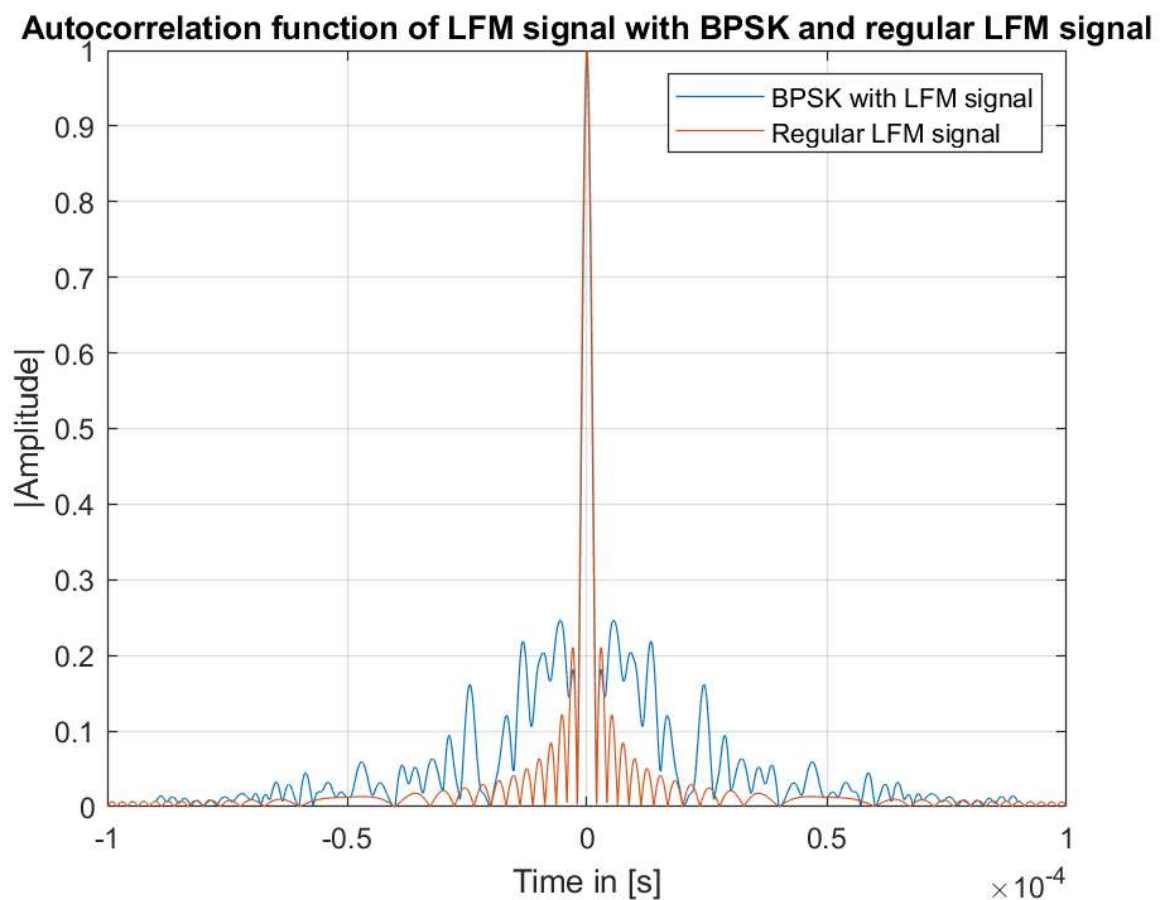


Figure 17 Autocorrelation function of LFM signal with BPSK and regular LFM signal.

3.7. BPSK symbol error rate

The performance of BPSK can be estimated with Monte Carlo simulations. With a MATLAB program of Ahmed [3-29] the symbol error rate is calculated and presented in Figure 18. However, the probability of error degrades if the energy of one bit increases. It is possible to integrate the energy of one bit over a longer time in that way the bit rate will decrease. The advantage is that the probability of error also will decrease. In order to integrate the energy of one bit the receiver must be synchronized.

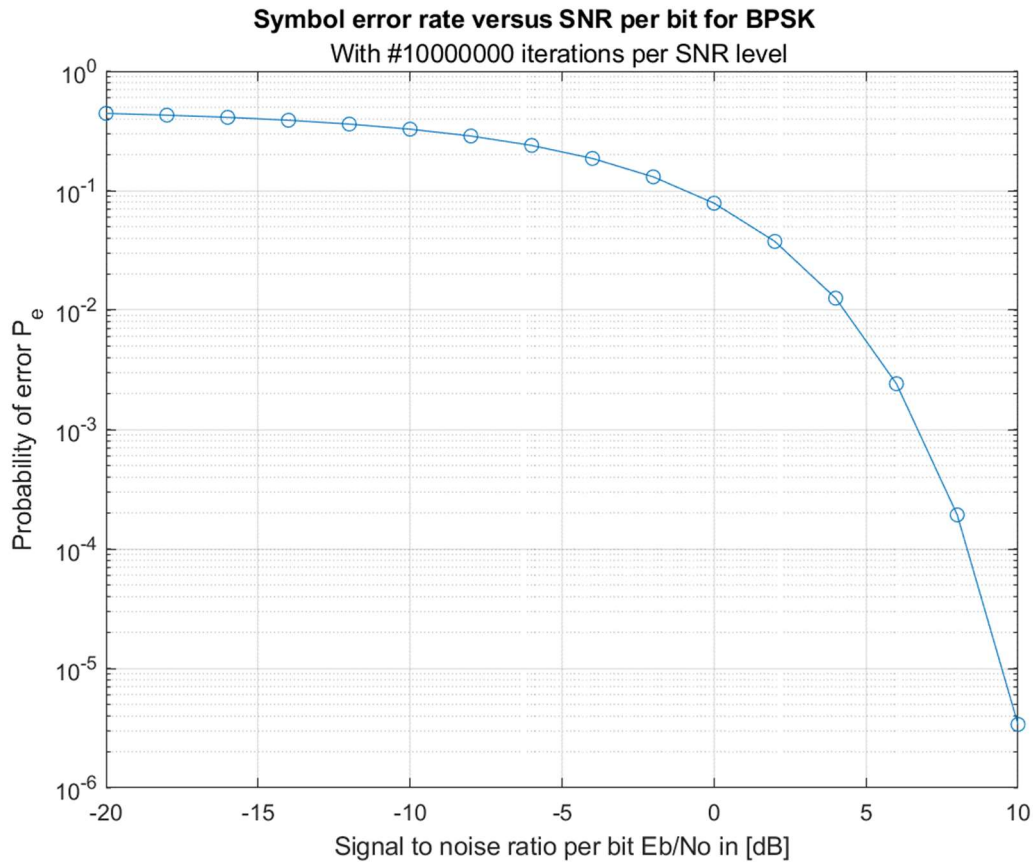


Figure 18 Simulated symbol error rate for BPSK as function of energy per bit.

3.8. Conclusions and State-of-the-art

In the literature research no cooperative hitchhiking radar is found and therefore an investigation in this new radar type is in place. There are no waveforms found which can communicate over an object-of-interest or without line-of-sight which do not degrade the primary radar performance. In this thesis the novelty lies in a novel joint radar waveform design which does not degrade the primary radar. The primary radar can operate without degradation and still communicate to the receive radar. Another novelty is the possibility to communicate over an object-of-interest in low SNR scenarios. By using coherent integration gain it is possible to use pulsed radar to communicate in a low signal-to-noise scenario. The principles of LFM-MSK and PC FMCW which are found in literature are described and their BPSK coding and waveforms are presented. The bit rate of BPSK is high. The downside of BPSK is the needed energy per bit to achieve a low symbol error rate. The next chapter shall introduce the new time delay between radar bursts waveform.

4 Time delay between radar bursts

4.1. Introduction

In this chapter the mathematical framework is presented of a novel technique to communicate with radar waveforms: time delay between radar bursts (TDBRB) communication. Further a feasibility analysis of TDBRB is performed and the theoretical maximal bit rate is derived and calculated. This technique will be compared to phased attached radar communication (PARC) and LFM-MSK pulsed radar which are described in the previous chapter.

4.2. Time delay between radar bursts

The way a radar operates is used as a starting point. To communicate in a robust way, a pulsed radar with additional time delay between bursts is proposed where coherent integration can be used. This technique makes use of an inserted time delay between two (or more bursts). This principle is shown in Figure 19 which is an extended version of Figure 1. This technique shall be referred to as TDBRB in this thesis.

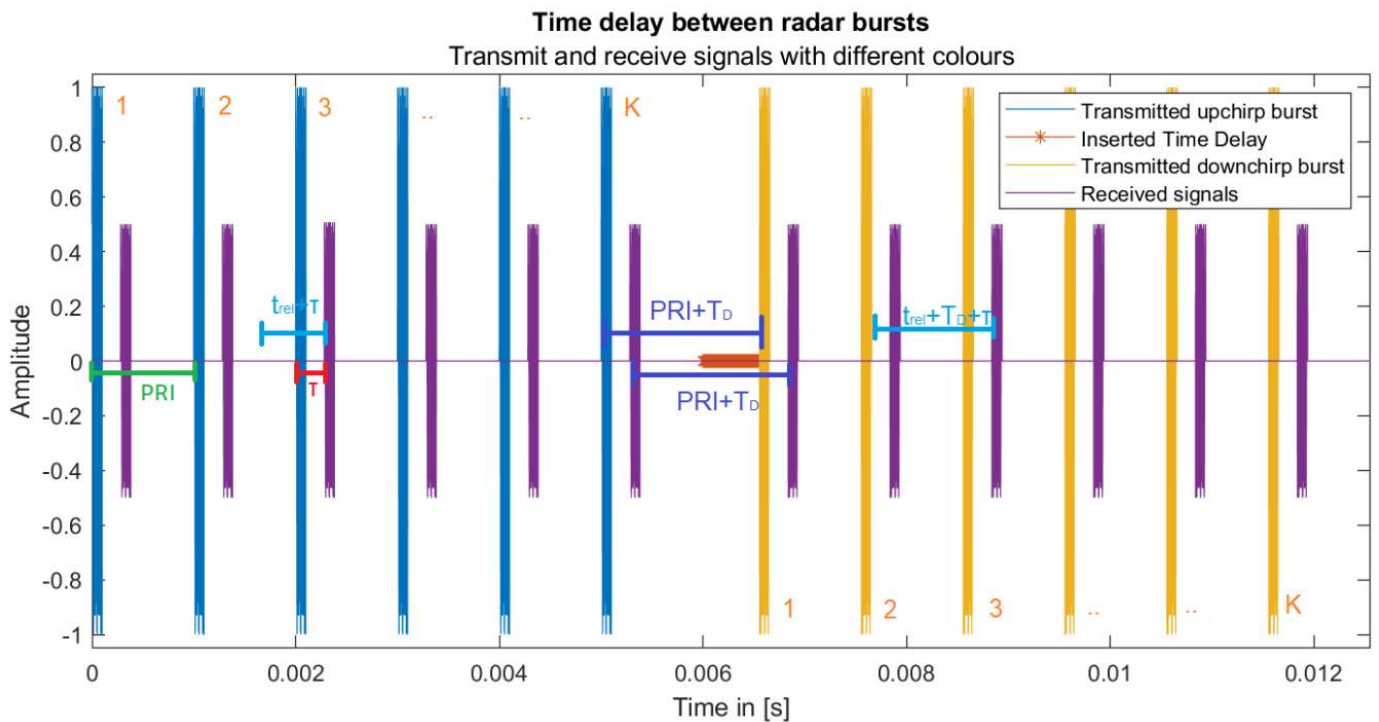


Figure 19 Principle of time delay between radar bursts with variables used in the equations.

TDBRB uses an inserted time delay which corresponds to a communication symbol. The inserted time delay is limited by 0 and the PRI. The receive radar uses a relative time. With this relative time the receive radar is able to correlate the response of the upchirp burst with the response of the downchirp burst. The inserted time delay is the output of this cross-correlation. The original time delay τ (in Figure 1) can not be recovered at the receive radar, only the inserted time delay. The number of communication symbols depends on the number of range cells as defined in (19). The maximum number of communication symbols N_s is equal to the maximum number of range cells.

In the block scheme of the time delay radar system is shown. It is similar as the block scheme of Figure 5 although there are some differences. The main differences are as follows. First, another LO is placed at the receive side. This LO must be synchronized for the down converting to work properly. Another difference is the inserted time delay at the pulse modulator of the primary radar. The last difference is besides the normal signal processing at the receive radar, the additional extraction of the time delay between the bursts.

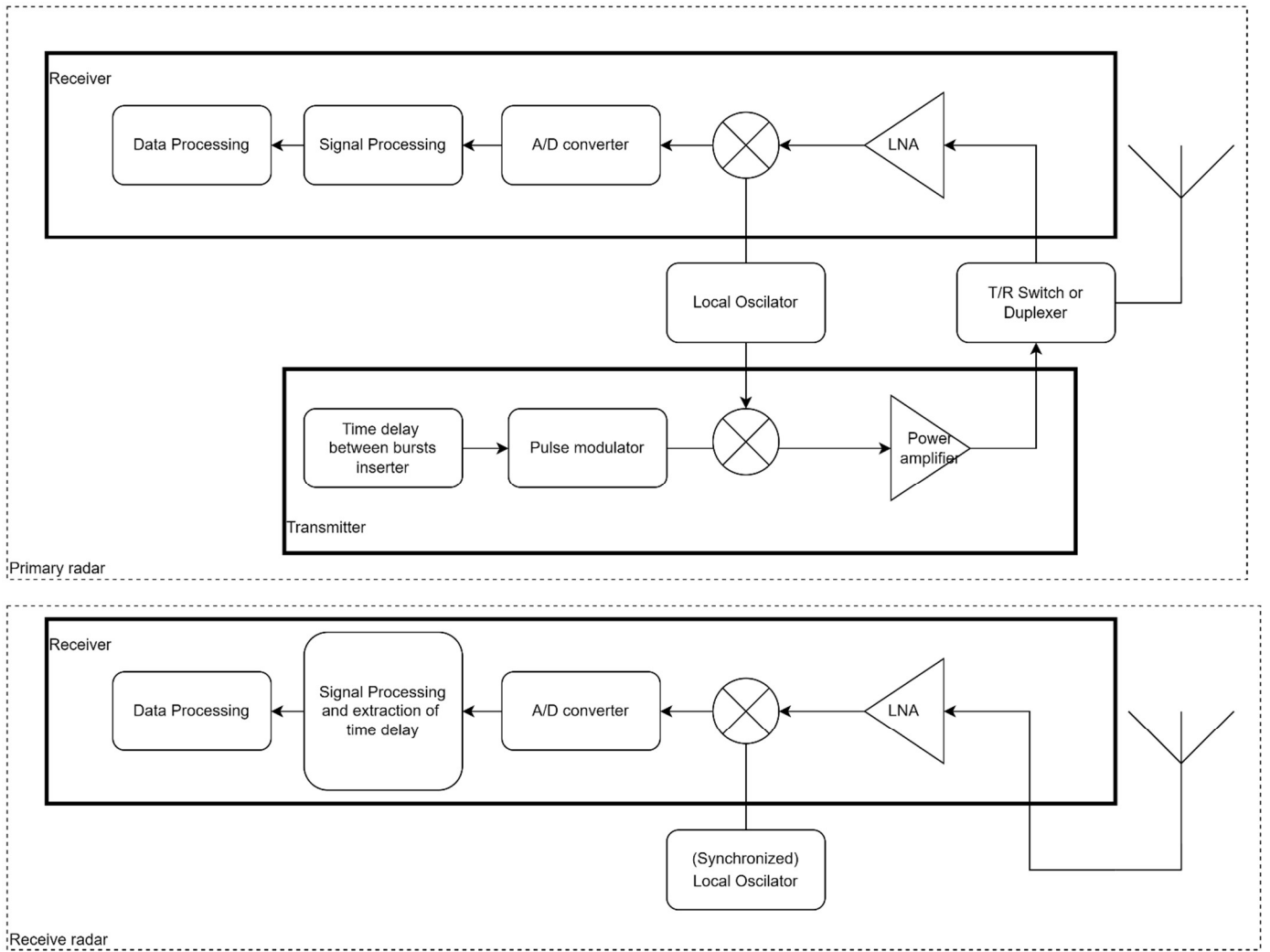


Figure 20 Block scheme of time delay radar system with primary radar and receive radar.

In this section the main steps for estimating the time delay at the receiver are described. Those main steps are stated below. In this case a pulsed Doppler radar is used with a linear frequency modulated signal.

1. Detect 2 intermitted bursts with matched filter.
2. Determine angular information angle of arrival (AoA)
3. Determine arrival time of first burst.
4. Determine arrival time of second burst.
5. Estimate the time difference between them.
6. Use AoA information and the estimated times to build up a TX radar picture.

In this experimental system setup, a matched filter for only one radar pulse is assumed and the pulse repetition interval T_{pri} is fixed. To detect the two intermitted bursts two sampling intervals are introduced. The first interval is during the PRI or the fast time. The second interval is between every PRI which correspond to the slow time. The AoA information must be processed for every possible angle. This processing will result in a high processing capacity. In the simplified case two bursts are detected for a certain AoA.

TDBRB works with a time delay T_D between an upchirp burst as defined in (14) and a downchirp burs. In the simplest form the two bursts consist of the same number of pulses K . The LFM upchirp is modelled in (10) similar the LFM downchirp pulse can be expressed as follows:

$$s_D(t) = e^{j2\pi B_{LFM}t} e^{-j\pi\gamma t^2} \quad (40)$$

In the latter equation a correction for the carrier frequency of $e^{j2\pi B_{LFM}t}$ should be added to have the upchirp and downchirp in the same frequency range. The pulse defined in (9) multiplied with $s_D(t)$ lead to:

$$s_{PD}(t) = e^{j2\pi B_{LFM}t} e^{-j\pi\gamma t^2} \cdot s_{pulse}(t) \quad (41)$$

Similar as for the upchirp before, the signal for the downchirp burst can be constructed. Considering that the upchirp burst is followed by a downchirp burst with the same number of pulses.

$$s_{BD}(t) = \sum_{n=K}^{2K-1} s_{PD}(t - n \cdot T_{PRI}) \quad (42)$$

With the use of (14), this will lead to the two successive bursts where a time delay is put between them:

$$s_{TdBUd}(t) = s_{BU}(t) + s_{BD}(t - T_D) \quad (43)$$

The information what is transferred with the time delayed signal between bursts can be designed depending on the different varieties of the proposed applications. The time delay which is measured by the primary radar which corresponds to the distance of the primary radar to the object-of-interest is an option. In (43) the last pulse of burst 1 is separated from the first pulse of burst 2 by one PRI and the inserted. In this case the primary radar can do its matched-filtering for the whole burst 1 before the new burst is transmitted. The next step is to modulate this signal on a carrier frequency f_c :

$$s_{TdLFM}(t) = e^{j2\pi f_c t} \cdot s_{TdBUd}(t) \quad (44)$$

To create some insights in the signal components all the previous signals are shown together in the same expression as (44):

$$s_{TdLFM}(t) = \sum_{k=0}^{K-1} A \cdot e^{j(2\pi f_c(t-k \cdot T_{PRI}) + \pi\gamma(t-k \cdot T_{PRI})^2)} \cdot (u(t - k \cdot T_{PRI}) - u(t - k \cdot T_{PRI} - T_p)) + \sum_{n=K}^{2K-1} A \cdot e^{j(2\pi(f_c + B_{LFM})(t-n \cdot T_{PRI} - T_D) - \pi\gamma(t-n \cdot T_{PRI} - T_D)^2)} \cdot (u(t - n \cdot T_{PRI} - T_D) - u(t - n \cdot T_{PRI} - T_p - T_D)) \quad (45)$$

At this point the transmit waveform is described. In the following section a more complex waveform is described.

4.3. Sophisticated waveforms

In (45) a waveform with two successive bursts with similar length K and the same PRF is described. The waveform can be made more complex with different PRFs and different number of pulses in the successive bursts. This is described in Richards [2-03] as a staggered waveform. In this case the pulse duration and carrier frequency are kept the same although they can be varied too. To create the highest data rate the signals with the smallest PRI (equal to high PRF) must be placed in the front of the waveform. That has to do to the fact that the first burst creates the starting point as relative time to determine the inserted time delay. However, this only works as the complete waveform is recovered at the receive radar. In case not the whole waveform is recovered ambiguities can occur when the inserted time delay between two successive bursts is limited to the smallest PRI of those. The maximum number of bits is limited by the PRI of the successive burst.

With different number of pulses (K_1, K_2, K_3) and PRIs ($T_{PRI1}, T_{PRI2}, T_{PRI3}$) a sophisticated waveform could be:

$$\begin{aligned}
s_{TdSWLFM}(t) = & \sum_{k_1=0}^{K_1-1} A \cdot e^{j(2\pi f_c(t-k_1 \cdot T_{PRI1}) + \pi\gamma(t-k_1 \cdot T_{PRI1})^2)} \cdot (u(t-k_1 \cdot T_{PRI1}) - u(t-k_1 \cdot T_{PRI1} - T_p)) \\
& + \sum_{\substack{k_2=K_1 \\ K_1+K_2+K_3-1}}^{K_1+K_2-1} A \cdot e^{j(2\pi(f_c+B_{LFM})(t-k_2 \cdot T_{PRI2}-T_{D1}) - \pi\gamma(t-k_2 \cdot T_{PRI2}-T_{D1})^2)} \cdot (u(t-k_2 \cdot T_{PRI2}-T_{D1}) - u(t-k_2 \cdot T_{PRI2}-T_p-T_{D1})) \\
& + \sum_{k_3=K_2}^{K_1+K_2+K_3-1} A \cdot e^{j(2\pi f_c(t-k_3 \cdot T_{PRI3}-T_{D2}) + \pi\gamma(t-k_3 \cdot T_{PRI3}-T_{D2})^2)} \cdot (u(t-k_3 \cdot T_{PRI3}-T_{D1}-T_{D2}) - u(t-k_3 \cdot T_{PRI3}-T_p-T_{D1}-T_{D2}))
\end{aligned} \tag{46}$$

As mentioned before to avoid ambiguities the following restrictions holds for the inserted time delay: $T_{PRI1} \geq T_{D1} \leq T_{PRI2}$ and $T_{PRI2} \geq T_{D2} \leq T_{PRI3}$. In Figure 21 an example of the sophisticated waveform of (46) is shown. The maximal inserted time delay between PRI2 and PRI3 is smaller as between PRI1 and PRI2 because PRI2 and PRI3 are smaller. In that case the maximal number of symbols is smaller, and the bit rate is lower.

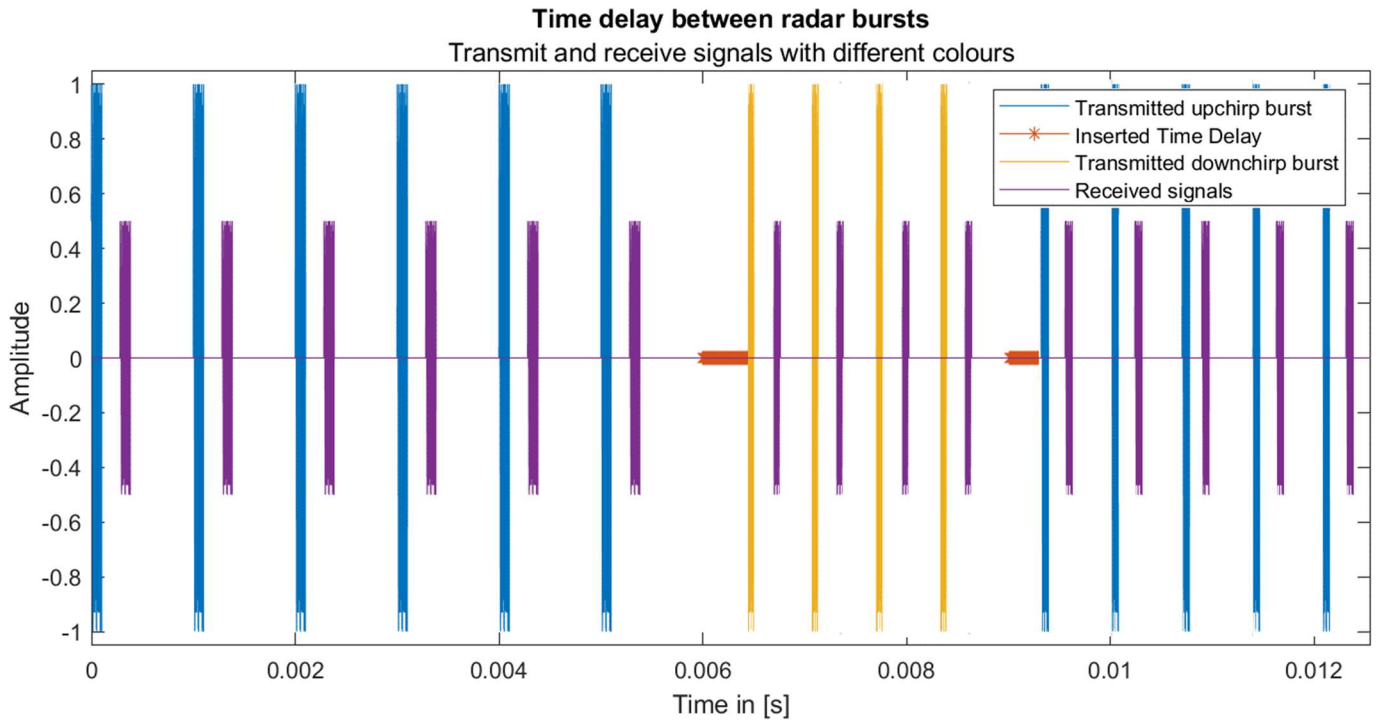


Figure 21 Sophisticated waveform with $K_1 = 6, K_2 = 4$ and $K_3 = 5$, different values for the PRI and two different inserted time delays.

Another sophisticated waveform which consists of two successive bursts with the same PRI looks as follows:

$$\begin{aligned}
s_{TdSWLFM2}(t) = & \sum_{k_1=0}^{K_1-1} A \cdot e^{j(2\pi f_c(t-k_1 \cdot T_{PRI1}) + \pi\gamma(t-k_1 \cdot T_{PRI1})^2)} \cdot (u(t-k_1 \cdot T_{PRI1}) - u(t-k_1 \cdot T_{PRI1} - T_p)) \\
& + \sum_{\substack{k_2=K_1 \\ K_1+K_2+K_3-1}}^{K_1+K_2-1} A \cdot e^{j(2\pi(f_c+B_{LFM})(t-k_2 \cdot T_{PRI1}-T_{D1}) - \pi\gamma(t-k_2 \cdot T_{PRI1}-T_{D1})^2)} \cdot (u(t-k_2 \cdot T_{PRI1}-T_{D1}) - u(t-k_2 \cdot T_{PRI1}-T_p-T_{D1})) \\
& + \sum_{\substack{k_3=K_2 \\ K_1+K_2+K_3+K_4-1}}^{K_1+K_2+K_3-1} A \cdot e^{j(2\pi f_c(t-k_3 \cdot T_{PRI2}-T_{D1}-T_{D2}) + \pi\gamma(t-k_3 \cdot T_{PRI2}-T_{D1}-T_{D2})^2)} \\
& \cdot (u(t-k_3 \cdot T_{PRI2}-T_{D1}-T_{D2}) - u(t-k_3 \cdot T_{PRI2}-T_p-T_{D1}-T_{D2})) \\
& + \sum_{k_4=K_3}^{K_1+K_2+K_3+K_4-1} A \cdot e^{j(2\pi(f_c+B_{LFM})(t-k_4 \cdot T_{PRI2}-T_{D1}-T_{D2}-T_{D3}) - \pi\gamma(t-k_4 \cdot T_{PRI2}-T_{D1}-T_{D2}-T_{D3})^2)} \\
& \cdot (u(t-k_4 \cdot T_{PRI2}-T_{D1}-T_{D2}-T_{D3}) - u(t-k_4 \cdot T_{PRI2}-T_p-T_{D1}-T_{D2}-T_{D3}))
\end{aligned} \tag{47}$$

In that case the first time delay can be as large as the PRI1 $T_{PRI1} \geq T_{D1}$. For the second inserted time delay holds: $T_{PRI1} \geq T_{D2} \leq T_{PRI}$ and successively $T_{PRI2} \geq T_{D2}$.

Another sophisticated waveform contains one prefix burst. This is the first upchirp burst followed by one similar PRI downchirp burst. After this burst every burst has a lower PRI in that way every inserted i^{th} time delay is maximal as large as the i^{th} PRI. This looks as follows:

$$\begin{aligned}
S_{TdsWLFM3}(t) = & \sum_{k_1=0}^{K_1-1} A \cdot e^{j(2\pi f_c(t-k_1 \cdot T_{PRI1}) + \pi (t-k_1 \cdot T_{PRI1})^2)} \cdot (u(t - k_1 \cdot T_{PRI1}) - u(t - k_1 \cdot T_{PRI1} - T_p)) \\
& + \sum_{\substack{k_2=K_1 \\ K_1+K_2-1}}^{K_1+K_2-1} A \cdot e^{j(2\pi(f_c+B_{LFM})(t-k_2 \cdot T_{PRI1}-T_{D1}) - \pi (t-k_2 \cdot T_{PRI1}-T_{D1})^2)} \cdot (u(t - k_2 \cdot T_{PRI1} - T_{D1}) - u(t - k_2 \cdot T_{PRI1} - T_p - T_{D1})) \\
& + \sum_{\substack{k_3=K_2 \\ K_1+K_2+K_3-1}}^{K_1+K_2+K_3-1} A \cdot e^{j(2\pi f_c(t-k_3 \cdot T_{PRI2}-T_{D1}-T_{D2}) + \pi \gamma (t-k_3 \cdot T_{PRI2}-T_{D1}-T_{D2})^2)} \\
& \cdot (u(t - k_3 \cdot T_{PRI2} - T_{D1} - T_{D2}) - u(t - k_3 \cdot T_{PRI2} - T_p - T_{D1} - T_{D2})) \\
& + \sum_{\substack{k_4=K_3 \\ K_1+K_2+K_3+K_4-1}}^{K_1+K_2+K_3+K_4-1} A \cdot e^{j(2\pi(f_c+B_{LFM})(t-k_4 \cdot T_{PRI3}-T_{D1}-T_{D2}-T_{D3}) - \pi (t-k_4 \cdot T_{PRI3}-T_{D1}-T_{D2}-T_{D3})^2)} \\
& \cdot (u(t - k_4 \cdot T_{PRI3} - T_{D1} - T_{D2} - T_{D3}) - u(t - k_4 \cdot T_{PRI3} - T_p - T_{D1} - T_{D2} - T_{D3}))
\end{aligned} \tag{48}$$

And as mentioned before $T_{PRIi} \geq T_{Di}$ if $T_{PRIi} \geq T_{PRI(i+1)}$.

It is possible to coherently integrate over a longer period in a configuration where the primary radar uses two different bursts of equal length. In that case the signal can be made periodic for the upchirp burst. This will have a positive effect on the coherent integration of the receive radar and the information is doubled. The primary radar can use its coherent integration operation by discarding the inserted time delays. The upchirp becomes periodical when, after the upchirp downchirp combination, an extra time delay with the duration $T_{PRI} - T_D$ is added. If the signal processing is also performed when first a downchirp arrives followed by an upchirp the same information has been transmitted only mirrored. This doubling will have a higher reliability although when the downchirp is not measured correctly both time delays (T_D and $T_{PRI} - T_D$) will be incorrect. This waveform is stated in (49):

$$\begin{aligned}
S_{TdLFM}(t) = & \sum_{k=0}^{K-1} A \cdot e^{j(2\pi f_c(t-k \cdot T_{PRI}) + \pi \gamma (t-k \cdot T_{PRI})^2)} \cdot (u(t - k \cdot T_{PRI}) - u(t - k \cdot T_{PRI} - T_p)) \\
& + \sum_{\substack{n=K \\ 2K-1}}^{2K-1} A \cdot e^{j(2\pi(f_c+B_{LFM})(t-n \cdot T_{PRI}-T_{D1}) - \pi \gamma (t-n \cdot T_{PRI}-T_{D1})^2)} \cdot (u(t - n \cdot T_{PRI} - T_{D1}) - u(t - n \cdot T_{PRI} - T_p - T_{D1})) \\
& + \sum_{\substack{m=2K+1 \\ 3K}}^{3K} A \cdot e^{j(2\pi f_c(t-m \cdot T_{PRI}) + \pi \gamma (t-m \cdot T_{PRI})^2)} \cdot (u(t - m \cdot T_{PRI}) - u(t - m \cdot T_{PRI} - T_p)) \\
& + \sum_{\substack{p=3K+1 \\ 4K}}^{4K} A \cdot e^{j(2\pi(f_c+B_{LFM})(t-p \cdot T_{PRI}-T_{D2}) - \pi \gamma (t-p \cdot T_{PRI}-T_{D2})^2)} \cdot (u(t - p \cdot T_{PRI} - T_{D2}) - u(t - p \cdot T_{PRI} - T_p - T_{D2}))
\end{aligned} \tag{49}$$

The periodic waveform is created because from the second to the third row in (49) the time delay will be $T_{PRI} - T_{D1} + T_{D1} = T_{PRI}$. Now coherent integration is possible for the upchirp for multiple upchirp bursts. In this equation the third line can also be written with a summation with m from $2K$ to $3K - 1$ and $(m - 1) \cdot T_{PRI}$. And here the inserted time delay from the first downchirp to the second upchirp is $T_{PRI} - T_{D1}$. This waveform is used in the experiment.

4.4. Received signals

The whole signal is received with a delay of τ_p at the primary radar.

$$s_{RP}(t) = S_{TdLFM}(t - \tau_p) \tag{50}$$

The received signal at the primary radar is for the upchirp bursts $s_{RPU}(t)$:

$$s_{RPU}(t) = \sum_{k=0}^{K-1} a \cdot e^{j(2\pi f_c(t-\tau_p-k \cdot T_{PRI})+\pi\gamma(t-\tau_p-k \cdot T_{PRI})^2)} \cdot (u(t-\tau_p-k \cdot T_{PRI}) - u(t-\tau_p-k \cdot T_{PRI}-T_p)) \quad (51)$$

Where a is related to the attenuation and RCS properties of the object-of-interest. The received signal at the primary radar is for the downchirp bursts where τ_p is assumed to be equal for the two sequential bursts:

$$s_{RPD}(t) = \sum_{k=0}^{K-1} a \cdot e^{j(2\pi(f_c+B_{LFM})(t-\tau_p-k \cdot T_{PRI})-\pi\gamma(t-\tau_p-k \cdot T_{PRI})^2)} \cdot (u(t-\tau_p-k \cdot T_{PRI}) - u(t-\tau_p-k \cdot T_{PRI}-T_p)) \quad (52)$$

As stated before, it is impossible to determine the distances R_0 and R_1 with (16) at the receive side without the knowledge of the exact moment when the burst is transmitted. However, it is possible to determine the transmitted time delay when two sequential bursts are received with the knowledge of the PRI. Therefore, a relative time t_{rel} is introduced which samples pulses on the interval $\{0, T_{PRI}\}$. The exact time t is transformed to $t_{rel} = t - \Delta t$. Here an unknown extra time delay Δt is introduced. The time delay at the receive radar is in that way relatively measured. For the radial velocities a similar relative velocity must be defined because the total bistatic velocity vector contains two components: $v_{bi} = (v_{rop} + v_{ror})/2$. With unknown arrival times, the bistatic velocity will be measured in relative time. However, this velocity is the same as the bistatic velocity therefore $v_{bi,rel} = v_{bi}$. The received signal at the receive radar will have the following form:

$$s_{RR}(t) = s_{TdLFM}(t_{rel} - \tau_r) \quad (53)$$

In the complete form it can be written as:

$$s_{RR}(t) = \sum_{k=0}^{K-1} a \cdot e^{j(2\pi f_c(t_{rel}-\tau_r-k \cdot T_{PRI})+\pi\gamma(t_{rel}-\tau_r-k \cdot T_{PRI})^2)} \cdot (u(t_{rel}-\tau_r-k \cdot T_{PRI}) - u(t_{rel}-\tau_r-k \cdot T_{PRI}-T_p)) + \sum_{n=K}^{2K-1} a \cdot e^{j(2\pi(f_c+B_{LFM})(t_{rel}-\tau_r-n \cdot T_{PRI})-\pi\gamma(t_{rel}-\tau_r-n \cdot T_{PRI})^2)} \cdot (u(t_{rel}-\tau_r-n \cdot T_{PRI}-T_D) - u(t_{rel}-\tau_r-n \cdot T_{PRI}-T_p-T_D)) \quad (54)$$

At this point the received signal at the receive radar is described. The following subsections contains the signal processing to determine the inserted time delay.

4.5. Signal processing

In Figure 22 the processing steps are shown at one AoA direction from which the signal is received. The first step is the down mixing of the carrier frequency. The next step is the matched filter. One matched filter for the upchirp signal and one for the downchirp signal. The result of the matched filter is stored in a data cube with the results of the matched filter for each slow time period (PRI). After this slow time sampling the results of the matched filter are Doppler processed. The coherent integration will be performed after every new matched-filtered slow time period. After this operation the data are stored. In case two bursts with length K are used the maximum storage is $2K + 1$ times the fast time samples of one PRI. In this storage the two bursts and the inserted time delay are stored. Every iteration both bursts can be detected and if two successive bursts are detected the inserted time delay can be estimated. The computational power for the signal processing of the receive radar is increased compared to the primary radar. The primary radar "knows" in which direction it sends its signals and therefore only has to process signals which are received from that direction. While for the receive radar this operation is performed for all AoA directions.

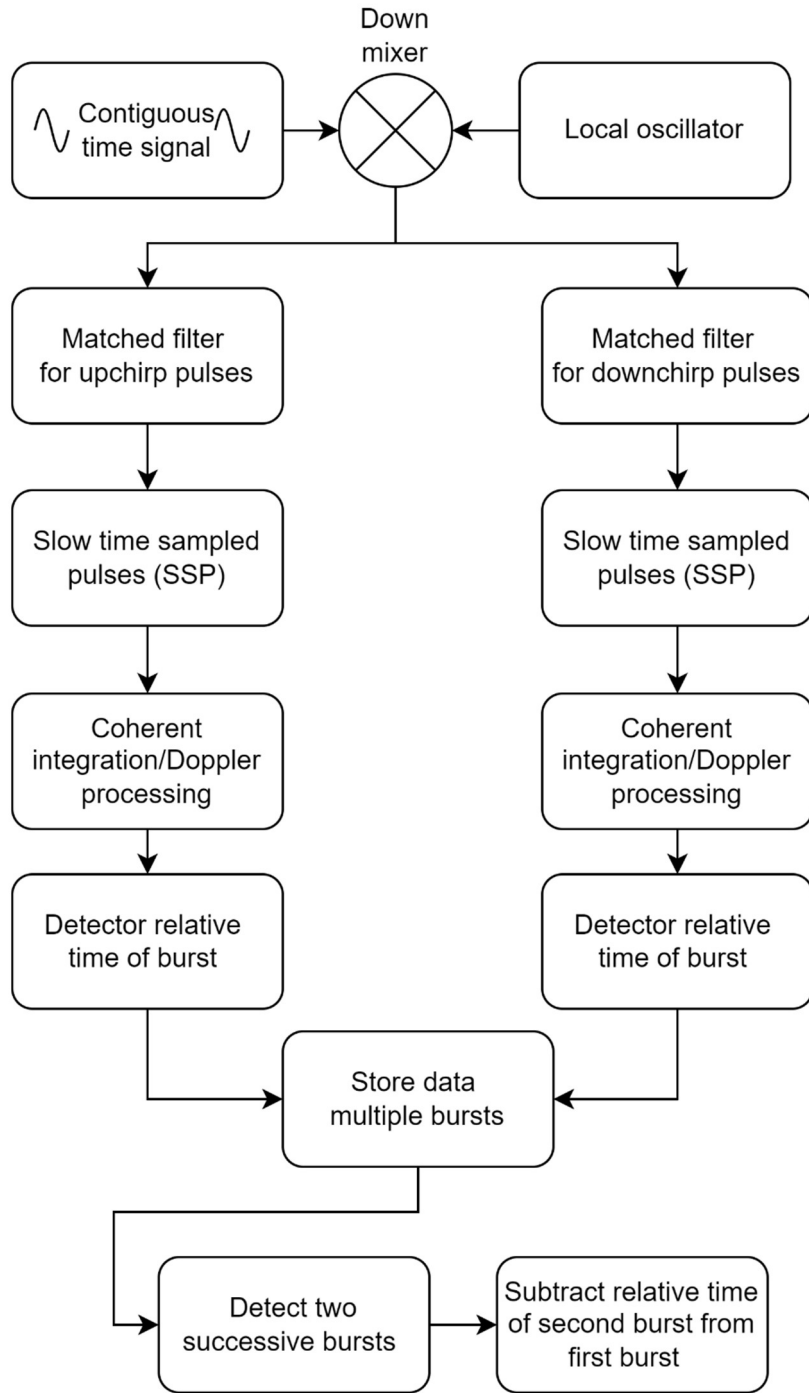


Figure 22 Block scheme of processing steps for a signal at one angle of arrival.

The first step is to convert the high carrier frequency down of the received signal. For the primary radar this will lead to the following equations. The received signal which is down converted at the primary radar is for the upchirp bursts $s_{RPUC}(t)$ using (15):

$$\begin{aligned}
 s_{RPUC}(t) = & \sum_{k=0}^{K-1} a \cdot e^{j\left(2\pi f_c \left(t - \frac{2(R_0 + v_{rop}t)}{c} - k \cdot T_{PRI}\right) + \pi \gamma \left(t - \frac{2(R_0 + v_{rop}t)}{c} - k \cdot T_{PRI}\right)^2\right)} \\
 & \cdot \left(u \left(t - \frac{2(R_0 + v_{rop}t)}{c} - k \cdot T_{PRI} \right) - u \left(t - \frac{2(R_0 + v_{rop}t)}{c} - k \cdot T_{PRI} - T_p \right) \right) \cdot e^{-j2\pi f_c t}
 \end{aligned} \tag{ 55 }$$

Where the received amplitude of the signal a is related to the attenuation and RCS properties of the object-of-interest.

The received signal at the primary radar is for the downchirp bursts:

$$S_{RPDC}(t) = \sum_{k=0}^{K-1} a \cdot e^{j\left(2\pi(f_c + B_{LFM})\left(t - \frac{2(R_0 + v_{rop}t)}{c} - k \cdot T_{PRI}\right) - \pi\gamma\left(t - \frac{2(R_0 + v_{rop}t)}{c} - k \cdot T_{PRI}\right)^2\right)} \cdot \left(u\left(t - \frac{2(R_0 + v_{rop}t)}{c} - k \cdot T_{PRI}\right) - u\left(t - \frac{2(R_0 + v_{rop}t)}{c} - k \cdot T_{PRI} - T_p\right)\right) \cdot e^{-j2\pi f_c t} \quad (56)$$

These equations are more complicated as the signals in (43) and (44). For the primary radar the inserted time delay, T_D is known. And therefore, the original envelopes of the upchirp burst and downchirp burst can be used to process the bursts.

$$S_{RPC}(t) = e^{j2\pi f_c \left(t - \frac{2(R_0 + v_{rop}t)}{c}\right)} \cdot S_{TdBUD}\left(t - \frac{2(R_0 + v_{rop}t)}{c}\right) \cdot e^{-j2\pi f_c t} \quad (57)$$

This can be simplified to the two different bursts:

$$S_{RPUC}(t) = e^{j2\pi f_c \left(t - \frac{2(R_0 + v_{rop}t)}{c}\right)} \cdot S_{BU}\left(t - \frac{2(R_0 + v_{rop}t)}{c}\right) \cdot e^{-j2\pi f_c t} \quad (58)$$

And without the inserted time delay:

$$S_{RPDC}(t) = e^{j2\pi f_c \left(t - \frac{2(R_0 + v_{rop}t)}{c}\right)} \cdot S_{BD}\left(t - \frac{2(R_0 + v_{rop}t)}{c}\right) \cdot e^{-j2\pi f_c t} \quad (59)$$

The two different bursts can now be evaluated with the assumption that the envelope is not influenced by the velocity:

$$\begin{aligned} S_{RPUC}(t) &\approx e^{j2\pi f_c t} \cdot e^{-j\frac{4\pi}{\lambda_c} R_0} \cdot e^{+j2\pi\frac{2v_{rop}t}{\lambda_c}} \cdot S_{BU}\left(t - \frac{2R_0}{c}\right) \cdot e^{-j2\pi f_c t} \\ &= e^{-j\frac{4\pi}{\lambda_c} R_0} \cdot e^{+j2\pi\frac{2v_{rop}t}{\lambda_c}} \cdot S_{BU}\left(t - \frac{2R_0}{c}\right) \end{aligned} \quad (60)$$

And without the inserted time delay:

$$\begin{aligned} S_{RPDC}(t) &\approx e^{j2\pi f_c t} \cdot e^{-j\frac{4\pi}{\lambda_c} R_0} \cdot e^{+j2\pi\frac{2v_{rop}t}{\lambda_c}} \cdot S_{BD}\left(t - \frac{2R_0}{c}\right) \cdot e^{-j2\pi f_c t} \\ &= e^{-j\frac{4\pi}{\lambda_c} R_0} \cdot e^{+j2\pi\frac{2v_{rop}t}{\lambda_c}} \cdot S_{BD}\left(t - \frac{2R_0}{c}\right) \end{aligned} \quad (61)$$

For the signals at the receive radar side similar equations can be calculated:

$$S_{RRUC}(t) \approx e^{-j\frac{2\pi}{\lambda_c}(R_0 + R_1)} \cdot e^{+j2\pi\frac{2v_{bi}t}{\lambda_c}} \cdot S_{BU}\left(t - \frac{R_0 + R_1}{c}\right) \quad (62)$$

And without the inserted time delay:

$$s_{RRDC}(t) \approx e^{-j\frac{2\pi}{\lambda_c}(R_0+R_1)} \cdot e^{+j2\pi\frac{2v_{bi}t}{\lambda_c}} \cdot s_{BD}\left(t - \frac{R_0 + R_1}{c}\right) \quad (63)$$

Where the first terms in the equations above are constants within a burst. The two equations above are correct when the time of transmission is known at the receiver. In the case where the time is relative it looks as follows:

$$s_{RRUC}(t_{rel}) \approx e^{-j\frac{2\pi}{\lambda_c}(R_0+R_1)} \cdot e^{+j2\pi\frac{2v_{bi}t_{rel}}{\lambda_c}} \cdot s_{BU}\left(t_{rel} - \frac{R_0 + R_1}{c}\right) \quad (64)$$

And for the downchirp without the inserted time delay:

$$s_{RRDC}(t) \approx e^{-j\frac{2\pi}{\lambda_c}(R_0+R_1)} \cdot e^{+j2\pi\frac{2v_{bi}t_{rel}}{\lambda_c}} \cdot s_{BD}\left(t_{rel} - \frac{R_0 + R_1}{c}\right) \quad (65)$$

As mentioned before the LOs are assumed to be synchronized. In Appendix A the calculations are shown when the LOs are not synchronized and how it affects the bistatic velocity. The matched filter which is used will consist of one pulse. Where afterwards coherent integration will be conducted. This integration will be executed in the relative time t_{rel} interval $\{0, T_{PRI}\}$. In that way, a maximum will occur when all the received pulses of a burst are added up. This is done because the exact time of the arrival of pulses is not known. In the ideal case for the first burst, all K pulses are received and added up. This relates to a match at the relative time $\tau_{r,rel}$. When the second burst arrives, there should be a match at another time $\tau_{r,rel} + T_D$. This coherent integration in relative time is performed for every K PRIs which arrives. In that case upchirp as downchirp matched filters can be executed on the coherent integrated signals of exactly one burst length. The first process in the simulation is to determine the inserted time delay when there is no or only one object-of-interest.

4.6. Time delay estimation

In this section the principle of the time delay estimation will be explained. To start with the explanation a definition of the burst length and duration is made. One burst length T_b is the number of pulses (K) in a burst multiplied by the time of one PRI (T_{PRI}).

$$T_b = K \cdot T_{PRI} \quad (66)$$

Continuously the signals are sampled in one period of the PRI. This is stored in a matrix before the integration (adding up) of the number of used pulses is performed. This matrix has a maximal size of $2K + 1$ times the number of range cells (fast time measurements).

In the case there is a reflection of one object-of-interest the whole burst or a part of the burst can be detected. With a detector the burst can be detected and linked to a relative time (related to the range cells or fast time measurement).

$$\begin{aligned} T_{B1} &\sim \tau_{r,rel} \\ T_{B2} &\sim \tau_{r,rel} + T_D \end{aligned}$$

The relative times and n times the PRI can be used to determine the added time delay if another burst is detected maximal twice burst lengths later.

This leads to the following expression:

$$T_D = T_{B2} - T_{B1} - l \cdot T_{PRI} \quad (67)$$

Where T_D is the estimated inserted time delay and l is an integer number of pulses. The maximum value of l is K the total number of pulses in a burst. T_{B1} is the relative time of burst 1 and T_{B2} the relative time of burst 2. When both bursts are completely detected the difference between them is exactly the delay time, plus the total number of pulses in a burst (K) times the PRI. When some pulses are missing, but still there are two bursts detected the inserted time delay can be estimated with a delay between of one T_{PRI} to K times the PRI.

When all the receive signals are sampled in relative time a detector is used to determine if there is a signal or not. This can be performed similar as in the radar which is used as primary radar. Therefore, the optimal detector which is already used for the proposed radar application should be used. The primary radar can off course use this detector which it already uses. For the receive radar the signal which is received is a signal of opportunity. Therefore, it is not known if a detection of an upchirp and downchirp is correct. With the slow time sampling all the received signals are placed in a matrix which has the size of the number of range cells (PRI interval) times the number of received signals. After this operation the detector is implemented to determine if there is a signal or not. In Figure 11 the two different kinds of detectors are shown which are used in the simulation of the TDBRB waveform. The coherent detector can be used for detecting Swerling case 1 and 3 objects-of-interest and determine their Doppler frequency. The noncoherent detector can be used for Swerling case 2 and 4 objects-of-interest.

4.7. Feasibility

A feasibility analysis is performed before the simulation starts. This is according to Kay [4-01] an assessment of the best possible performance. Where one must take in mind that the performance of the simulations is always better as in practice. The main idea is to use a primary radar which can operate under its regular conditions and a receive radar which can built its own radar picture. The degradation of the primary radar is described in the next subsection. Followed by the theoretical maximal bit rate calculations when the algorithm works as designed from a communication perspective.

One of the main constraints of the research questions is to not degrade the primary radar. This is possible when only a time delay after a burst is added. The radar operates with its regular pulses and bursts for its designed purposes. Now it is possible to calculate the degradation in performance because of the added time delay. The degradation in the performance can be calculated as a function of the number of bursts. The signals have the same properties as without a time delay, but it loses only an inserted time. When the inserted time is of random duration with an equal chance of each detectable time slot within 1 PRI the distribution is uniform. With the uniform distribution the expected value of the loss of time $E(T_l)$ is the PRI divided by two.

$$E(T_l) = 0.5 \cdot T_{PRI} \quad (68)$$

Where E_{tl} is expected value of the time loss, T_{PRI} the PRI. The mean time loss ratio TLR is in that case $E(T_l)$ divided by the number of pulses times the PRI:

$$TLR = \frac{K \cdot T_{PRI}}{K \cdot T_{PRI} + E(T_l)} = \frac{2 \cdot K}{(2 \cdot K + 1)} = 1 - \frac{1}{(2 \cdot K + 1)} \quad (69)$$

Where K the total number of pulses in one burst. The maximum absolute time loss is one PRI with (69) this will become:

$$TLR = \frac{K \cdot T_{PRI}}{K \cdot T_{PRI} + E(T_l)} = \frac{K}{(K + 1)} = 1 - \frac{1}{(K + 1)} \quad (70)$$

The mean time loss ratio can be converted to a loss of time related to the number of pulses in a burst. For the maximum value this is: $1/(K + 1)$. This loss of time has an influence on the Doppler resolution as stated in (22). When the primary radar operates as scanning radar the mean time loss will not influence objects-of-interest with high signal-to-noise ratios. However, the update rate will decrease with the TLR . The degradation can be limited if an adjustable communication mode is used for the suggested application of the radar. When communications are not necessary it can be turned off. Or the communications are only performed at a fixed time schedule for instance when the radar scans or when an object-of-interest is detected.

The only degradation for the primary radar is a lower duty cycle. This loss of duty cycle results in a lower SNR which increases the chance of a missed detection. The mean transmit power depends on the duty cycle and the peak power. The mean transmit power degrades with the *TLR* when an additional time loss is introduced. This is shown in Figure 23.

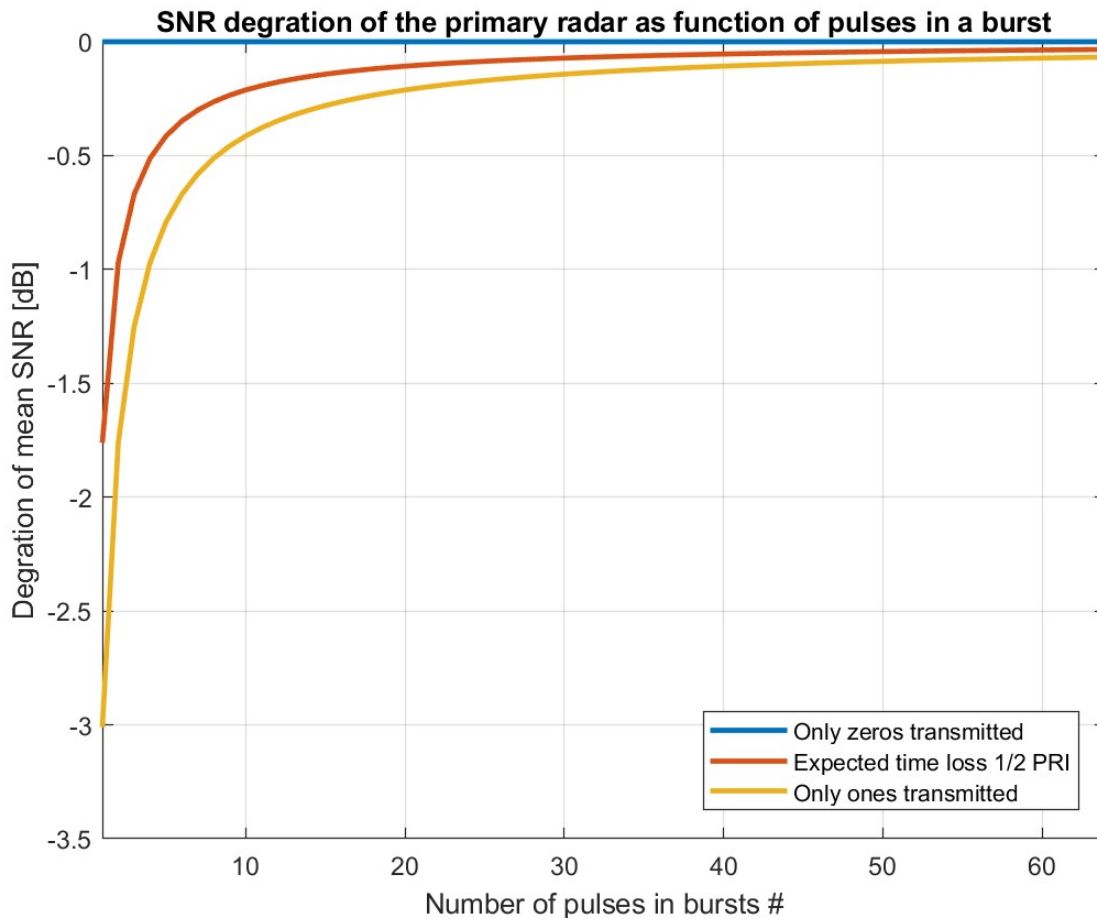


Figure 23 Degradation of the primary radar.

When the PRI is translated range cells which corresponds to symbols who represents for instance 10 bits. The inserted time delay is 0 when 10 zeros are transmitted. In that case there is no degradation. The expected mean loss degradation as calculated with the mean time loss in (69) is the line in the middle. In that case an equal number of ones and zeros are transmitted what results in a time delay of one PRI. The largest degradation is when only ones are transmitted what corresponds to a time delay of exactly one PRI. In Table 4 the time delay per bit sequence is shown for a signal with 10 information bits, 1024 range cells and a pulse repetition frequency of 1 kHz. In this table the range cell starts at time 0 this will correspond to the start of the pulse repetition interval.

Range cell	Symbol	Bit sequence	Time delay
0	1	000000000	0.0000 μ s
1	2	000000001	0.9766 μ s
2	3	000000010	1.9531 μ s
3	4	000000011	2.9297 μ s
4	5	000000100	3.9063 μ s
...
1019	1020	11111111011	0.9951 ms
1020	1021	11111111100	0.9961 ms
1021	1022	11111111101	0.9971 ms
1022	1023	11111111110	0.9980 ms
1023	1024	11111111111	0.9990 ms

Table 4 Time delay with 10 information bits, 1024 range cells and pulse repetition frequency of 1 kHz.

4.8. Bit rate TDBRB

One way to look at the proposed TDBRB communication is to see it from the communication perspective. The first step is to determine the maximum bit rate for a pulsed radar without pulse compression. The second step is to determine the maximal bit rate with pulse compression (or better range resolution). Those calculations are made for perfect communication conditions and without error correcting codes. The last step is to describe possible error correcting codes.

In communications the bit rate determines the performance of a modulation form. Although the primary radar uses range cells to determine the range of an object-of-interest, the receive radar uses communication symbols. Those symbols correspond to the range cells, they do not represent range (however it could be), only a time delay. The number of range cells in a period of one PRI determines the number of symbols. In case two similar radars are used to communicate, with the time delay signal, the number of range cells can be transformed to the number of communication symbols. This is shown in Figure 24.

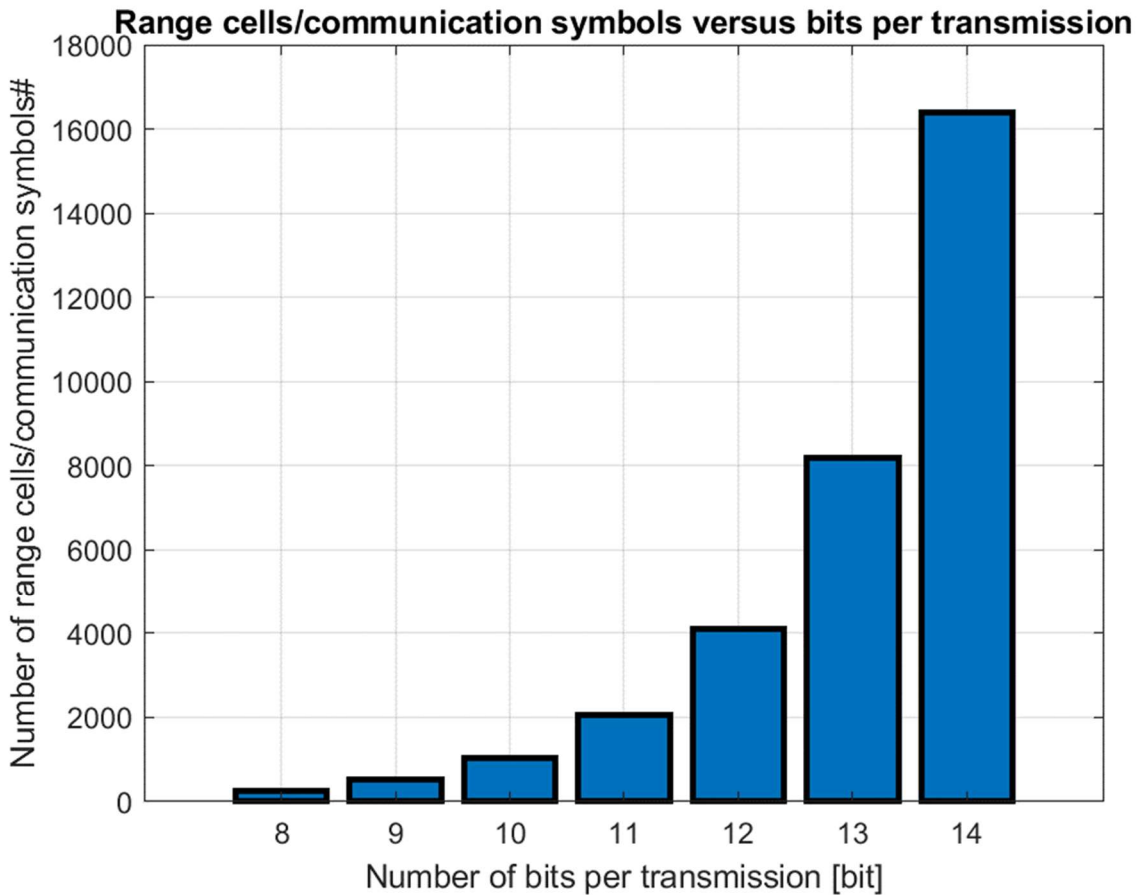


Figure 24 Range cells/communication symbols versus bits per transmission.

In Figure 24 the 256 to 16,384 range cells are shown which corresponds to the number of symbols and the number of bits (8 to 14) which they represent calculated with the following equation:

$$N_{bit} = \log_2(N_{RC}) \tag{71}$$

Where the number of bits N_{bit} is defined by the number of range cells N_{RC} . When the number of range cells is not a power of two this equation must be rounded down. This amount is floored to relate the range cells to bits and for digital communication. However, it is possible to use the range cells which are not used with when the bit rate is floored. This is possible when more data are transferred with several delay times, and the number of range cells is less as an integer power of two. For example, when 700 range cells are available and 11 bits (corresponds to 2048 symbol) must be sent then the data can be split into three sections of 700, 700 and 648 (or 700 where only 648 symbols are used). In that way more data can be transferred. In that

case the communication protocol consists of 4 successive bursts with the three sections as inserted time delays between them.

With (29) and (30) the and the bit rate or baud of TDBRB can be determined. In the TDBRB communication T_s is of a variable length what might indicate that it is an analogue way to communicate. The baud can be used when the number of range cells is not a binary value.

The application can be engineered for only one information transfer per two successive bursts like the waveform in (45). In that case there are only two bursts with one time delay after the first burst. If that is the case, every transmission only contains one information symbol (the maximum number of range cells). Another way to use this TDBRB communication is with a continuous stream of bursts with after each burst an inserted time delay. This are the sophisticated waveforms as presented in equations (46),(47),(48) and (49). In that case a bit rate per unit of time can be calculated. TDBRB communication can also be engineered with a sequence of different burst lengths if the receive radar “knows” what to expect and can evaluate the received transmissions.

In Figure 25 the number of range cells as function of the PRF is shown when the radar has a pulse duration of 0.1 μ s to 1 μ s without pulse compression. In this case there are 1000 possibilities when a low PRF of 1000 Hz is used with a pulse duration of 1 μ s. And only 10 possibilities in case of a high PRF of 100 kHz with this same pulse duration of 1 μ s. If the message is transmitted in bursts of 10 pulses, it is possible to calculate a bit rate. In this calculation we use 1024 possibilities (a low PRF of 976.6 Hz) of different range cells which corresponds to 10 bits. The bit rate is with only one pulse is 9766 bit/s. When this is 10 times retransmitted (10 pulses in a burst) the bit rate becomes 976 Bits/s. The inserted time delay introduces an extra PRI therefore the maximum bit rate will be divided by 11 ($K + 1$) instead of 10 (K) in the example. This will result in 887 bit/s. The special feature of this kind of communication is that there is no specific time frame as in traditional communication systems. Therefore, the length of the transmission will be smaller when only zeros are transmitted and longer when all ones are transmitted (exactly one PRI). In the worst case, the whole transmission consists of ones. In that case the result is 887 bit/s. However, when zeros and ones occur with equal chances the transmissions are $PRI/2$ times longer. In that case the bit rate of one pulse is divided by 10.5 what results in a bit rate of 930 bit/s. These calculations show that the pulse duration and PRF corresponds directly to the bitrate.

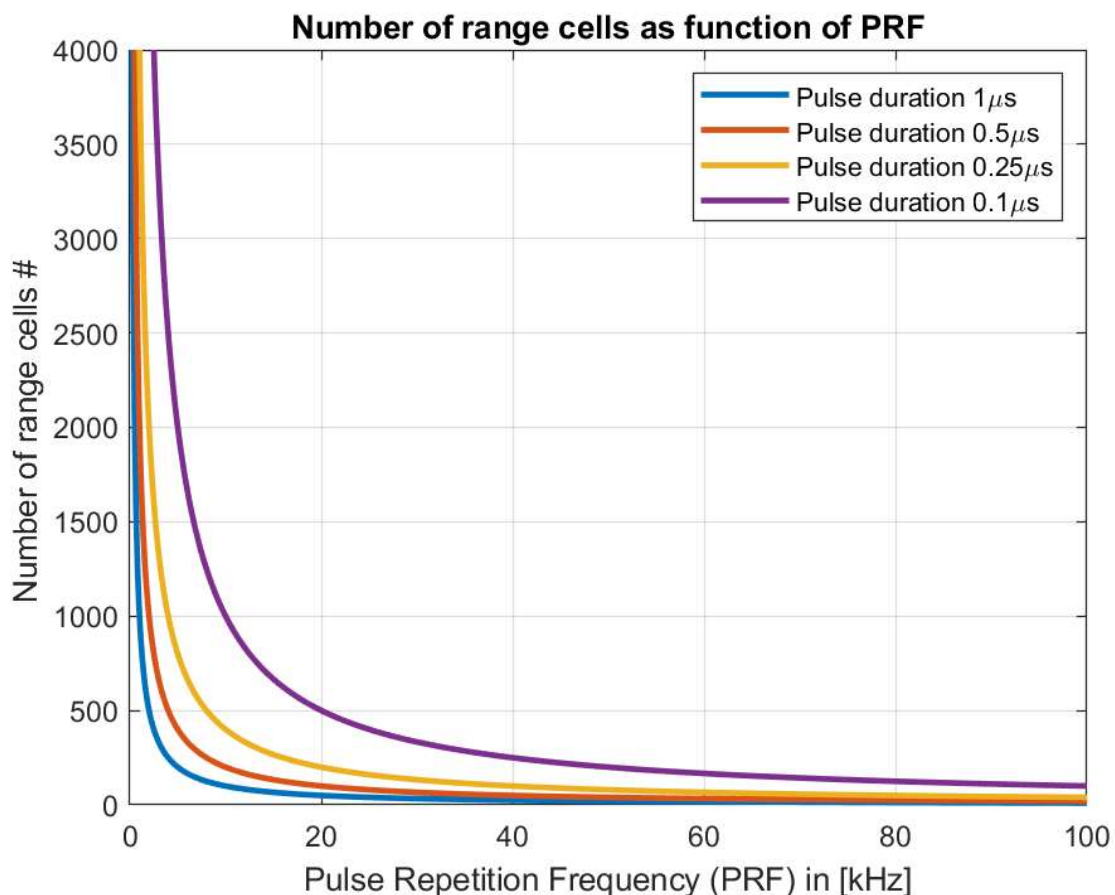


Figure 25 PRF versus number of range cells for different pulse durations.

The time of one symbol T_S is related to the number of pulses in a burst and the PRI and showed in the following equation:

$$T_S = (K + T_{S,RB}) \cdot T_{PRI} \quad (72)$$

The more pulses in a burst are used, the longer the symbol time T_S in [s]. Further there is a variable real symbol time $T_{S,RB}$ in [s] which is related to the range cell where the burst is detected. And T_{PRI} is the duration of one PRI in [s]. This is placed on the interval $\{0, PRI\}$. Where range cell 0 stands for all zeros and the maximum range cell stand for alle ones. In an equation this is represented as the maximum bitrate (with alle zeros):

$$R_{B,max} = \frac{N_{bit} \cdot PRF}{K} \quad (73)$$

The minimum bit rate which is the most conservative calculation (worst case with all ones):

$$R_{B,min} = \frac{N_{bit} \cdot PRF}{(K + 1)} \quad (74)$$

And for the case where zeros and ones occur in equal chances the mean bit rate \overline{R}_B :

$$\overline{R}_B = \frac{N_{bit} \cdot PRF}{(K + \frac{1}{2})} \quad (75)$$

With the number of range cells equation cells stated in (19) and (71) the total mean bit rate becomes:

$$\overline{R}_B = \frac{\log_2(T_{PRI} \cdot B_{LFM}) \cdot PRF}{(K + \frac{1}{2})} = \frac{\log_2(T_{PRI} \cdot B_{LFM})}{(K + \frac{1}{2}) \cdot T_{PRI}} \quad (76)$$

In this equation the trade-off between the PRI and PRF is visible. It is of course the same design variable. What is visible in (76) is that by increasing the PRF the bit rate increases however at the same time the bit rate decreases because the number of bits will drop with the ratio $\log_2(T_{PRI})$.

If we take a look at the mean baud following from (29) the maximal mean symbol rate becomes:

$$\overline{D} = \frac{T_{PRI} \cdot B_{LFM}}{(K + \frac{1}{2})T_{PRI}} = \frac{B_{LFM}}{(K + \frac{1}{2})} \quad (77)$$

Which only depends on the bandwidth and the number of pulses in a burst.

In Figure 26 the bit rate is shown as function of the number of pulses in a burst. In the histogram the worst case (transmitting only ones) is used with (74). The pulse duration and range accuracy are set on 1 μ s. The more pulses are used in a burst, the lower the bit rate. To put this low bit rate in perspective: in GSM it is possible with a bit rate of 13.2 kbit/s to make a phone call. In this case it is not possible to perform a phone call with a radar with those settings. The main showstopper here is the PRF of 976.6 Hz. As the number of range cells increases, more symbols can be transmitted, and the bit rate will increase.

Bit rate versus #pulses burst (with PRF 976.6 Hz and 1024 range cells=10bits)

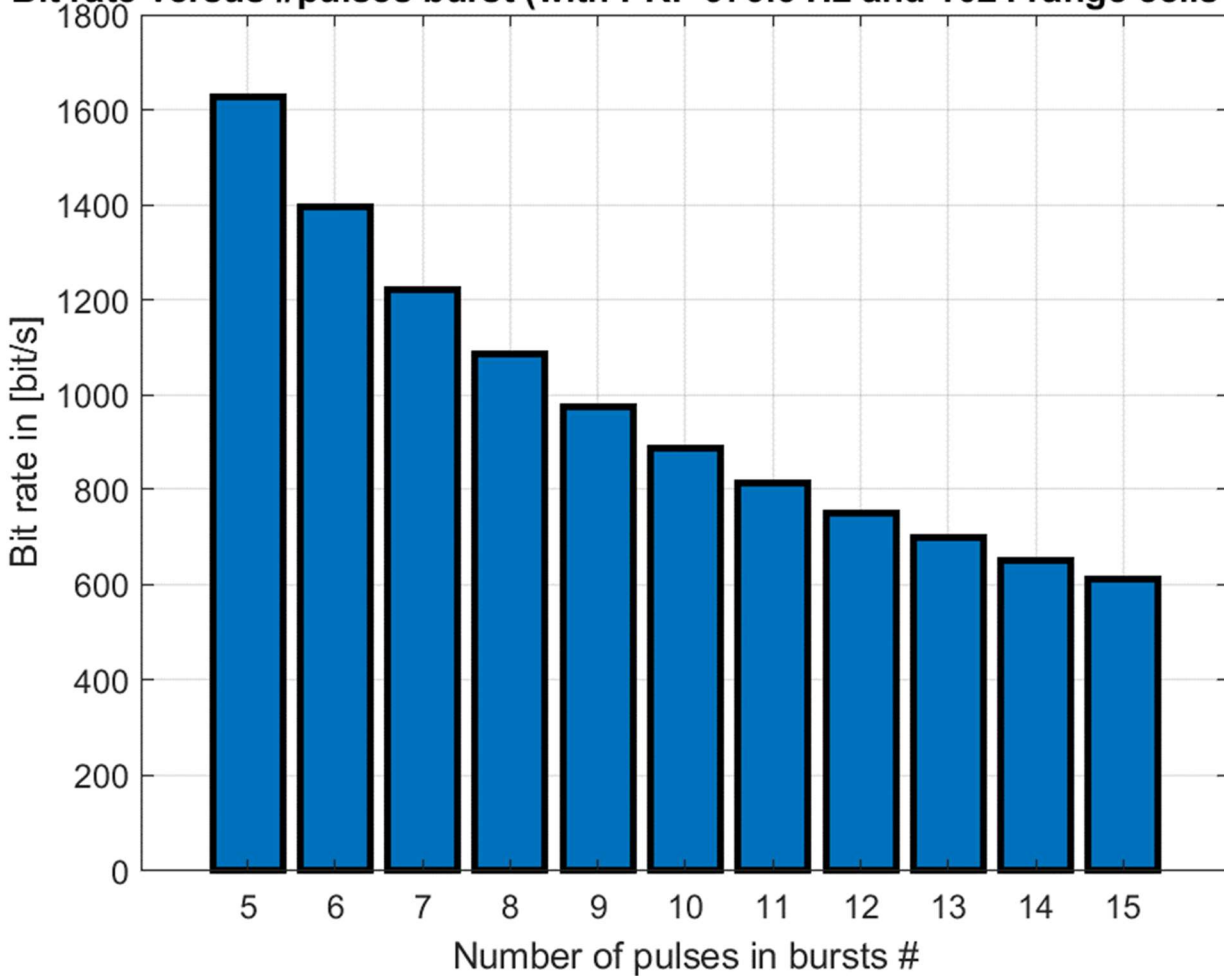


Figure 26 Bit rate as function of number of pulses in a burst with a pulse width of 1 μ s.

The range resolution will increase when pulse compression is used. This is useful in TDBRB communication. With a higher range resolution more communication symbols can be transmitted. The bit rate as function of number of pulses in a burst is shown in Figure 27. In this figure 10 bits per transmission for different pulse repetition frequencies are used. To compare, the dotted line represents the GSM data rate. The high data rates are only possible when the pulse duration (and range resolution) is small or when pulse compression is used. In Figure 28 the bit rate as function of number of range cells is shown for a PRF of 60 kHz versus different number of pulses in a burst.

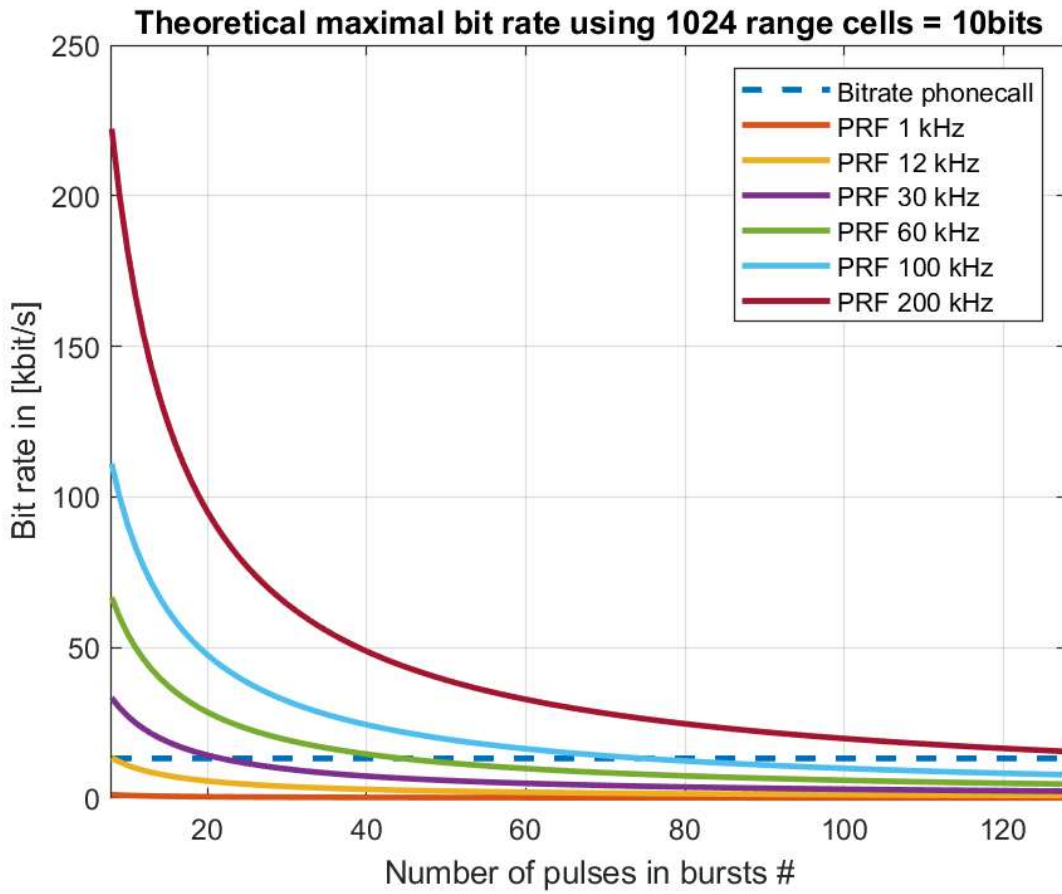


Figure 27 Bit rate as function of PRF, number of pulses in a burst with 1024 range cells or 10 bits per transmission.

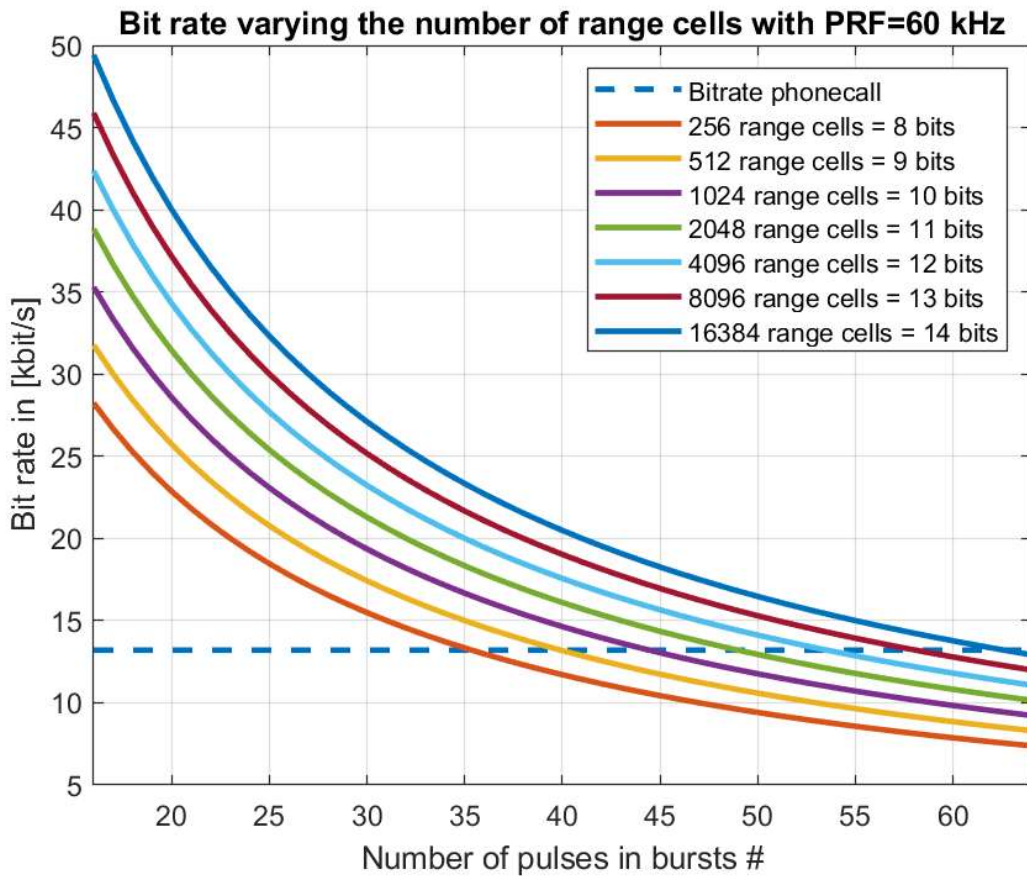


Figure 28 Different bit rates for a PRF of 60 kHz while the number of ranges bins is varied.

4.9. Error correction codes TDBRB

At this point it is clear that it is possible to transmit data with a radar in a radar way (TDBRB). It is feasible to communicate in a simplex way. In the proposed setup the receive radar does not transmit, therefore an automatic repeat request cannot be used. However, in the case where TDBRB communication is used for communication purposes in a duplex way an ARQ could be send. In that case a protocol could be made for both radars to not interfere with each other. However, with simplex TDBRB communication it is possible to use forward error correction.

4.10. Conclusions TDBRB

In this section conclusions of the TDBRB waveform and system setup are given. The TDBRB waveform is derived for an upchirp burst and a successive downchirp burst. It is feasible to use TDBRB communication in a simplex way and the maximal bit rate is determined by PRF, bandwidth and number of pulses in a burst. Two of the main waveforms which are presented in equations will be implemented in the simulations and experiment. For the simulation one TDBRB signal with one time delay as presented in (45) will be used. A data stream which consists of the sophisticated waveform where the information is doubled as presented in (49) will be used for the experiment. The degradation of the primary radar with TDBRB is only a degradation of the time on target. The dependence of the PRF, number of range cells and number of pulses in a burst on the bit or symbol rate has been derived. The duration of the transmission is not fixed because the length of the inserted time delay varies.

5 Simulations

5.1. Introduction

In this chapter the simulations of the novel TDBRB waveform are presented. The general simulation model is shown in Figure 29. This simplified scheme shows the steps which are taken in the simulations. First the primary radar transmits the waveform. This waveform travels through the environment which can be subject to clutter and is possibly scattered on an object-of-interest. The primary radar and receive radar both receive this waveform and perform their signal processing on it. The performance of the waveform depends on the chosen variables like PRI, carrier frequency, LFM sweep etc. To compare the waveforms in a similar way these variables are fixed. The primary radar and receive radar are assumed to have similar specifications. Both radars can perform the two roles. Therefore, both radars have the same antenna gains and thermal noise figures. And for simplicity the transmit and receive antenna gains are set to be equal.

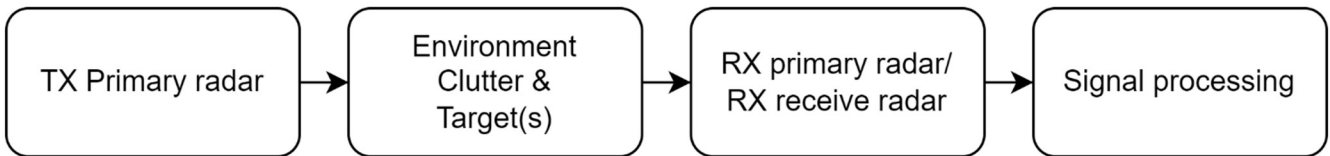


Figure 29 Simulation model.

5.2. MATLAB computer simulation

The performance analysis is an essential part in measuring the performance of the proposed algorithm. Different algorithms can be compared in a fair way with similar simulation variables. With the equations of chapter 4 the signal can be implemented in MATLAB. The starting point is (54) which describes the complete signal for one upchirp burst followed by the inserted time delay and one downchirp burst. The first MATLAB program simulator is only for one measurement. This is programmed with different figures to assess what happens with the signal and assess if faults occur. In the following subsections the programmed MATLAB simulator is described.

The first part of the MATLAB program is setting the variables. The used settings, variables (both in MATLAB and in the thesis) with values and units are shown in Table 5. The main setting which influences the algorithm are the number of pulses K . The pulse duration can be set in the simulation at any value. To check the working of the algorithm the inserted time delay can be set for all the times which are possible with the number of range cells. The amplitude of the signal versus the amplitude of the noise can be set and tested for different settings. This will correspond to the received signal-to-noise ratio. The time delay between the radars is in the first part to check if the primary radar works properly. With the variables T_{PRI} and f_s a time vector is created for the PRI from where the signal is built up and shown in the next section.

Setting	Variable MATLAB	Variable Thesis	First Simulations	Simulations and Experiment	Unit
Pulses in a burst	K	K	6/8/16*	2/4/8/16/32/64/128	#
Pulse duration	T_p	T_p	1×10^{-4} *	62.5×10^{-9} *	s
Pulse repetition frequency	PRF	PRF	1×10^3	4.0×10^6	Hz
Pulse repetition interval	PRI, T_{pri}	PRI, T_{PRI}	1×10^{-3}	2.5×10^{-7}	s
Inserted time delay	T_d	T_D	$\{0..998\} \times 10^{-6}$ *	$\{0..234.4\} \times 10^{-9}$ *	s
Carrier frequency	fc	f_c	10×10^9	10×10^9	Hz
Bandwidth	BW	B, B_{LFM}	0.5×10^6	64×10^6	Hz
Sampling frequency	fs	f_s	1×10^6	128×10^6	Hz
Number of samples	Rb	N_{samp}	1000	32	#
Number of range cells/symbols	Rb/2	N_{RC}, N_s	500	16	#
Number of bits per time delay	NB	N_{bit}	8	4	bit
Amplitude transmitted signal	a	a	1	1	~ V
Amplitude received noise	an	a_n	1*	1*	~ V
Distance between the radars	RI	L	42.2×10^3	42.2	m
Speed of light	c	c	299792458	299792458	m/s
Time delay between radars	taup	τ_p	2.81×10^{-4}	2.81×10^{-7}	s
Threshold	Th	T	0, 13	0, 3 and 13	dB

Table 5 MATLAB simulation variable settings, *all variables which are varied.

The two signals for the upchirp and downchirp are created in MATLAB and shown in Figure 30. The real part and imaginary part for the upchirp are presented to picture the whole waveform. In the last figure the real part of the downchirp is shown. The imaginary signal is shown to see the created phase shift. In the following figures only, the real part is shown. The signals are sampled with twice the bandwidth and therefore spikey. At the start of the real signal upchirp the signal starts at amplitude 0.5. This is because of the use of the Heaviside function. With a higher sampling frequency, the signal becomes smoother however the algorithm will not perform better.

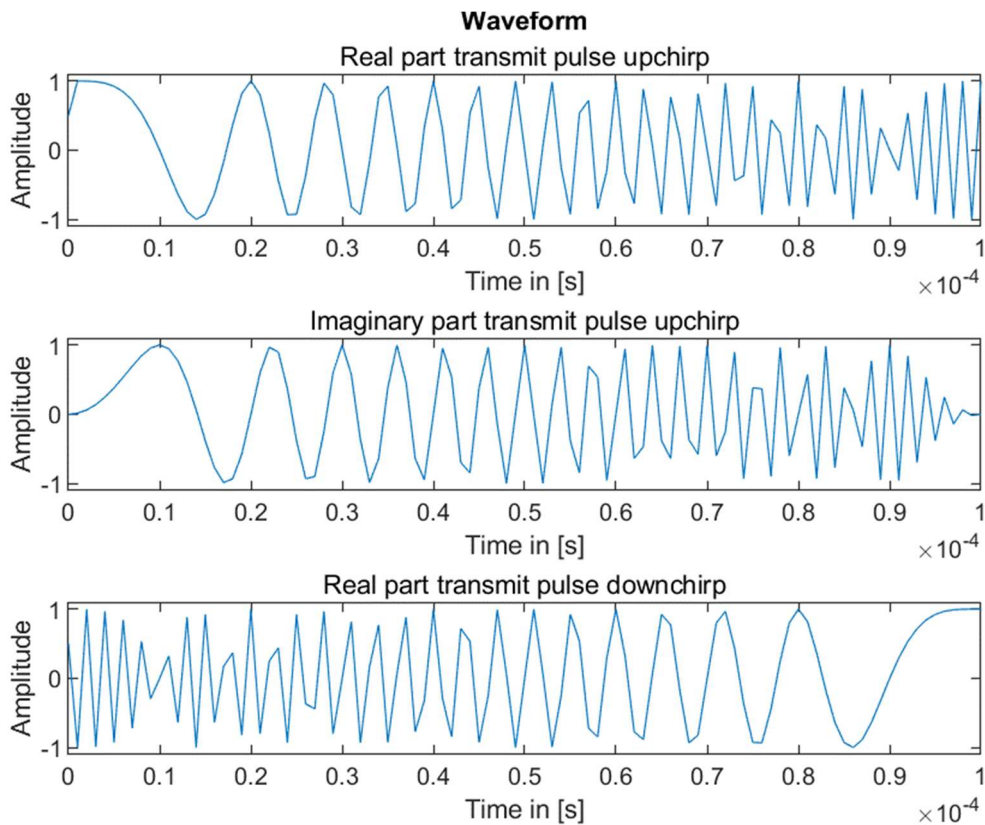


Figure 30 Upchirp and downchirp waveform during one pulse duration.

The next step is to place the transmit signal in one PRI. Those vectors with the complex signal in one PRI have the dimension of 1x1000. In Figure 31 the LFM pulse with the remaining of the PRI is shown.

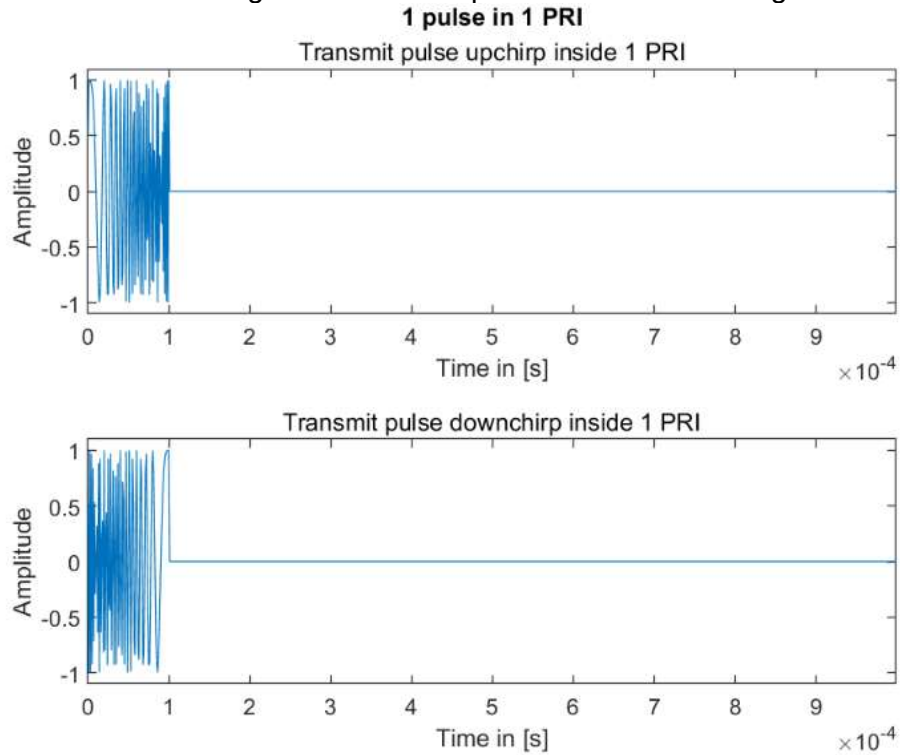


Figure 31 Upchirp and downchirp in one PRI.

Figure 32 is created with 6 upchirp and downchirp pulses placed in a sequence. The upchirp and downchirp vectors have the size of an 1x6000 vector. At this point both bursts are created the next step is to place them with an inserted time delay between them.

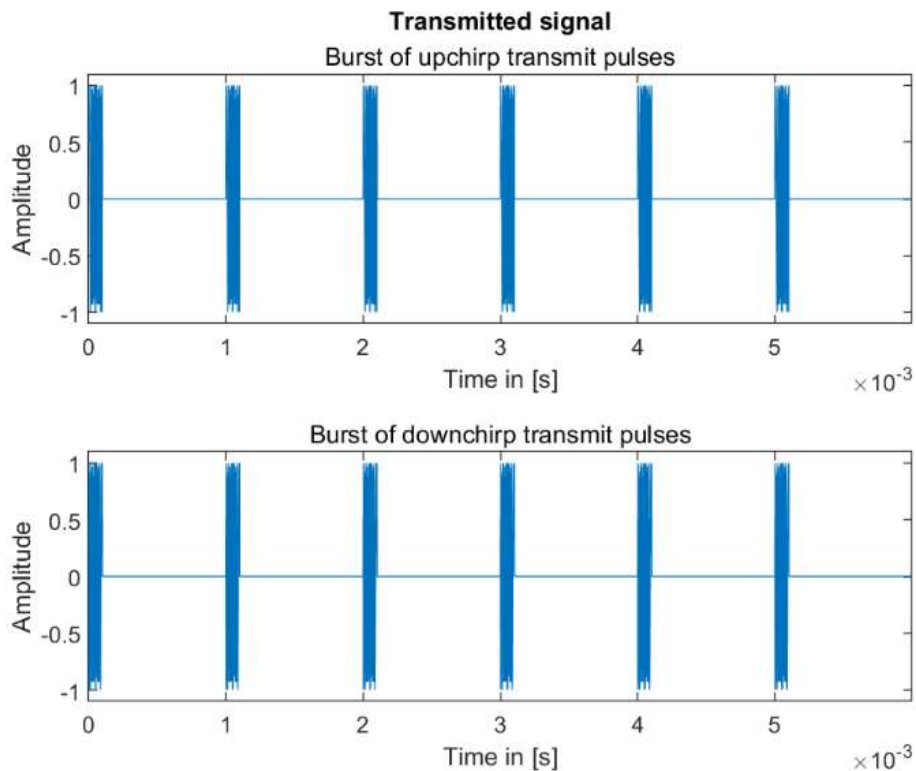


Figure 32 6 Pulses upchirp and 6 pulses downchirp.

In Figure 33 the transmitted signal is shown. To visualise the different parts the lower figure shows the segments of the signal with a different colour. For the visual presentation a time delay of 555 μs is used. At this point the vector of the transmit signal has a size of 1×6000 (up) + 1×555 (time delay) + 1×6000 (down) = 1×12555 . When the time delay is varied also the size of the transmit signal will vary.

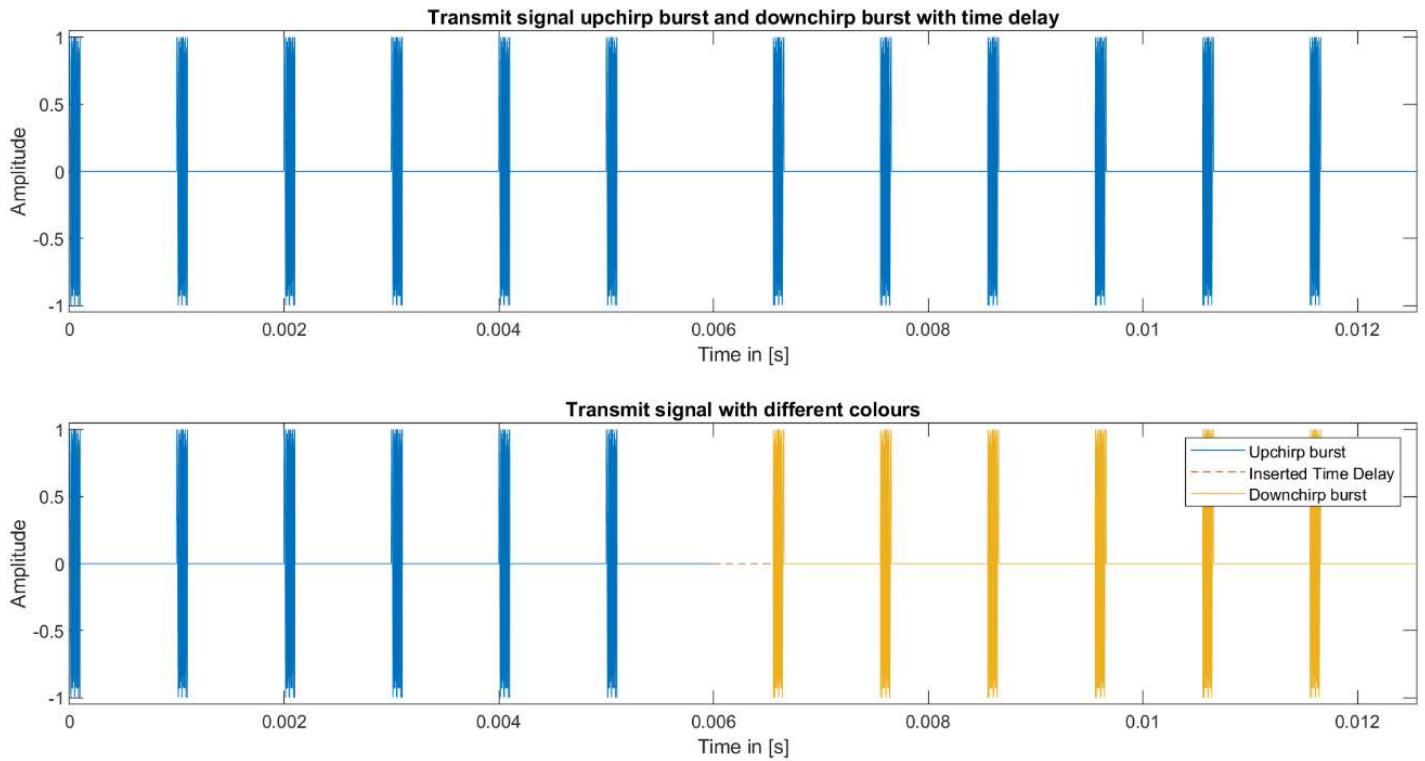


Figure 33 Total transmit signal.

The next step is to simulate the noise. In MATLAB the random function is used to create complex white Gaussian noise. The random noise n_i is calculated. In an equation this is shown as follows:

$$n_i = a_n \frac{\text{randn}(s_{TdBUD}) + j \cdot \text{randn}(s_{TdBUD})}{\sqrt{2}} \quad (78)$$

The random noise is multiplied by the amplitude of the noise a_n which can be varied for the different SNR levels. Where the noise vector n_i is created with two random components with the size of vector s_{TdBUD} . The received signal contains noise which is added to the transmitted signal which creates the transmitted signal covered in noise. This is shown in Figure 34. As expected, the original signal cannot be seen clearly in this plot.

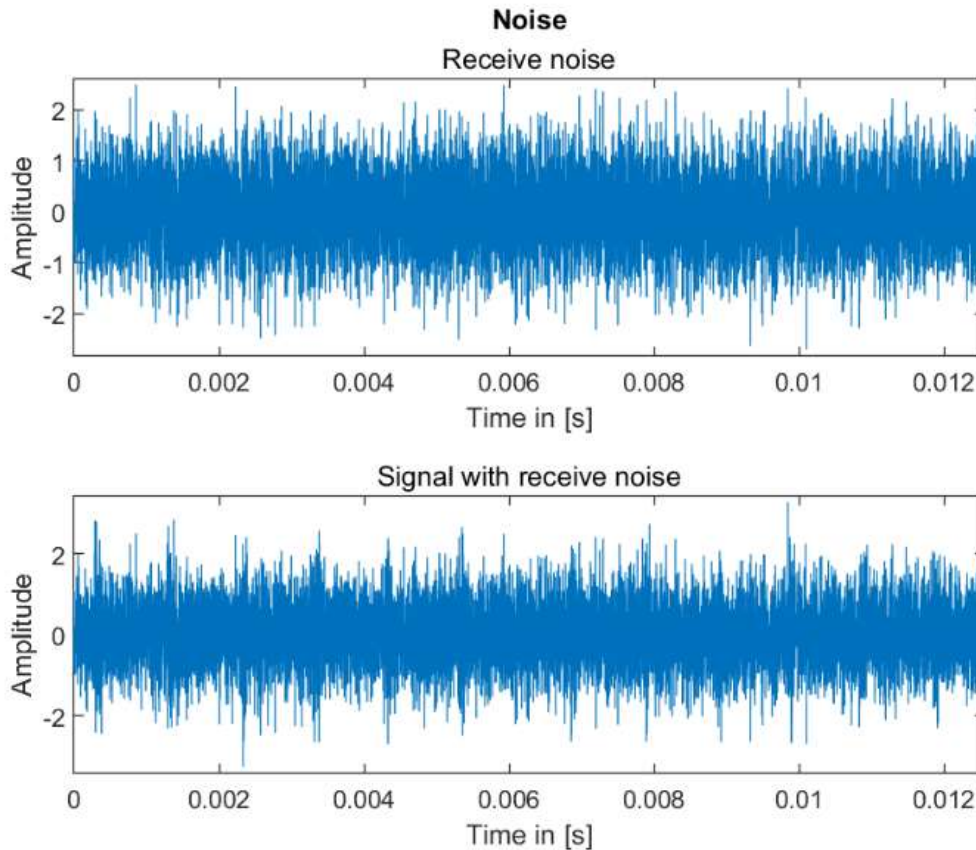


Figure 34 Noise with and without the transmit signal.

To simulate that the signal reflects on an object-of-interest a time relative to this delay is added to the signal. A fixed distance of 42.2 km is simulated as distance between transmitter and receiver. This corresponds with the speed of light to a delay of 2.81×10^{-4} s for the primary radar and 1.41×10^{-4} s for the receive radar. The Swerling case of the object-of-interest is at this point 0 (ideal object without any fluctuations).

To simulate that the signal which is received at the receive radar at another time as the primary radar an additional part of noise is introduced. In the MATLAB simulation a random start of the sampling time (the relative time t_{rel}) on interval $\{0, T_{PRI}\}$ is introduced. With 1000 samples this corresponds to a random number of 0 to 999 of additional delay between the transmitted signal and the arrival at the receive radar. The simulated scattered waveform is not related to the arrival of the signal at the receive radar in the real time. This real time is only available at the primary radar. The receive radar uses a relative time. This is simulated with a noise vector of random length which is inserted before the transmitted waveform.

The following subsections describes the operations which are used in the MATLAB simulation. These operations are presented in Figure 35. This starts with the simulated receive signal as vector which is cut into sections of one PRI and forms a 2D matrix. The next step is the coherent integration and Doppler processing of a burst for the upchirp and downchirp signal where the receive signal is transformed to a matrix. This is performed in steps of one PRI. In that way the result of the upchirp burst can be compared to the result of the downchirp burst K and $K+1$ PRIs later. The maximum of this comparison is used as input for the detector followed by the estimation of the time delay. In Figure 35 the used 2D and 3D matrix dimensions are shown.

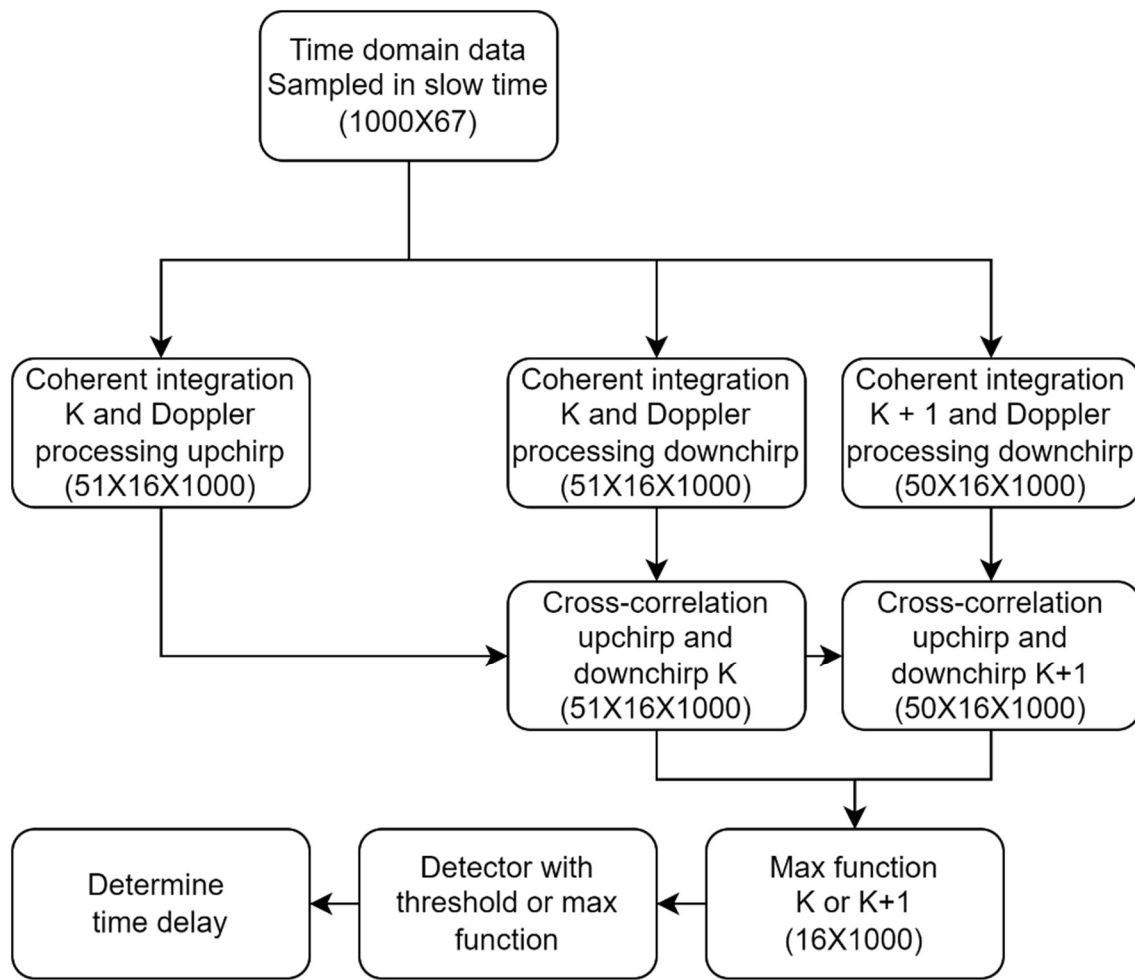


Figure 35 Signal processing steps MATLAB simulation with the size of the vector or matrix between brackets.

With the receive signal simulated, the signal processing can be started. The first step is implementing the matched filter. This is done with a convolution (or cross-correlation) in the time domain and with an FFT by transforming the signals to the frequency domain. Both simulations worked, however the choice to continue the simulations fell on the convolution because the time delay communication happens in the time domain. The matched filter is performed twice for both upchirp as downchirp on parallel data streams.

The first simulations are performed in the static domain where the object-of-interest is stationary. There the Doppler frequency is 0 Hz. The coherent integration can be performed by summing up the relative time samples of the PRIs. The next step is to perform the coherent integration with Doppler processing. Therefore, a random Doppler frequency on the interval $\{-PRF/2, PRF/2\}$ is simulated. The coherent integration is performed in slow time, therefore every PRI a new set of K PRIs is taken and coherently integrated. To have enough space for all the coherent integration an additional noise vector is introduced. Before and after the two successive bursts an additional number of PRIs with noise are added. The total length of this additional noise vector is two times K . This additional noise vector is split into two parts of a random number of PRIs and placed before and after the received signal.

The Doppler processing is performed with an FFT before the time domain data stream is transformed into a matrix. Therefore, the vector is cut into pieces of one PRI (1000 samples). For every K (in this example 16) successive PRIs the coherent integration is performed. In this example the matrix after the matched filter is of size 1000X67. This is reshaped into 51 successive sections of 1000X16 samples as the input data before the FFT.

The novel radar set up is a matched filter which is performed as a sliding window over the data in real time. With a MATLAB simulation data can be processed afterwards, this is the case for the experiment. In a radar network of opportunity, the detection of a upchirp burst can be seen as a prefix and the receive radar can search for a downchirp in the upcoming data. Every PRI a new matched filter operation with coherent integration is executed. When the number of PRIs increases first an upchirp is detected and later the downchirp is detected. By comparing the peaks in a sliding window K or $K + 1$ pulses later the maximum value can be used to determine the inserted time delay. This principle is shown in Figure 36 where the response of the matched filter is calculated every PRI. With the detection threshold set at -13 dB the time delay can already be calculated at the 21st PRI. However, in the simulation the maximum values are taken for the upchirp at the 11th PRI and the downchirp at the 26th PRI.

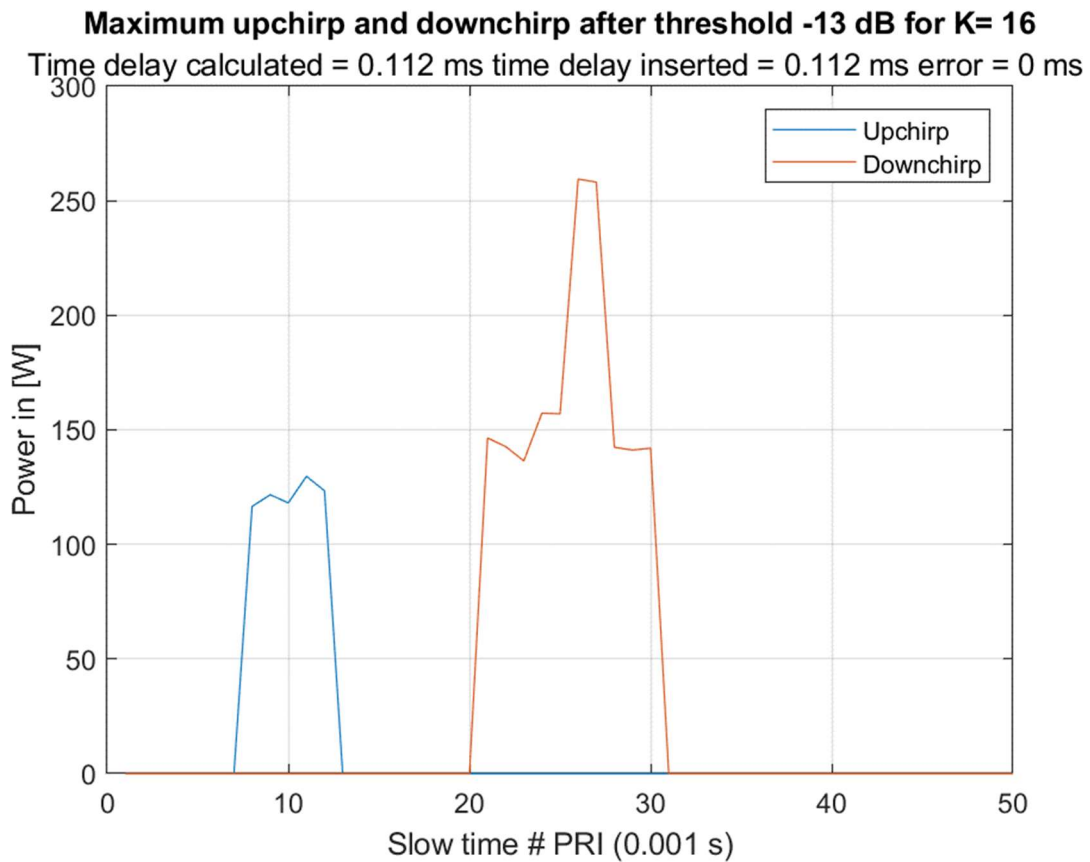


Figure 36 Plot upchirp and downchirp response on the matched filter per PRI.

The simulation can be performed with a continuously updating figure to visualize this procedure. In Figure 37 the two maximums of the upchirp and downchirp are shown. These are at position 17 and 33. To prove that the algorithm can operate with moving objects or radial bistatic velocities the inserted (random) Doppler frequency and the calculated Doppler frequency are shown. With Doppler resolution defined in (22) as function of the time on target, the Doppler resolution is calculated as function of the input PRF:

$$\Delta f_d = \frac{PRF}{K} \tag{ 79 }$$

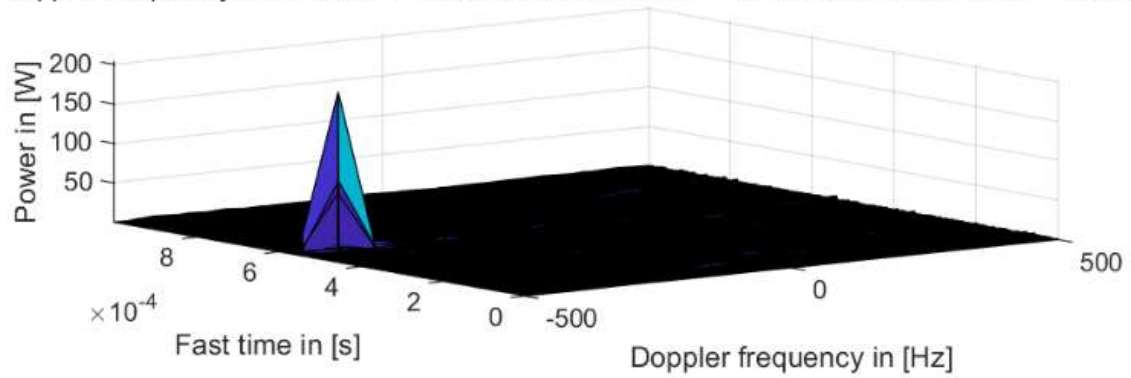
Where the integration time is only the number of pulses in a burst K . This leads to $1000/16 = 62.5$ Hz. In Figure 37 both peaks of the upchirp and downchirp measure -433.3 Hz. The inserted Doppler frequency is -454.5 Hz. The difference between both maximums is 21.1 Hz what fits the Doppler resolution.

The next step is a detector to detect two successive bursts. First a threshold of 13 dB is executed. The next step is a cross-correlation of the maximum of $2K+1$ successive PRIs. This will be executed for the upchirp as well as the downchirp. When a value above the threshold for the upchirp is detected, this is compared to the maximum of the downchirp. In Figure 38a. the flipping point where both upchirp as downchirp are visible is shown. There, both sides have integrated 8 pulses of the complete burst of 16 pulses. Depending on the noise level this is visible. The threshold will remove all the noise. This is visible in Figure 38b. In case there is no noise both peaks lay exactly K or $K + 1$ separated from each other in slow time. This is calculated in the simulation and shown as 16 before "Pulse Repetition Intervals Later" in Figure 38b. Also, the position in relative sampled time is shown for the maximum of the upchirp as well for the downchirp. In this case the inserted time delay T_D is 0.112 ms. The difference of the position of the downchirp burst (0.653 ms) and upchirp burst (0.541 ms) is exactly the inserted time delay. It could be possible that the upchirp and downchirp are folded or multiple folded objects-of-interest give reflections. With the cross-correlation a positive time delay or negative time delay is calculated. By shifting the negative time delay to the positive side and take the maximum of this cross-correlation the correct time delay is found. Folding of multiple targets or folding of the downchirp signal is repaired. Because the knowledge of an upchirp must be followed by a downchirp is used in the cross-correlation.

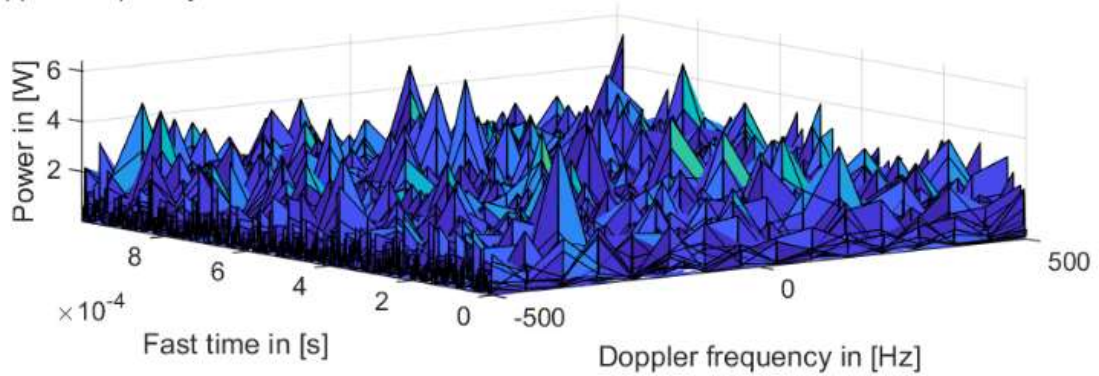
a.

Doppler processed Upchirp and Downchirp signal for K = 16

Doppler frequency calculated = -433.3333 Hz inserted = -454.4818 Hz Resolution = 62.5 Hz



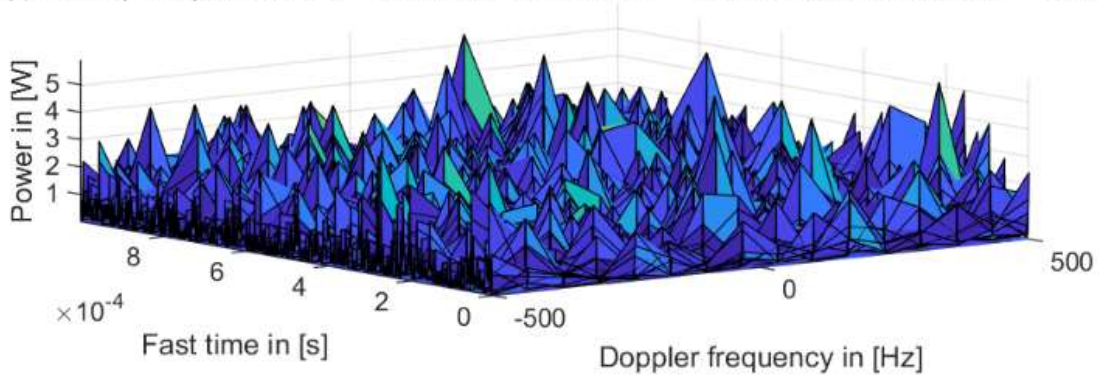
Doppler frequency calculated = -166.6667 Hz inserted = -454.4818 Hz Resolution = 62.5 Hz



b.

Doppler processed Upchirp and Downchirp signal for K = 16

Doppler frequency calculated = 366.6667 Hz inserted = -454.4818 Hz Resolution = 62.5 Hz



Doppler frequency calculated = -433.3333 Hz inserted = -454.4818 Hz Resolution = 62.5 Hz

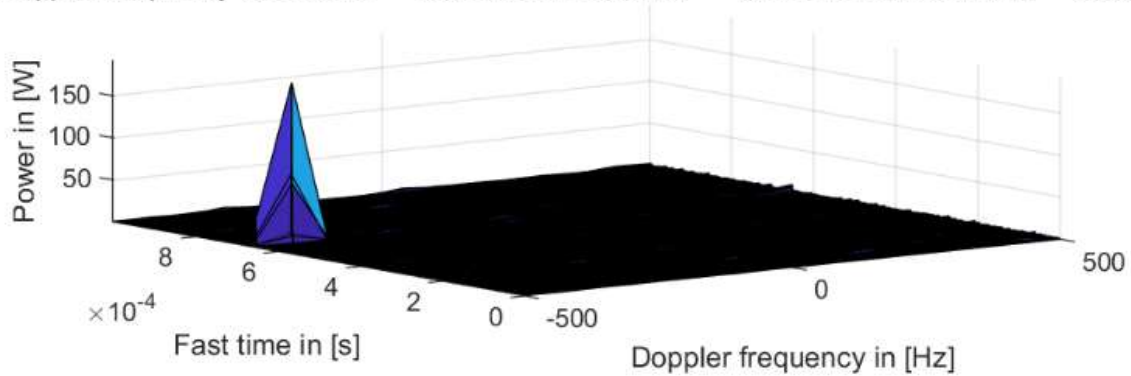
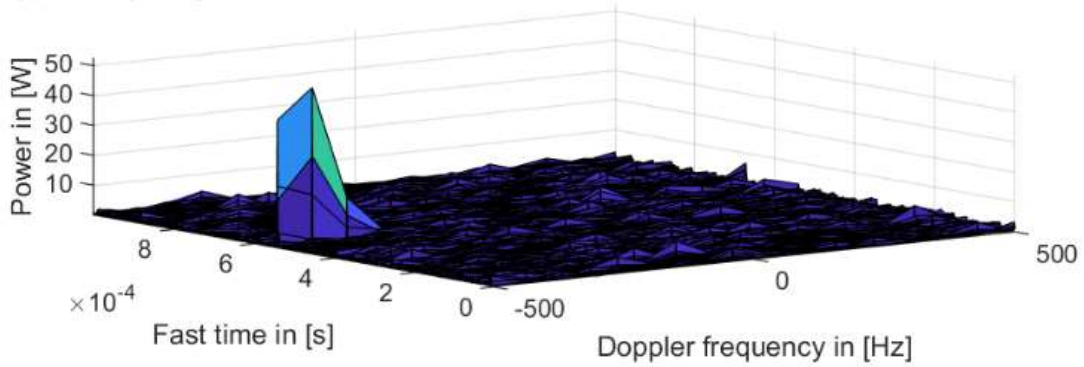


Figure 37 Maximum of coherent integrated signals with inserted and calculated Doppler frequency. a. Upchirp. b. Downchirp.

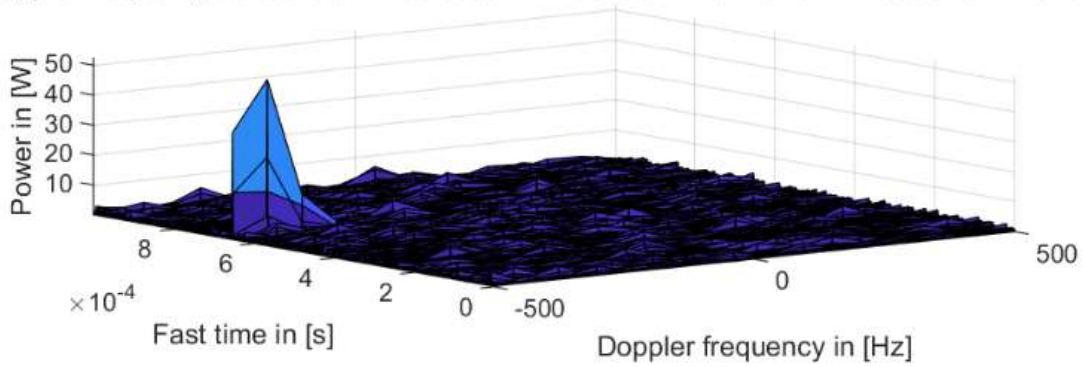
a.

Doppler processed Upchirp and Downchirp signal for K = 16

Doppler frequency calculated = -433.3333 Hz inserted = -454.4818 Hz Resolution = 62.5 Hz



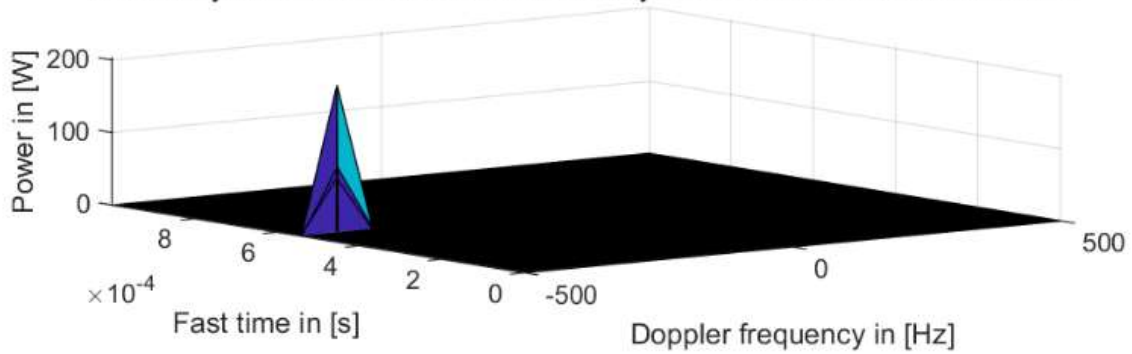
Doppler frequency calculated = -433.3333 Hz inserted = -454.4818 Hz Resolution = 62.5 Hz



b.

Maximum Upchirp after threshold -13 dB for K = 16

Time delay calculated = 0.112 ms time delay inserted = 0.112 ms error = 0 ms



Maximum Downchirp 16 Pulse Repetition Intervals later

Maximum time Upchirp = 0.541 ms and Downchirp = 0.653 ms

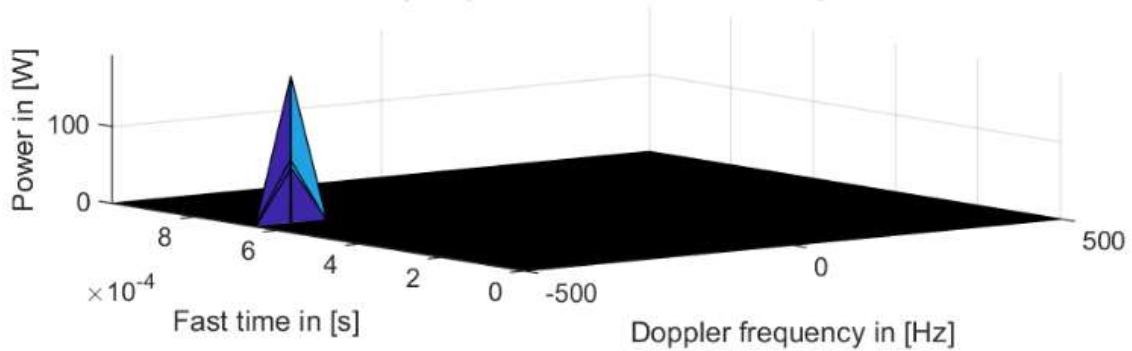


Figure 38 a. Both upchirp and downchirp are part of the coherent integration b. Maximum of upchirp and downchirp after the threshold.

5.3. Results TDBRB simulations

In this section the results of the simulations are presented. With the MATLAB simulation different aspects of the performance are measured. With different MATLAB programs it is possible to determine the performance of the proposed TDBRB. The performance is measured in bit rate and bit error rate or symbol error rate.

With Monte Carlo simulations the performance can be estimated. The radar performance is assumed to be similar to the performance of the primary radar. This should not change in means of probability of detection, false alarm rate or missed detections. Only a degradation of time as indicated in Figure 23. Therefore, the only performance measures of the novel TDBRB waveform are bit rate and bit error rate or symbol error rate. In the simulation the signal-to-noise level is varied, and all the different communications symbols are simulated with a uniformly distribution. In the Monte Carlo simulation, the simulation is performed for a fixed number of iterations (repeating the MATLAB program) per signal-to-noise level. The symbol error rate per SNR level SE_{SNR} is calculated as follows:

$$SE_{SNR} = P_{e,SNR} = \frac{\#Errors}{\#Iterations} \quad (80)$$

Where $P_{e,SNR}$ is the probability of an error per SNR level. And everything what is not the correct symbol is counted as incorrect. And therefore, the number of errors can be divided by the number of iterations.

5.3.1. Max function

The first MATLAB simulation consisted of coherent integration and without a threshold. With a max function the maximum of the correlation between the information in the range plot of the upchirp is compared to the range plot of the downchirp. Both range plots are sampled in a relative PRI (what means that the exact time of transmission is unknown). The response of the same object-of-interest for the upchirp as downchirp is shown in Figure 39 where the inserted time delay is 0.35 ms. In a static (non moving) scenario this is the case.

Coherent integrated signals. T_D calculated = 0.555 ms. Inserted T_D = 0.555 ms. Error = 0 ms

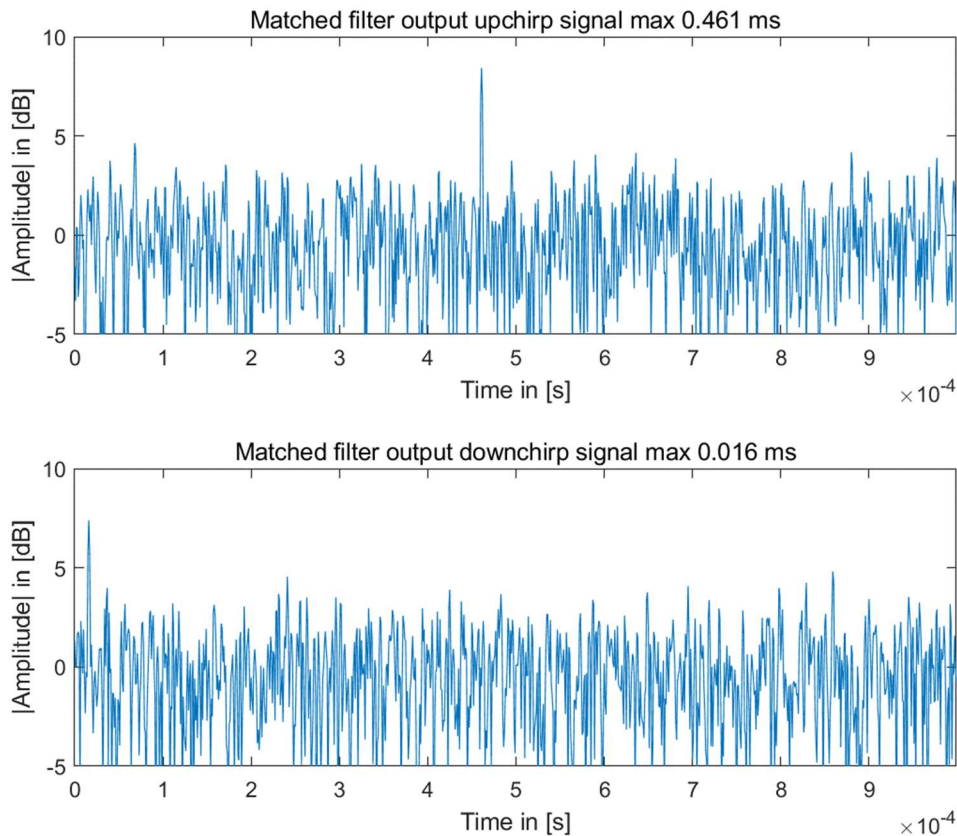


Figure 39 Response of the same object-of-interest for the upchirp and the delayed downchirp.

With a high matched filter gain and coherent integration of the pulses the symbol error rate as presented in Figure 40 is calculated. This static case will not work for a moving scenario because the pulses with a Doppler shift will not be added up. The graph shows a same probability of error for -13 and -14 dB SNR level. This is due to the maximum number of simulations (iterations) per SNR level the limit is in this case $P_{e,-13\text{ dB}}=1/2000=0.0005$. The SNR is the input SNR. If the simulation has more iterations per SNR level the probability of error can be estimated with more precision.

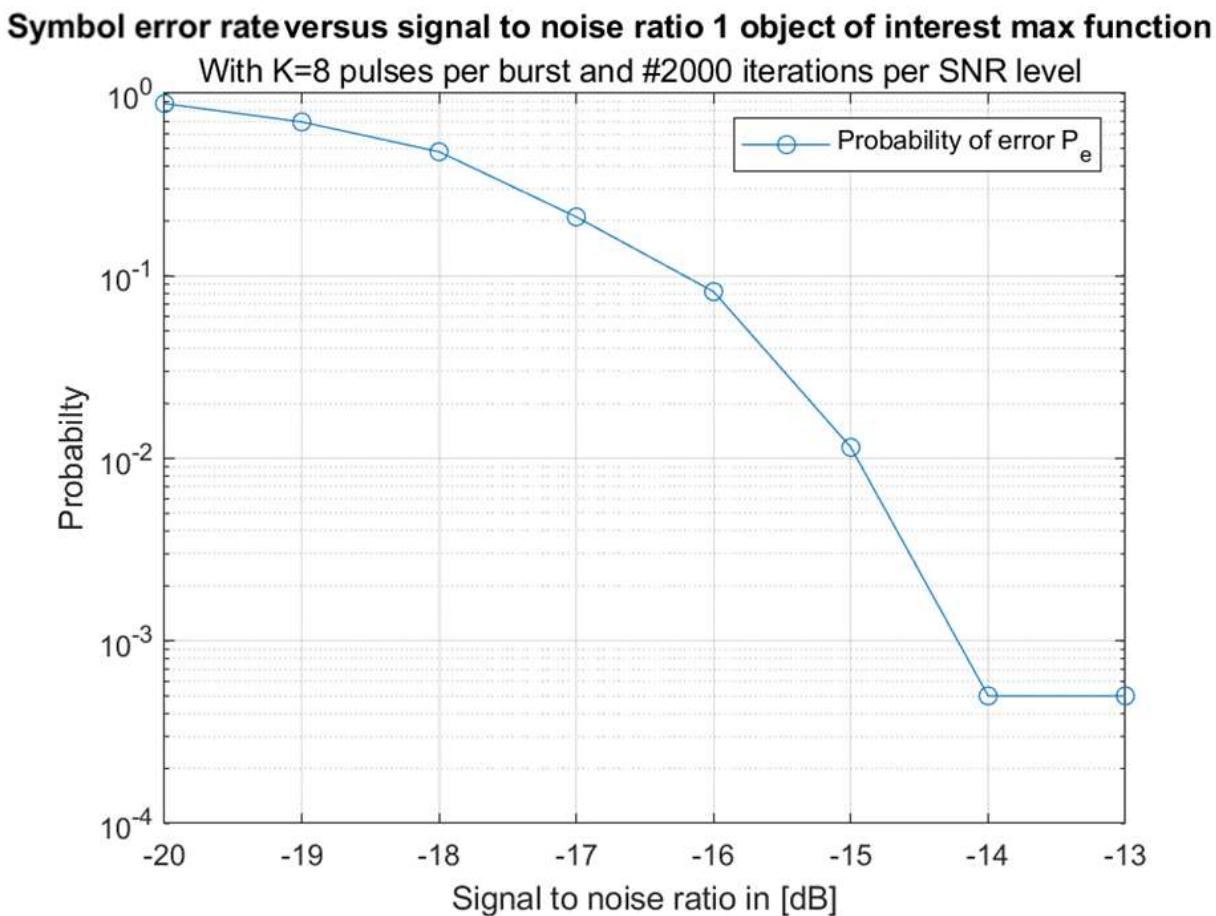


Figure 40 Symbol error rate as function of SNR for the static case with coherent integration.

5.3.2. Straddle loss

In the first static simulation the same number of range cells as samples is used. The number of samples are equal to number the number of range bins. The results are useful. However, every regular radar has problems with straddle or straddling loss. The inserted time delay was on the exact moment of sample. In static communication scenarios this is possible, but not in a radar scenario. Straddle loss is described in Richards et al. [2-03] as follows: the samples after matched filter which do not capture the important features of the matched-filtered output. At least two samples per range cell or transmitted symbol must be used with TDBRB communication. This phenomenon is because the output of the matched filter can be exactly on the border of two range bins. What the probability of correct estimation of the inserted time delay $P_{c,SL}$ with straddle loss will reduce to $P_{c,SL} = 0.5$. In Figure 41 the effect on the symbol error rate due to straddle loss is shown. The signal is shifted in steps of $0.1 \mu\text{s}$ on an interval of 0 to 0.5 times the time of one sample ($1 \mu\text{s}$). In this figure it is clearly visible that the shifted time does not influence the doubled sampling frequency. From $0.1 \mu\text{s}$ to $0.4 \mu\text{s}$ with the sampling frequency of 1 MHz the bit error rate increased with similar signal-to-noise ratios. For the $0.5 \mu\text{s}$ shift the inserted time delay can only be calculated with a probability of a correct symbol of $P_{c,SL} = 0.5$.

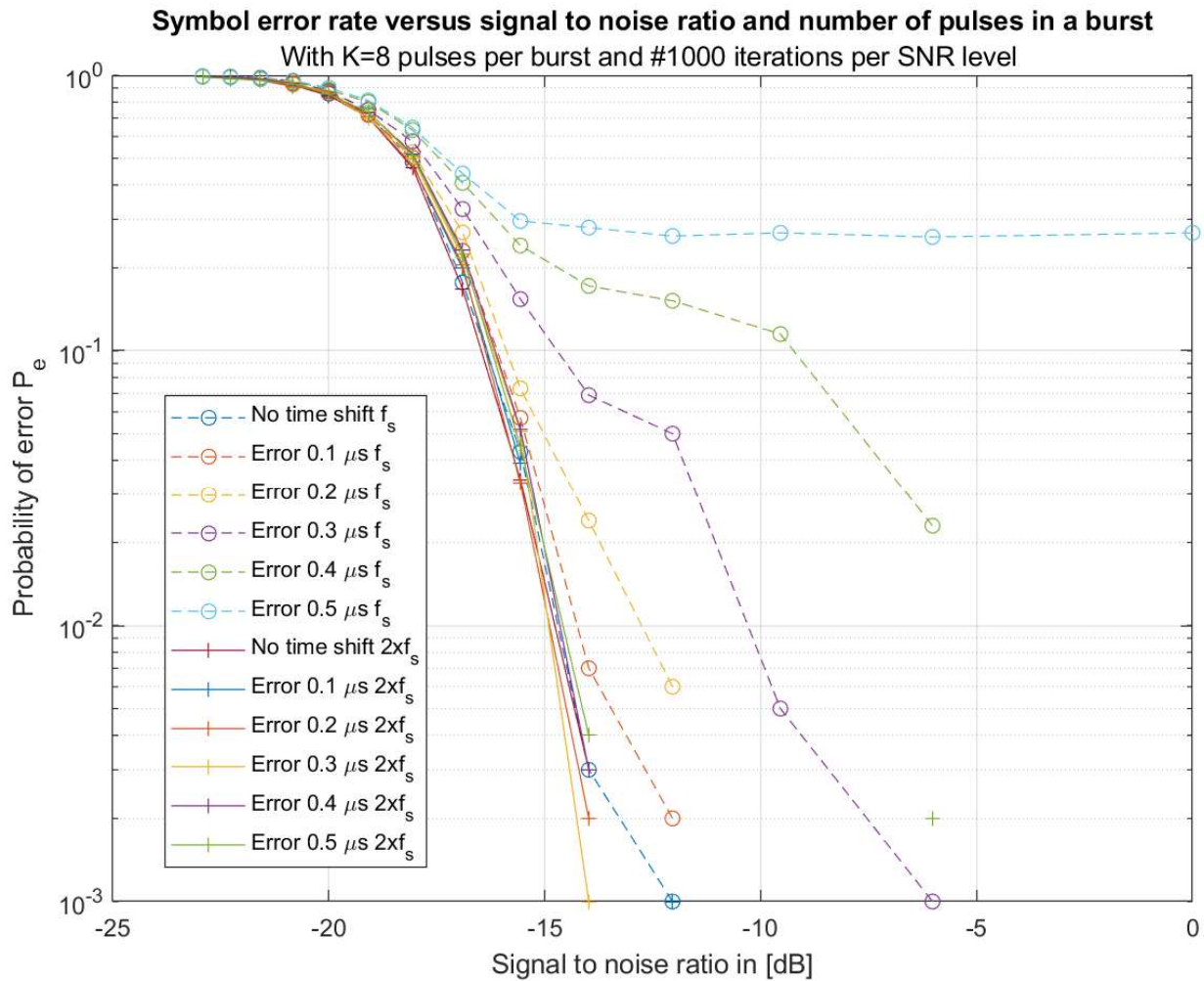
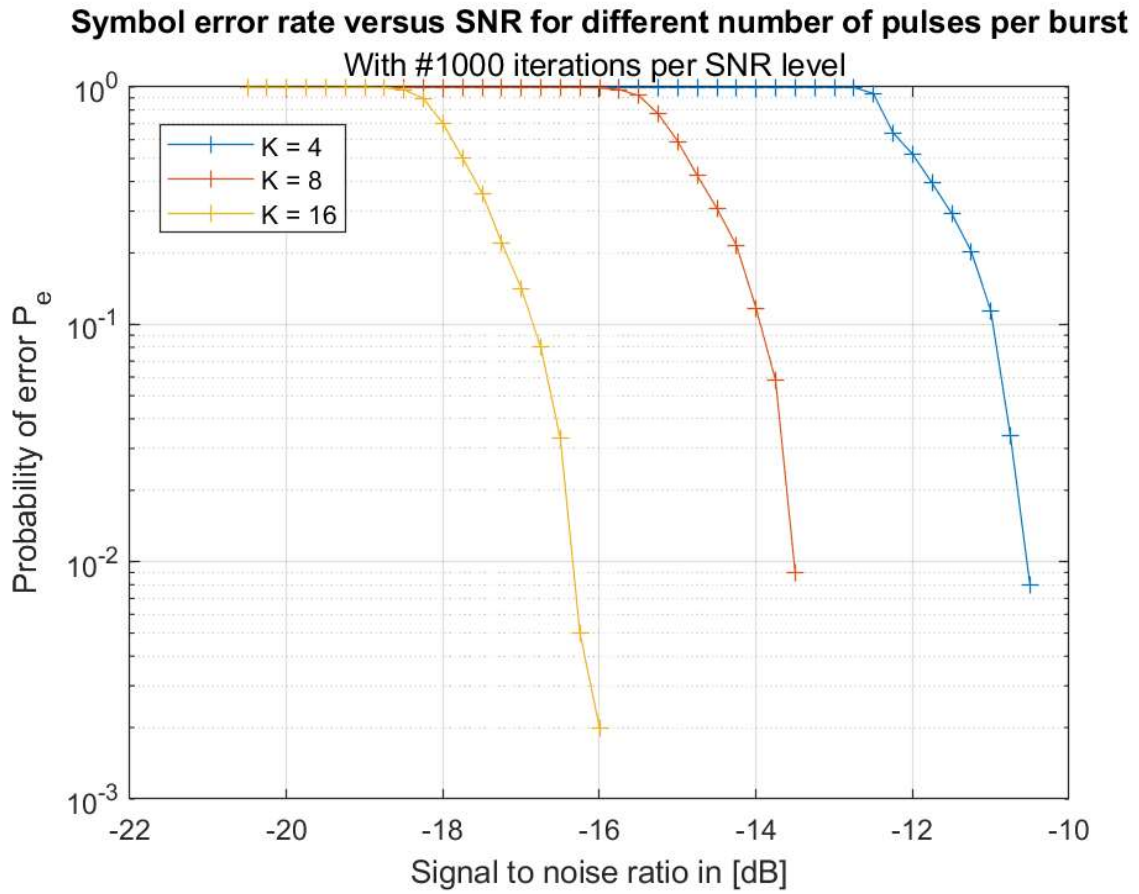


Figure 41 Symbol error rate with and without straddle loss with sampling frequency $f_s = 1$ MHz and a doubled sampling frequency $2xf_s = 2$ MHz.

5.3.3. Number of pulses in a burst

To simulate the moving scenario a random Doppler frequency is added to the receive signal. As showed in section 5.2 it was possible to determine the inserted Doppler frequency within the Doppler resolution. In Figure 42 the SER as function of the SNR is presented for the moving case. The results are similar as the SER for the static case. By varying the number of pulses in a burst it is also visible that doubling the number of pulses in a burst will shift the SER graph 3 dB. This is as expected from the theory concerning the number of pulses K in white noise in (5) and (6). The difference of 3 dB corresponds to the doubling of number the of pulses from $K = 4$ to $K = 8$, $K = 8$ to $K = 16$ and $K = 16$ to $K = 32$ (only in Figure 42b).

a.



b.

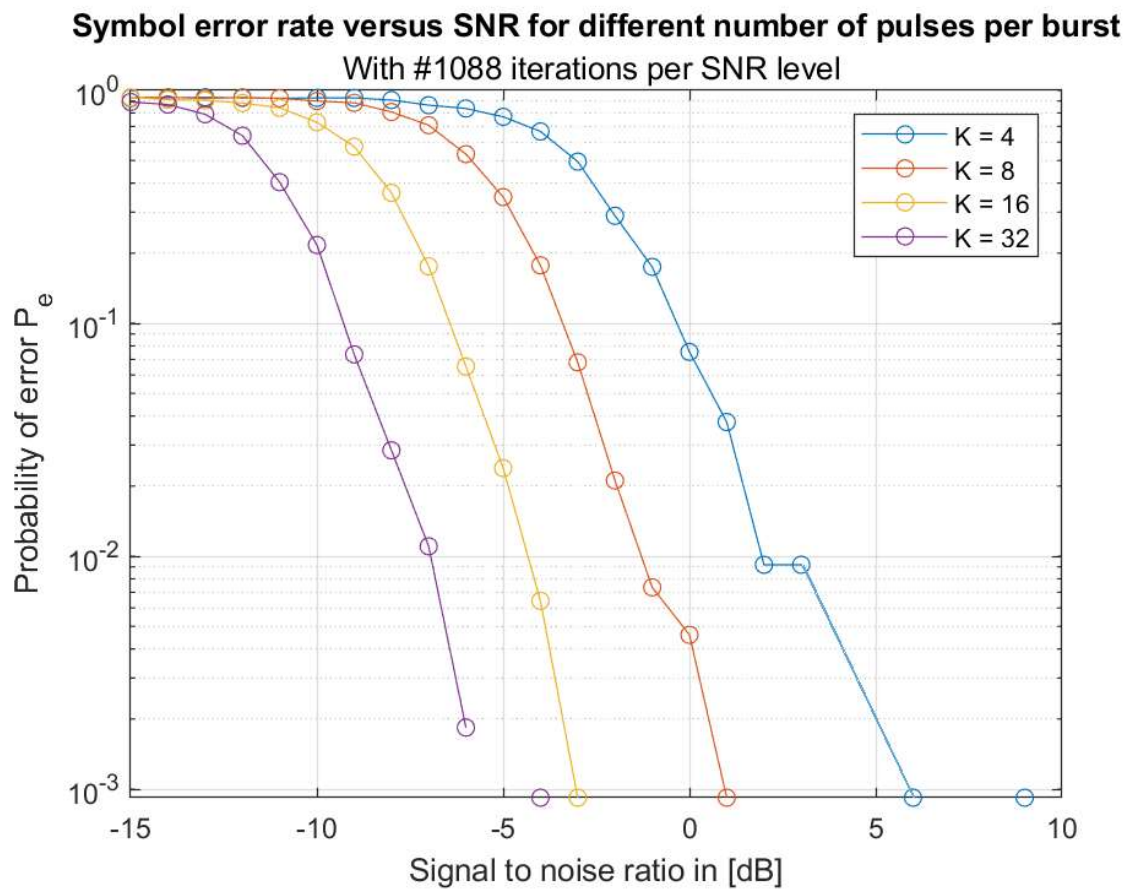


Figure 42 SER as function of SNR for the moving case with varied values of K number of pulses in a burst. a. Original simulation parameters. b. Adjusted parameters for the experiment with lower matched filter gain and 16 range cells or different symbols.

5.3.4. Detection probabilities

The next step is to simulate the regular radar performance. The main idea is to have two similar radars with similar radar performances. In that case the radars use similar thresholds to prevent false alarms. However, the receive radar is working with a signal of opportunity. This can result in only a detection of one upchirp or downchirp burst. However, only a complete detection of the upchirp and downchirp is assumed in the calculation of the probability of detection. The scheme stated in Table 3 is used to determine the hypothesis and probabilities scheme for the primary radar. For the receive radar this is similar only extended with a probability of detection $P_{D,U\&D,T_d}$ which is used in a similar way as the probability of detection. The scheme which is used for the receive radar is stated in Table 6 below.

Hypothesis	Signal is transmitted	Signal is not transmitted
$H_1(\text{Signal} + \text{Noise}):$	P_D or $P_{D,U\&D,T_d}$	P_{fa}
$H_0(\text{Noise}):$	P_M	P_{ND}

Table 6 Hypothesis and probabilities scheme regular (primary) radar.

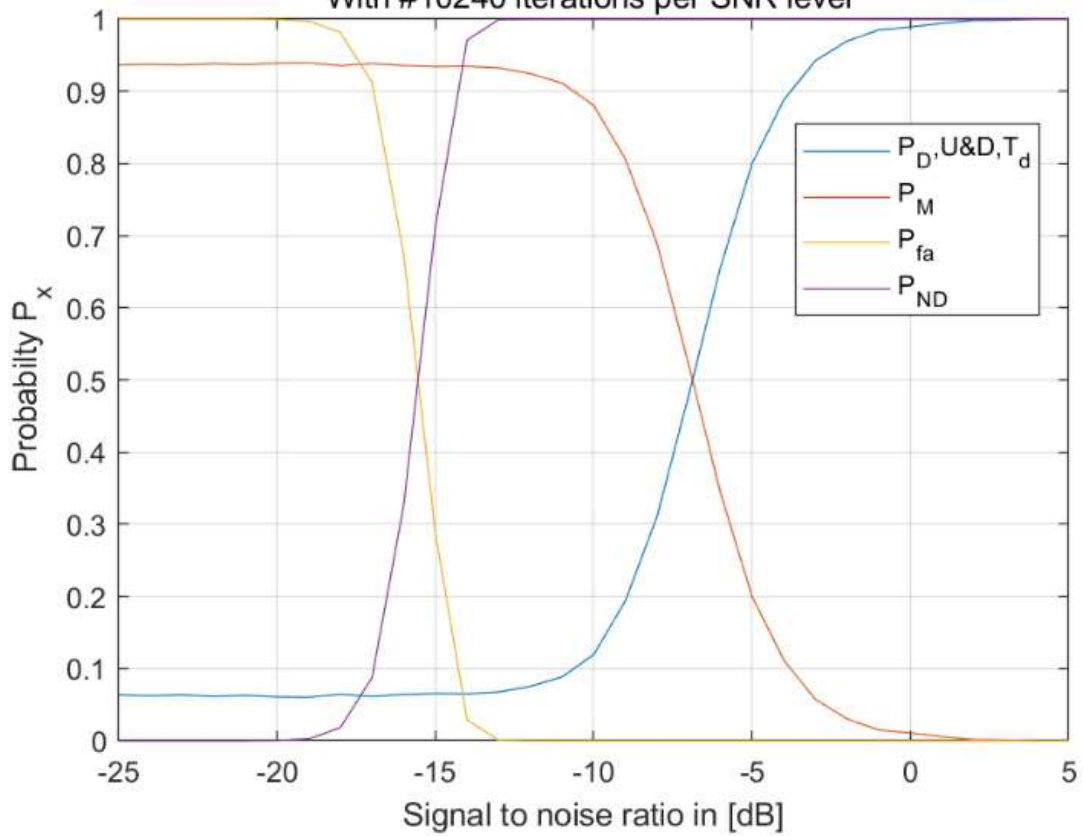
For the TDBRB algorithm the main probability of detection $P_{D,U\&D,T_d}$ (also called probability of correct communication P_C) is when the upchirp and downchirp are correctly detected and the inserted time delay is correctly calculated. In the low SNR region, the noise is large compared to the signal. The amplitude of the signal is set on 1. The amplitude of the noise is varied. For the calculation of the false alarm probability the SNR is used as if a signal with an amplitude of 1 is transmitted.

In Figure 43 multiple figures are shown for the different probabilities as introduced in Table 6. The probability of detection is simulated by calculating the probabilities when a signal is transmitted for different signal-to-noise levels. This operation is repeated 10240 times per SNR level. For the false alarm rate, the processing is performed without a signal. In this simulation the signal is replaced with a vector of zeros with the same length. The signal with communication is with a lower SNR level calculated properly, however the downside is that when there is no signal the false alarm rate is high.

a.

Probabilities of detection, no detection, missed detection and false alarm

With #10240 iterations per SNR level



b.

Probabilities of detection, no detection, missed detection and false alarm

With #10240 iterations per SNR level

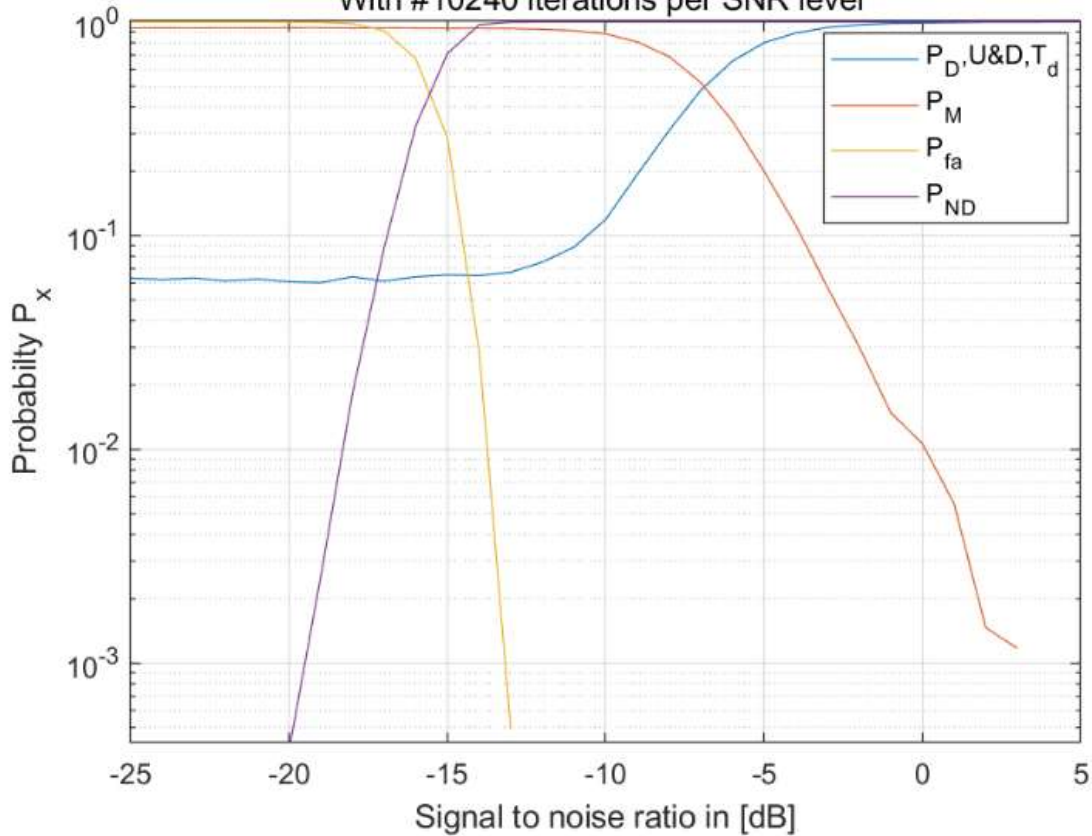


Figure 43 Probabilities of detection TDBRB for 8 pulses in a burst and 16 symbols for different SNR values with 13 dB threshold.
a. All probabilities in one figure b. All probabilities logarithmic scale.

The probabilities as stated in Table 3 are calculated for the primary radar for one burst (upchirp is similar as downchirp). Therefore, the same variables are used as in Figure 43. The results are presented in Figure 44. This figure shows that the radar performance is not influenced by the inserted time delay.

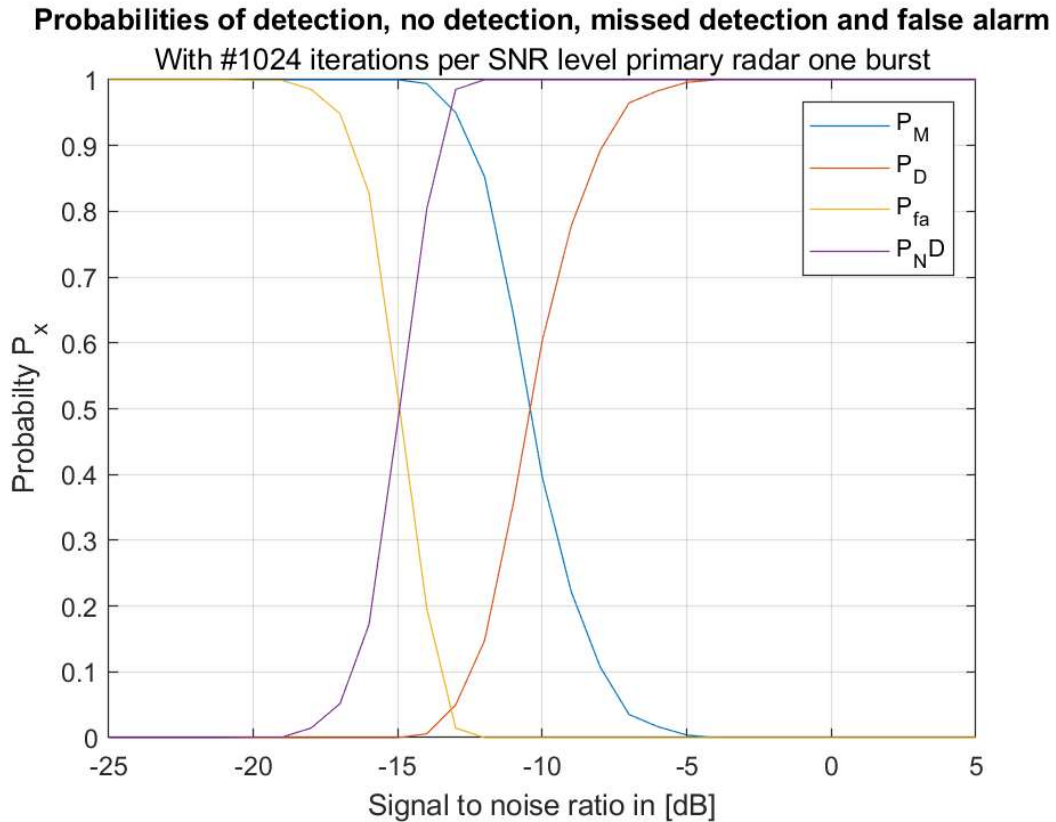


Figure 44 Probabilities of detection for one burst with a regular radar with 13 dB threshold

5.3.5. Pulse duration

In this section the influence of the pulse duration is simulated. The difference when a longer pulse duration is used is simulated just as in the moving scenario with a random Doppler shift. The expectation is that the matched-filtering gain is increased when the pulse duration is longer. This is similar as the variation of number of pulses. In Figure 45 the influence of the pulse duration on the SER is shown. In this figure it is visible when the pulse duration doubles the SER graph is shifted 3 dB to the left. This pattern is clearly visible for the pulse duration 1/16 times the PRI, 2/16 times the PRI and 4/16 times the PRI.

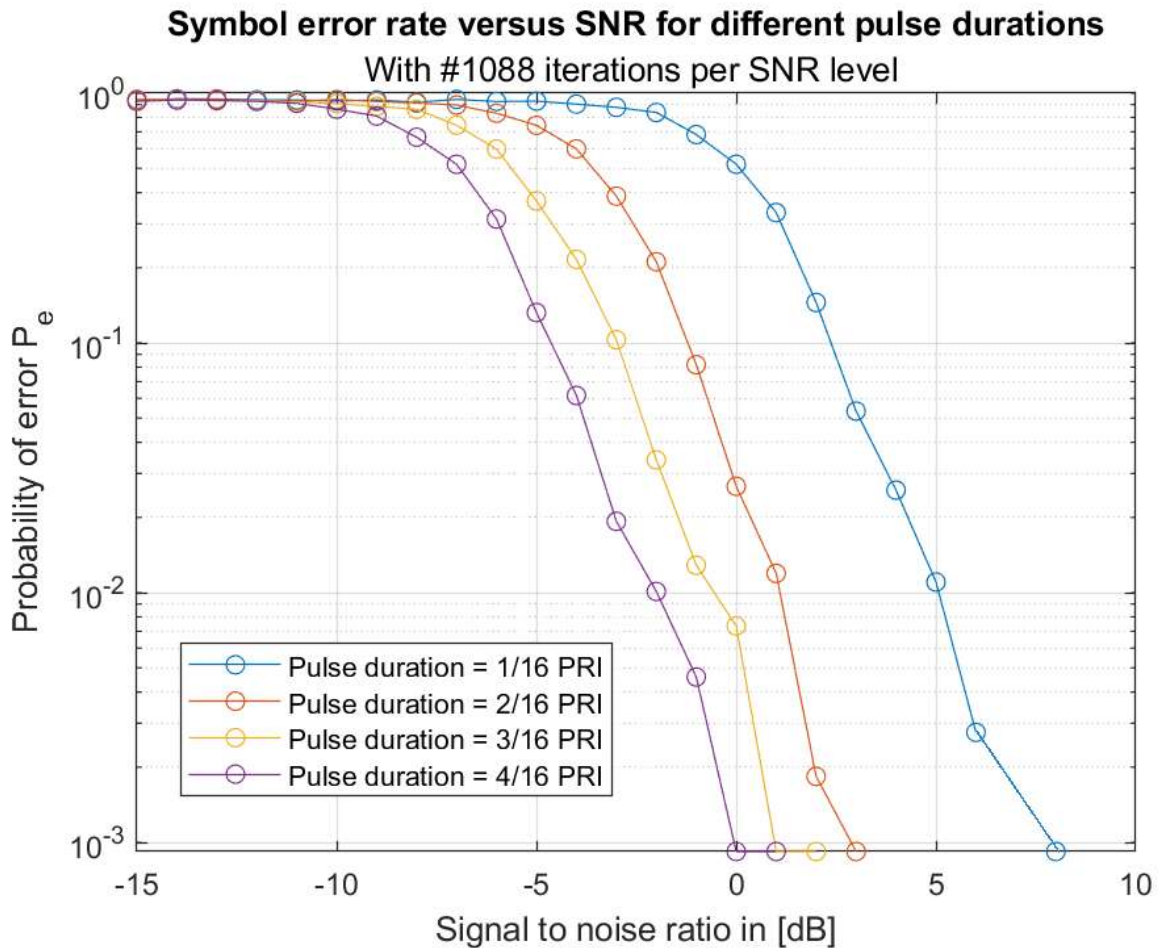
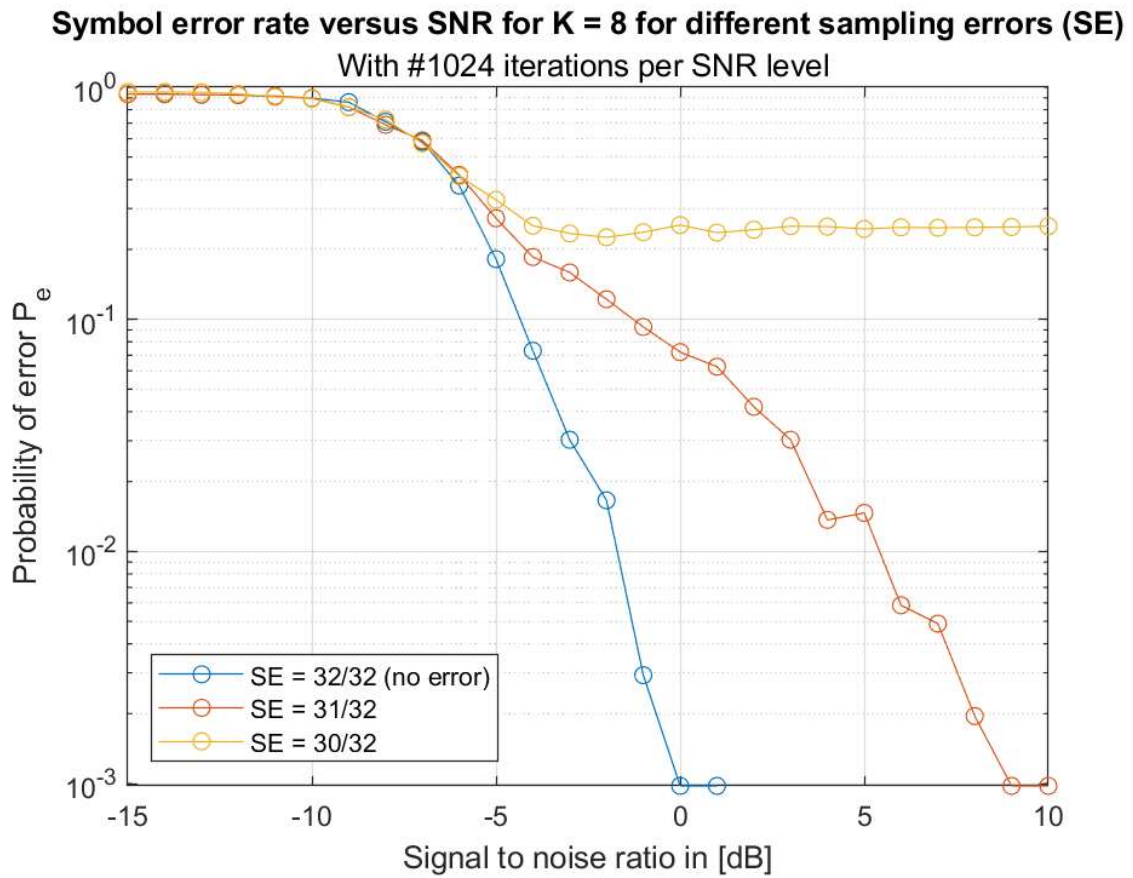


Figure 45 Influence of pulse duration on SER with 8 pulses in a burst.

5.3.6. Sampling errors

In this section the influence of errors in the sampling timing between the primary and receive radar is simulated. In the ideal situation the sampling frequency and timing of the primary radar and the receive radar are exactly the same. In this simulation the fluctuations in the timing of the samples are simulated. The start of a new pulse repetition period and the number of samples are kept the same. In this simulation 32 samples are used in one PRI. Due to the straddle loss 16 symbols can be transmitted with this number of samples per PRI. In this modulation an error is introduced in the timing before the matched filter of the receiver. The time vector of 32 samples is multiplied with $31/32$ and $30/32$. In that case the samples and symbols at the start will experience less error as the ones at the end. The results of this simulation compared to the zero error case are shown in Figure 46a. In this figure it is clearly visible that when the sampling is incorrect more errors occur. In the case of $30/32$ every last symbol (and probably more of the symbols before) is detected incorrect and therefore the SER will not converge to zero. In Figure 46b the influence of a small error on the interval of $\{31/32..32/32\}$ with steps of $0.2/32$ is shown. In that case some small errors like $31.6/32$ and $31.8/32$ have almost no effect on the SER.

a.



b.

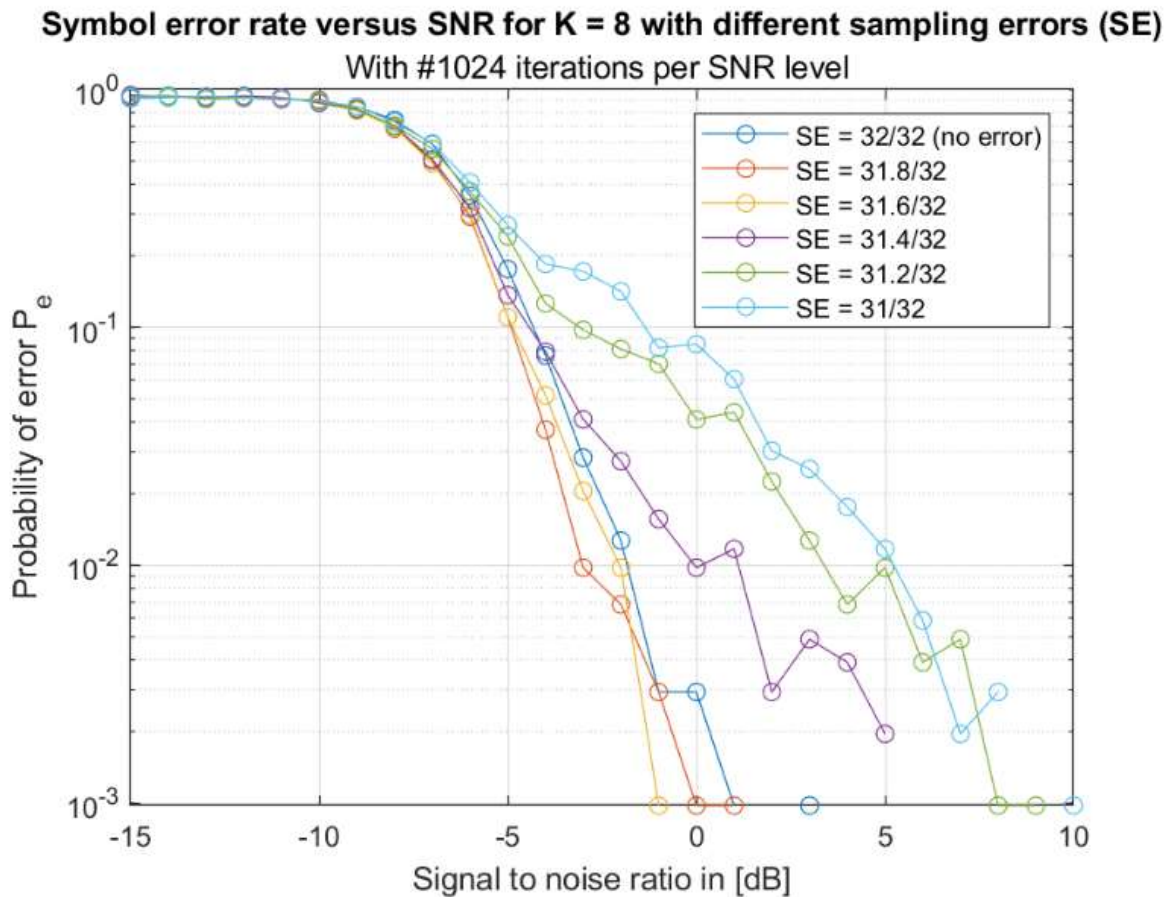


Figure 46 Influence of sampling error on SER. a. Large sampling errors b. Small sampling errors.

Another type of error is when every sample has a random error which can be maximal a multiplication on the interval $\{31/32..32/32\}$. In this simulation every time sample on the time vector is multiplied with this error and a random uniform distributed variable on the interval $\{0..1\}$. In Figure 47 the influence of these errors on the SER is shown. What can be seen in this figure is that the SER is less influenced because the random scaling can be zero. However, when the error which is multiplied is larger (31/32) the SER is more influenced. In this figure it looks as if 31.8/32 and 31.6/32 give a better performance. This can be due to the random calculations and coincidence. In the previous figure (Figure 46b) this is also visible. It is also possible that this is due to the decision algorithm which decides in which range cell the time delay is placed. For the last sample this can be in range cell 0 or 15. It is possible that because of the 31.8/32 or 31.6/32 multiplication transmitted symbol 15 will be better detected with an error. In that case it is clearer that the transmitted symbol is in range cell 15 because more energy is detected there.

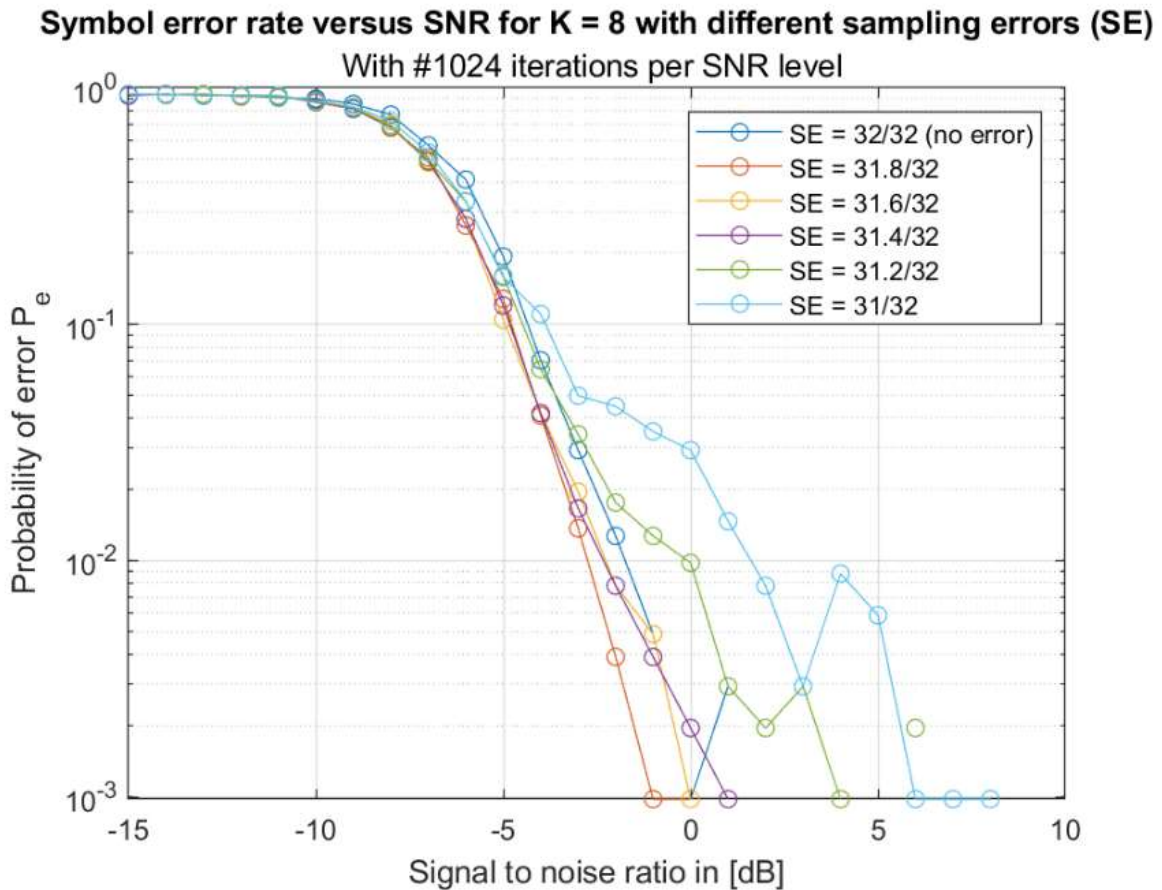


Figure 47 Influence on the SER of random errors on every sample.

5.3.7. Range or symbol accuracy

In Figure 48 four graphs are calculated with the same data to determine the accuracy of the algorithm. Therefore, the parameters for the experiment are used. The bandwidth is 64 MHz, and the sample frequency is 128 MHz. With a PRI of 4 MHz and a pulse duration of $\frac{1}{4}$ times the PRI this results in a pulse duration of 62.5 ns. The $B_{LFM} \cdot T_p$ product (bandwidth times the pulse duration) becomes 4. Therefore, the matched-filtering gain is 4. The range resolution δR is defined in (17) and the relation to the total number of range cells or maximal usable symbols is defined in (19).

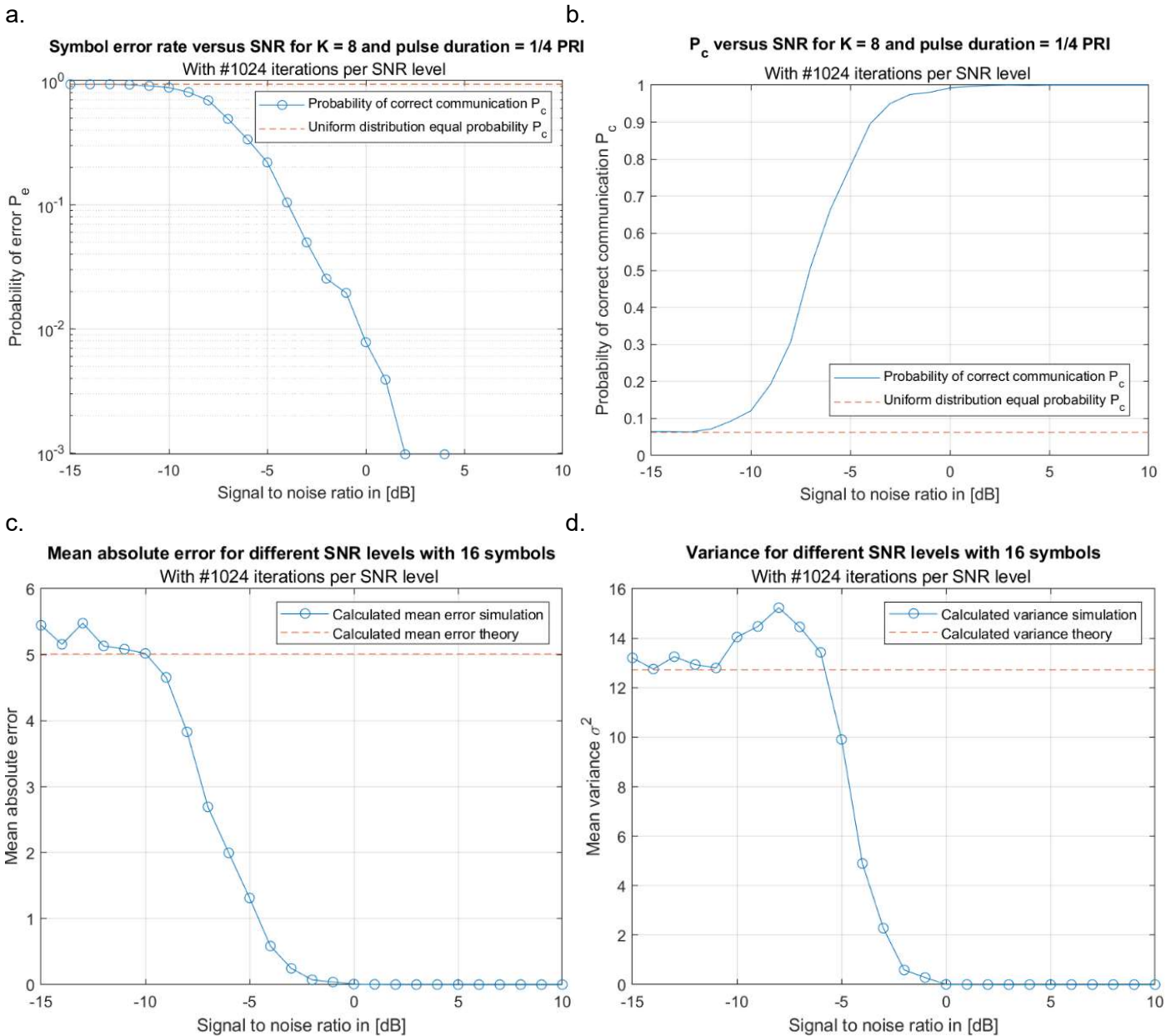


Figure 48 Accuracy of TDBRB for 8 number of pulses in a burst and 16 symbols for different SNR values.

a. Symbol error rate b. Probability of correct communication. c. Mean absolute error (symbols). and d. Mean variance (symbols).

The accuracy of the range measurement depends on the SNR as shown in (20). When we take a look at Figure 48c and d it is visible that the mean absolute value of the error and the variance of the error will converge to zero for large signal-to-noise scenarios, as is expected for a signal in white noise scenario.

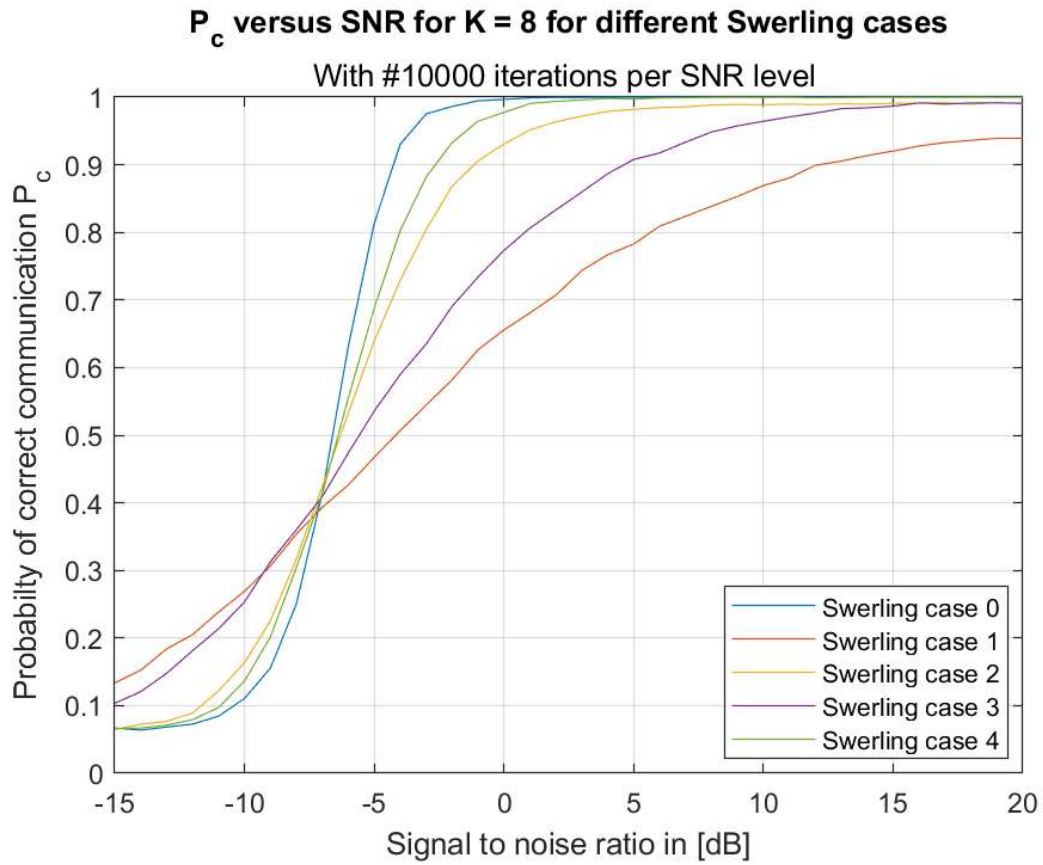
If the SNR level is too low, for instance at -15 dB, the expectation is that the probability of a correct detection is one over the number of symbols. In that case the distribution is uniform with equal chances. This is for 16 symbols a chance of $1/16 = 0.0625$ what is shown in Figure 48b. For the same reason the SER starts at $1-1/16 = 0.9375$. In Figure 48c and d the mean absolute value and the mean variance of the error is calculated. The 16 symbols consist of the values 0 to 15. One of them is correct and therefore the error lays on the interval $\{0,15\}$. At the limit on the left of the graphs the distribution leads to a uniform distribution.

The mean absolute error and variance do not match the uniform distribution. The value of the upchirp is withdrawn from the downchirp therefore the variance and mean are not of a uniform distribution. In MATLAB the mean and variance are simulated. This is performed with a random number on the uniform distributed interval $\{0,15\}$ minus another random number on the same uniform distributed interval. By taking the absolute value of this result the absolute error is calculated. This is repeated 100 million times what resulted in a variance of 12.72 and mean of 5.01. These values are plotted in Figure 48c and d. As is visible in those plots the limit for low signal-to-noise scenarios are those simulated values. However, if the signals are beneath the threshold the noise is too high to have reliably detections and no detection is made.

5.3.8. Swerling cases

All previous simulations are performed with a constant RCS. Fluctuations in the RCS will impact the performance of the TDBRB algorithm. Fluctuations in phase will destroy a coherent integration operation. To compare the different Swerling cases a noncoherent integration is performed. In this section the Swerling case 0 is compared to the other Swerling cases. The algorithm in its current form uses a coherent integration of the pulses and a fixed threshold. For the automotive scenario Swerling 1 and 3 (fluctuations scan-to-scan) are expected however, also the other two Swerling cases with fluctuations from pulse-to-pulse can be simulated. The expectation is that for fluctuations from scan-to-scan the algorithm works properly with coherent integration. In this simulation the assumption is made that in one scan the upchirp burst and downchirp burst experience the same fluctuation. For the pulse-to-pulse fluctuations noncoherent integration should give a better performance. In Figure 49 the influence of the different Swerling cases on the algorithm is shown for different SNR levels and compared to a graph of Harrison [2-06] which was already presented in Figure 12. The expectation for the TDBRB is that the probability of communication is similar as the probability of detection for a regular radar. This similarity is clearly visible in the figure and corresponds to this expectation. The only difference is a signal to noise ratio of approximate 9 dB. The graph of TDBRB is 9 dB shifted to the left. This difference is due to the use of 8 pulses in a burst instead of the single pulse signal-to-noise ratio. This leads to a gain of $10 \cdot \log_{10}(8) = 9.031$ dB.

a.



b.

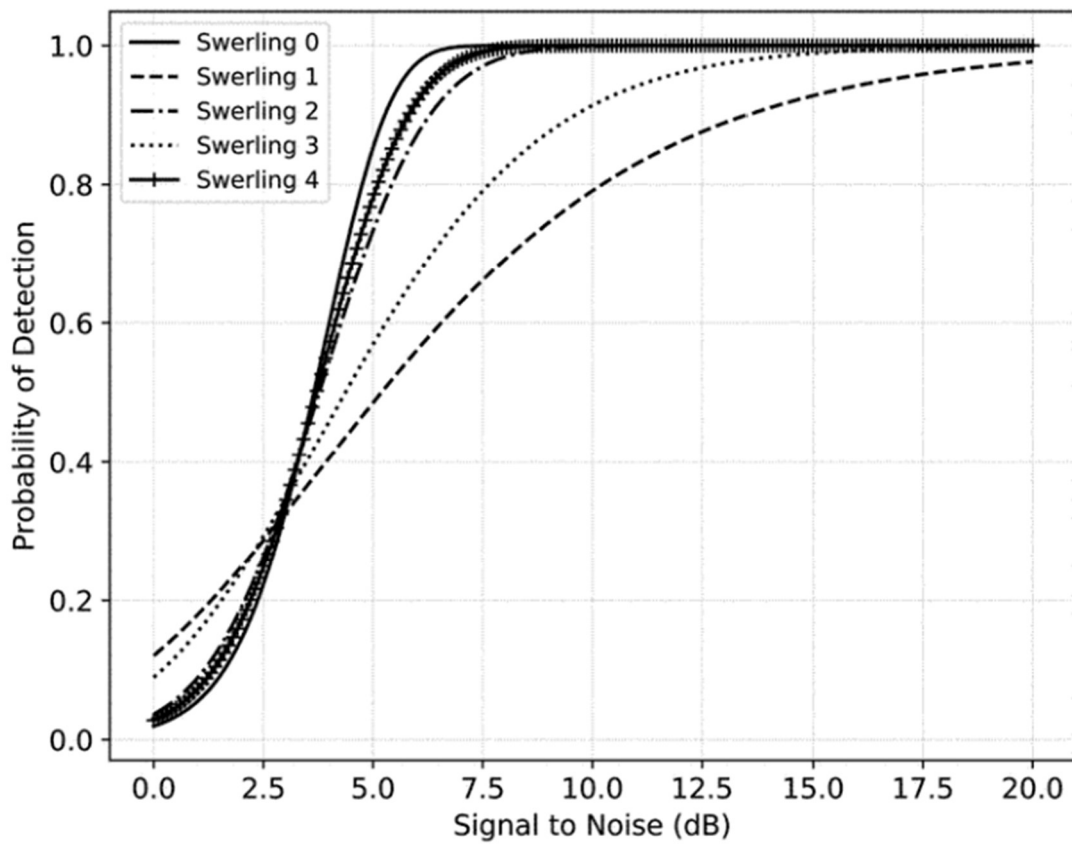


Figure 49 Influence on the SER for the different Swerling cases without coherent integration. a. Simulation. b. Graph from Harrison [2-06].

Swerling case 1 and 3 (fluctuations scan-to-scan) have a worse performance as 2 and 4 (fluctuations pulse-to-pulse). Low RCS reflections for a complete scan will destroy the detection probability. It is also visible that Swerling case 1 and 3 have a better performance as the Swerling case 0 (no fluctuations) in the region with a low SNR. This is due to the possibility that the exponential function gives a higher amplitude due to a higher RCS.

The next step is the influence of the algorithm on the different Swerling cases with coherent integration. In Figure 50 the results of the TDBRB waveform with coherent integration are presented. In Edde [2-02] multiple figures of the probability of detection are presented. The original graphs are presented in Meyer et al. [5-01]. Those graphs exist of three lines: one for Swerling case 0 with the best probability of detection. Swerling case 3 and 4 also give a good performance and Swerling case 1 and 2 give the worst performance. Those lines are also visible in the simulation of the TDBRB algorithm.

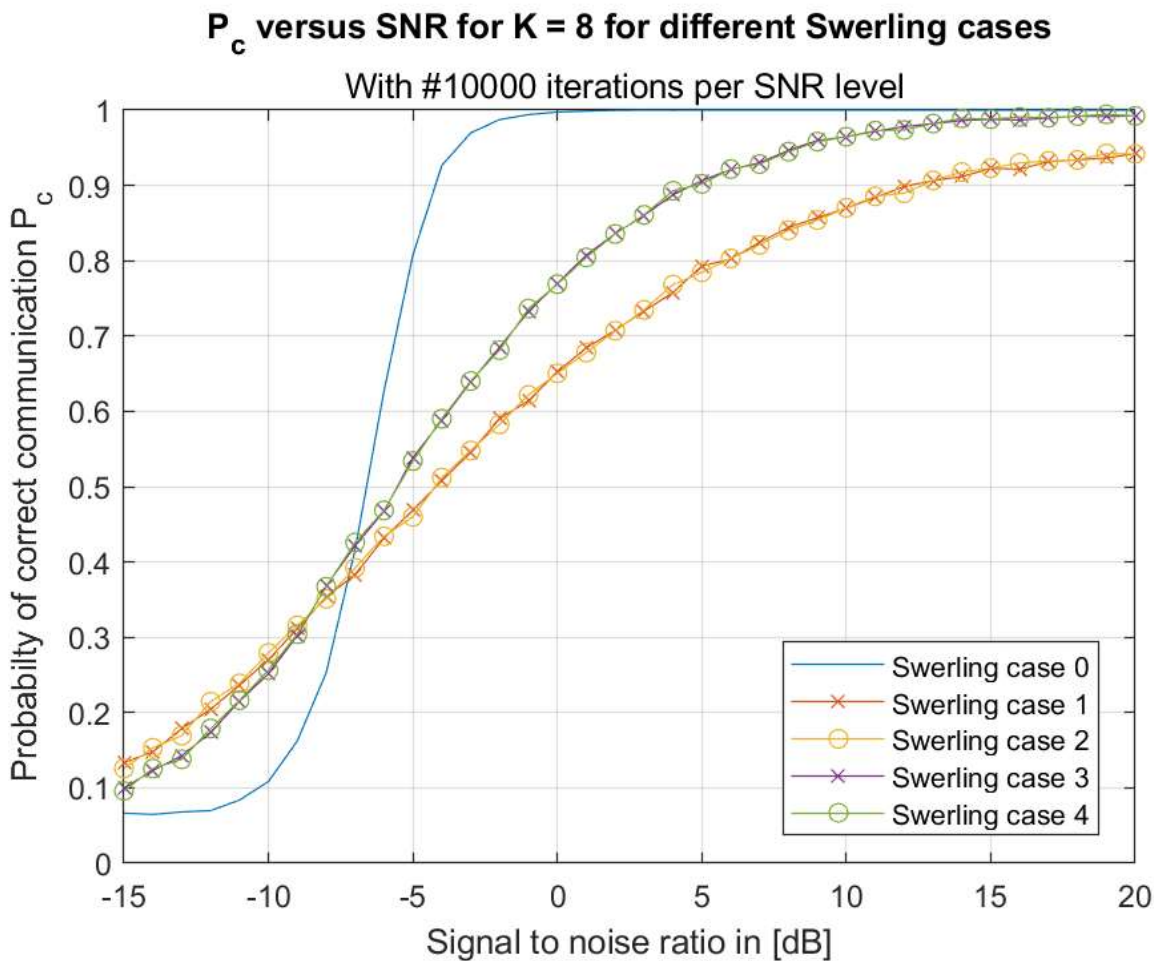


Figure 50 Influence on the SER for the different Swerling cases with coherent integration.

5.4. Discussion and Conclusions simulations

As showed in the simulation the receive radar is able to determine the Doppler frequency. The resolution is limited to the number of pulses in a burst. By using the waveform as suggested in (49) it is possible to perform the coherent integration over multiple bursts. In this waveform the upchirp burst will start every time at the same position inside the relative PRI. In that way the coherent integration can be performed with multiple upchirp bursts what will improve the Doppler resolution.

The threshold for the receive radar is kept the same as for the primary radar to get a similar performance. In that case the receive radar should have similar detection probabilities as the primary radar. Of course, the bistatic RCS can be different for the receive radar as the RCS towards the primary radar. The false alarm rate should be similar as a regular radar; however, the regular radar “knows” that it has sent a signal while the receive radar does not “know” if, or when a signal is transmitted. The information can be detected when it is possible to insert clear headings and footers in the information. In that case the false alarm rate is still high but only when the heading and footer are detected the algorithm shall decide that a detection is done.

The simulation of the different Swerling cases is performed with the same scan-to-scan variation for the upchirp and downchirp. In this thesis the assumption is made that the object-of-interest has a similar Swerling case for the upchirp burst as downchirp burst. The expectation is that the performance is worse when the scan-to-scan variation differs from burst-to-burst. In that case the worst detection of the upchirp or downchirp burst will determine the probability of detection. More simulations can be executed with multiple objects-of-interest to determine the reaction of the combination of different Swerling cases on the performance of the communication.

The first MATLAB simulations are performed with noncoherent integration and with 1 sample per range cell. One conclusion of the simulations is that due to the straddle loss at least 2 samples per range cell must be used. The next step were simulations with coherent integration. For the static case with a max function (without threshold) the best SER was found. This is only feasible in a static communication environment where the distance between transmit and receive radar is fixed on the best performance.

The impact of a higher number of pulses and a longer pulse duration are found. By increasing these variables, the bit or symbol error rates drops. However, this is at the cost of a lower bit rate. By using similar thresholds as a regular radar, the detection probabilities are similar for the primary as receive radar. Errors in the sampling will influence the performance of the communications. When the error is one range cell per PRI the probability of error will be high. With an error which is smaller as 0.5 range cell (this is one range bin) there is an influence, but the error will still converge to zero. The accuracy of the calculated time delay which represents a symbol depends on the SNR. With a high SNR the variance of the error will converge to zero. For the low SNR cases the error will be uniform distributed. Fluctuations in the RCS will impact the performance of TDBRB. Similar results as in literature for regular radar systems are found for the five Swerling cases. This result holds for coherent as well as noncoherent integrated signals.

6 Experiment and comparative analysis

6.1. Introduction

In this chapter the experiment where TDBRB is compared to BPSK modulation is described. The purpose of this experiment is:

- Prove that TDBRB is a communication method where communications with a low SNR can be performed.
- Prove that other communication methods (BPSK) are not suited for communications with a low SNR.
- Prove that reliable communications are possible without line-of-sight (communications over an object-of-interest).
- Prove that the performance of the primary radar is not degraded.

The main constraint of the experiment is the synchronization. Synchronization in time domain, as well as the frequency of the local oscillator. This experiment is performed with the 4 channel Keysight radar system. With this system it is possible to use one channel for the primary radar and another channel for the receive radar. However, this experiment is performed with one system, so the local oscillator and sampling frequency are per definition synchronized (actually the same local oscillator is used). Two images of the TNO logo are used to make the communication visible. These images of the TNO logo are shown Figure 51. Figure 52, on the following two pages, shows the experiment setup for the line-of-sight and non-line-of-sight scenario.

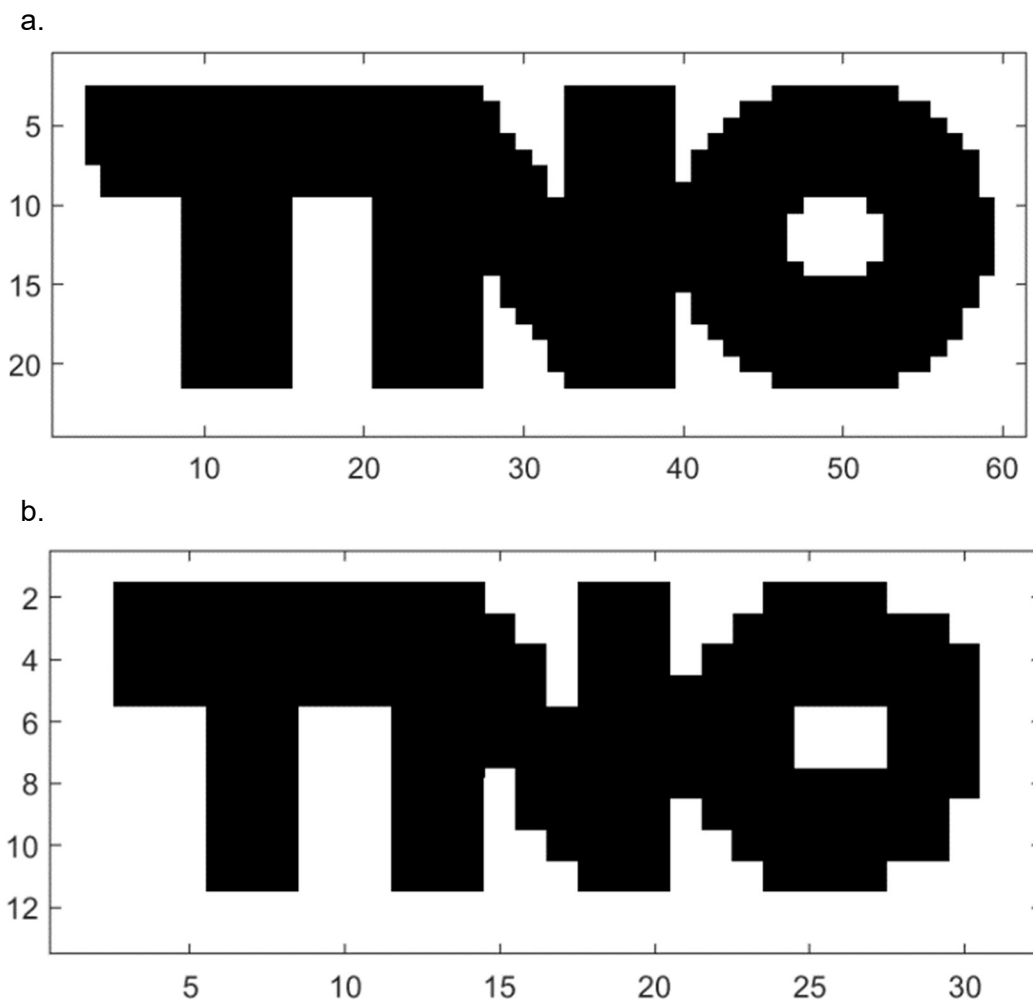


Figure 51 a. Large TNO logo with heading and footer 1528 bits. b. Small TNO logo for $K = 128$ in total 480 bits.

a.



b.

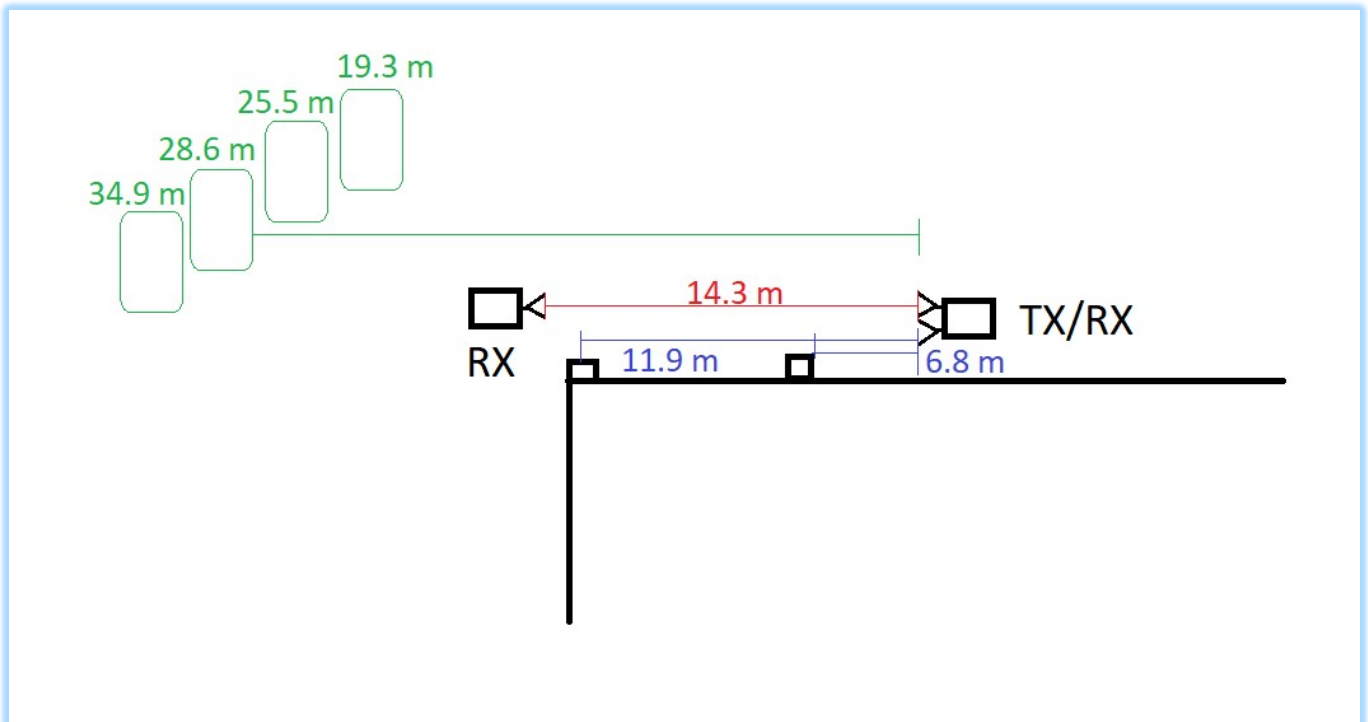


Figure 52 Experimental setup a. Line-of-sight scenario b. Schematic view LOS

c.



d.

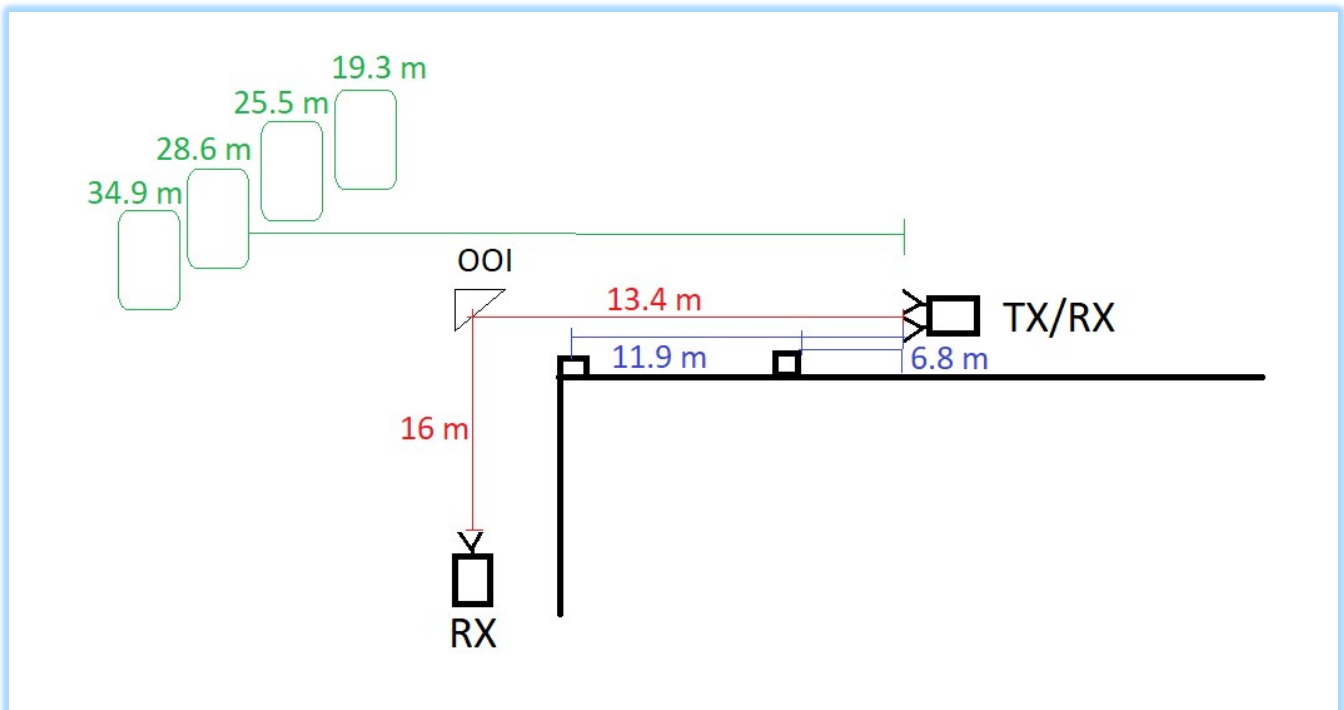


Figure 52 c. Non-line-of-sight scenario d. Schematic view NLOS.

There are two major system setups which both are shown in Figure 52. One with line-of-sight connection. The other without line-of-sight. The receive antenna is in this image not visible. TDBRB shall be compared to BPSK modulated on the carrier frequency. The hypothesis is that with a low signal level or a high noise level TDBRB communication is possible, while with BPSK this is not possible. The transmit power can be decreased, the RCS can be decreased, or the noise level can be increased to achieve this. A reflector as presented in the left image is used as object-of-interest is. In that case an equal amount of energy is scattered to the primary radar as the receive radar. In the line-of-sight of the primary radar multiple cars were parked these are not visible on the images. The distances of the radar to the objects and object-of-interest (OOI) are shown in Figure 52b and d. The receive channel of the primary radar is for both setups (LOS and NLOS) in a regular radar configuration which uses the radar equation as stated in (1). The receive radar has in the line-of-sight setup a line-of-sight connection as in (3). In the other setups the receive radar makes uses of the bistatic configuration as stated in (2).

The experiment is performed with a Keysight M8190A arbitrary waveform generator (AWG) and a Keysight M9703B digitizer. The intermediate frequency (IF) was 1 GHz. An upconverter and downconverter shifted the IF on the carrier frequency of 10 GHz. For this experiment a signal of 20 ms is used. This is generated in MATLAB with a sampling frequency of 640 MHz. This is digitally up sampled in the systems computer. The AWG sampled this signal at 5.67 GHz and digitizer at 2.88 GHz. The system has multiple channels. Three are used: two receive and one transmit channel. The channel which corresponds to the receive radar is connected to the Keysight system with a 40 m cable (eight connected cables of 5 m). Three SAGE Millimeter, Inc. quad-ridged horn antennas (model SAC-0231831225-SF-S4-DP) are used. The antennas have a gain of 12 dBi and beamwidth (3 dB) of 22° in horizontal polarization. Inside the system one central local oscillator is shared between the transmitter and receivers. The received signal (of approximately 20 ms) is digitally down sampled to 640 MHz and saved in the same MATLAB format as the transmit signal. The data are down sampled in MATLAB to 128 MHz for further signal processing.

6.2. Variables

Due to the limitations of the experimental range, as well as the Keysight radar system, alternative variables are chosen comparing to the simulations. The first variable is the maximum range of 37.5 meter which will limit the PRI. The number of range cells is set on 16, this means 32 samples in one PRI. The following parameters are set:

- Maximum unambiguous range (r_{ua}) set for the primary radar on 37.5 m.
- The PRI of one pulse is in that case: $PRI = \frac{2 \cdot r_{ua}}{c} = \frac{2 \cdot 37.5}{3 \times 10^8} = 0.25 \mu s$ and the $PRF = 4 MHz$.
- With 16 range cells the size of time of those cells is: 15.62 ns (0.25 μs /16).
- This leads to the bandwidth of 64 MHz.
- The sample time needs to be 0.5 times the duration of one range cell because of the straddle loss, therefore: 7.81 ns (0.25 μs /32).
- The bandwidth should be doubled because of the straddle loss and therefore the sampling frequency will be 128 MHz.

For the experiment a TNO logo is transformed into a sequence of bits. These logos are presented in Figure 51. A white bin corresponds to a 0 and the black bin to a 1. This bit sequence is placed together with a header and footer (1568 bits in total) inside the 20 ms signal. The bits are converted to symbols. Each 4 bits represent a symbol in the interval {0..15}. The bits are transformed to symbols with the simple binary-coded decimal (SBCD) or BCD 8421 scheme. Those symbols are fitted between the upchirp and downchirp bursts. For the TDBRB the waveform as presented in (49) has been used. In this waveform the first time delay between the upchirp and downchirp is the regular symbol. With a cross-correlation between the upchirp and downchirp this symbol is recovered. However, the same information is doubled because after the downchirp the PRI minus the time delay is inserted. Therefore, the information has been sent twice. Only the symbols are inverted. First the regular symbol is inserted followed by the inversed symbol. The latter information can be retrieved with a cross-correlation where the downchirp and upchirp are shifted.

For BPSK with a data rate of 32 Mbit/s 418 images of the TNO logo fitted in the data. For the TDBRB waveform the data rate depends on the number of pulses in a burst as calculated in (75). The number of images of the TNO logo which fits in the 20 ms signal per waveform are stated in Table 7.

Waveform	Bitrate	Number of figures
BPSK	32 Mbit/s	418
BPSK	16 Mbit/s	209
BPSK	8 Mbit/s	104
BPSK	4 Mbit/s	51
TDBRB K=2	6.4 Mbit/s	41 (and 41 inverted)
TDBRB K=4	3.556 Mbit/s	23 (and 23 inverted)
TDBRB K=8	1.882 Mbit/s	12 (and 12 inverted)
TDBRB K=16	969.7 kbit/s	6 (and 6 inverted)
TDBRB K=32	492.3 kbit/s	3 (and 3 inverted)
TDBRB K=64	248.1 kbit/s	1 (and 1 inverted)
TDBRB K=128	124.5 kbit/s	2 (smaller figures and 2 inverted)

Table 7 Data rate and number of figures per 20 ms signal.

6.3. Bit rate

The bit rates as calculated in Table 7 are correct because the images of the TNO logo are recovered for all different number of pulses in a burst. With this information the bit rates are proved. Also, the calculation inside the MATLAB program gave the calculated bit rate. This was calculated as follows:

$$R_{B,Exp,K<128} = \frac{2 \cdot N_{bit,transmitted}}{t_{figure}} = \frac{2 \cdot 1528}{t_{figure}}$$

$$R_{B,Exp,K=12} = \frac{2 \cdot 480}{t_{figure}} \quad (81)$$

Because the information is doubled two images of the TNO logo (the original and inversed information) are sent. With this information the bit rate is calculated for $K = 4$. The time of a transmission of two images of the TNO logo is 0.859 ms. What leads to a bitrate of 3.556 Mbit/s. And for the small image of the TNO logo with $K = 128$ the duration of two images of the TNO logo is 7.71 ms and this leads to a bit rate of 124.51 kbit/s.

6.4. Demodulation TDBRB

The MATLAB program compares a peak for the first upchirp burst with $K \cdot PRI$ delayed version of the successive downchirp burst and performs the cross-correlation. After this step this is repeated for the first burst with a $(K + 1) \cdot PRI$ delayed version. After this operation the maximum of the cross-correlation is taken and used to determine the inserted delay. Because of the header and footer, the signal can be found and plotted in a MATLAB figure what shows the image of the TNO logo. This MATLAB figure is updated with every demodulated image of the TNO logo and looks like a video when it is processed in MATLAB. The bit error rate and symbol error rate can be calculated. In the MATLAB program the inserted signals in a sequence of symbols and a sequence of bits are available. Where (80) uses the simulated symbol error rate will the following equation give the actual measured SER.

$$SER_{meas} = \frac{\#Errors}{\#Symbols_{trans}} \quad (82)$$

The MATLAB program calculates the mean symbol error rate of all the symbols which are transmitted. Also, the bit error rate can be computed. The expectation is that this rate is lower because one symbol which contains 4 bits can be wrong but still 3 bits can be correct.

The BER is calculated as follows:

$$BER_{meas} = \frac{\#Errors}{\#Bits_{trans}} \quad (83)$$

The receive channel for the primary radar is called Y1. The receive channel of the receive radar is called Y2. The BER and SER of the last images of the TNO logo are presented in the title of the MATLAB figure. The mean BER and SER of all the previous and the last image of the TNO logo are presented in the subtitle. By saving the last figure the mean BER and SER can be found. An example is presented in Figure 53. The incorrect bits are presented as grey bits to visually present the errors. This is performed with the MATLAB commands “pcolor” and “flipud”. The downside of these commands is that the first row and last column are not presented. The BER and SER calculations are made with these column and row and are therefore correct. In Figure 53 after “Figure #” 12 is presented. This means that twelve images of the TNO logo were found in the data. In Appendix B the last MATLAB figures for all the measurements are presented.

Figure # 12 K = 8 Bit error rate = 0.0068306 Symbol error rate = 0.013123
 Mean bit error rate = 0.0093352 mean symbol error rate = 0.017279

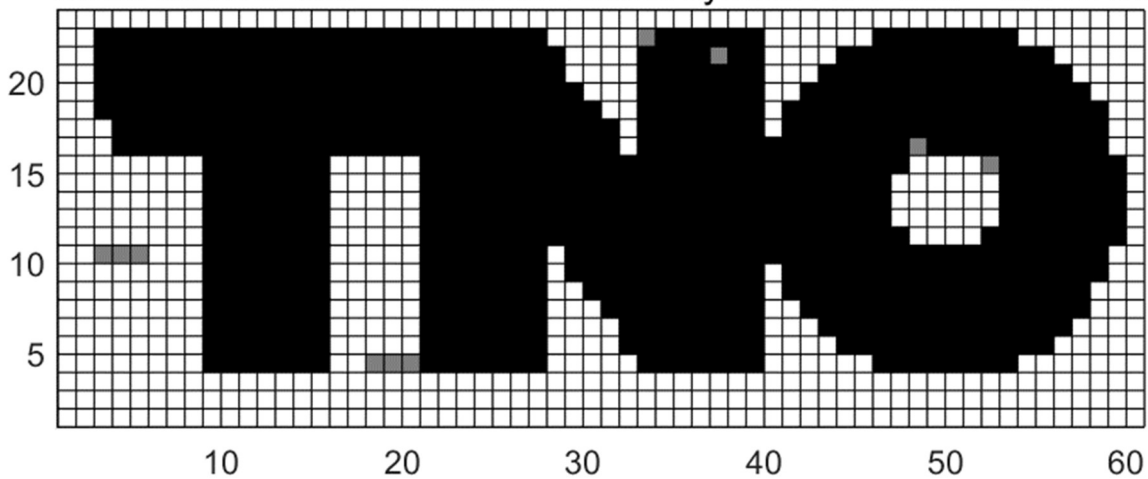


Figure 53 Signal processing result line-of-sight connection of the primary radar (channel Y1) for K=8.

The results for the line-of-sight measurement are presented in Table 8 the BER and Table 9 the SER.

Waveform	Primary (Y1)	Receive (Y2)
TDBRB K=2	0.090264	0.081417
TDBRB K=4	0.051328	0.0994
TDBRB K=8	0.0093352	0.0076275
TDBRB K=16	0.0081967	0.00045537
TDBRB K=32	0.004326	0
TDBRB K=64	0	0
TDBRB K=128	0	0

Table 8 LOS TDBRB mean bit error rate.

	Primary (Y1)	Receive (Y2)
TDBRB K=2	0.18578	0.16318
TDBRB K=4	0.08456	0.21146
TDBRB K=8	0.017279	0.018591
TDBRB K=16	0.014873	0.0017498
TDBRB K=32	0.0069991	0
TDBRB K=64	0	0
TDBRB K=128	0	0

Table 9 LOS TDBRB mean symbol error rate.

In Table 10 the mean BER of the non-line-of-sight are shown for the different TDBRB waveforms with different number of pulses in a burst. The same calculation is performed for the SER. This is presented in Table 11.

Waveform	Primary (Y1)	Receive (Y2)
<i>TDBRB K=8</i>	0	0.03514
<i>TDBRB K=32</i>	0	0.0015938
<i>TDBRB K=64</i>	0	0
<i>TDBRB K=128</i>	0	0

Table 10 NLOS TDBRB mean bit error rate.

Waveform	Primary (Y1)	Receive (Y2)
<i>TDBRB K=8</i>	0	0.068533
<i>TDBRB K=32</i>	0	0.0034996
<i>TDBRB K=64</i>	0	0
<i>TDBRB K=128</i>	0	0

Table 11 NLOS TDBRB mean symbol error rate.

In the tables it is clearly visible that for higher number of pulses in a burst the bit error rate drops. This can be seen in both the LOS as NLOS setup. Another remark which can be made is the difference between LOS and NLOS performance especially for the primary radar. No errors occur for the highest number of pulses in a burst in the LOS scenario. On the contrary in the NLOS scenario no errors occur for the primary radar.

6.5. Regular radar performance

The regular performance of the primary radar can be shown by the range plot of the primary radar. In Figure 54 the range plot of all the radar bursts for the transmission of one TNO image is shown. The radar bursts are matched filtered and noncoherent integrated. The results for the upchirp are presented in the upper figure. In the bottom figure the same result for the downchirp is shown. The upchirp gives a high reflection for all the 382 range plots (the number of symbols used to transfer the image) around 14.3 m where the receive radar is located (see the experimental setup in Figure 52). The downchirp burst results are not corrected for their time delay. The primary radar “knows” when it transmitted the downchirp burst and can therefore correct for this delay and make a similar plot for the upchirp. In this figure the working of the TDBRB algorithm is clearly visible. The range plot of the downchirp is delayed for the different symbols. Therefore the peaks at different ranges for the downchirp occur.

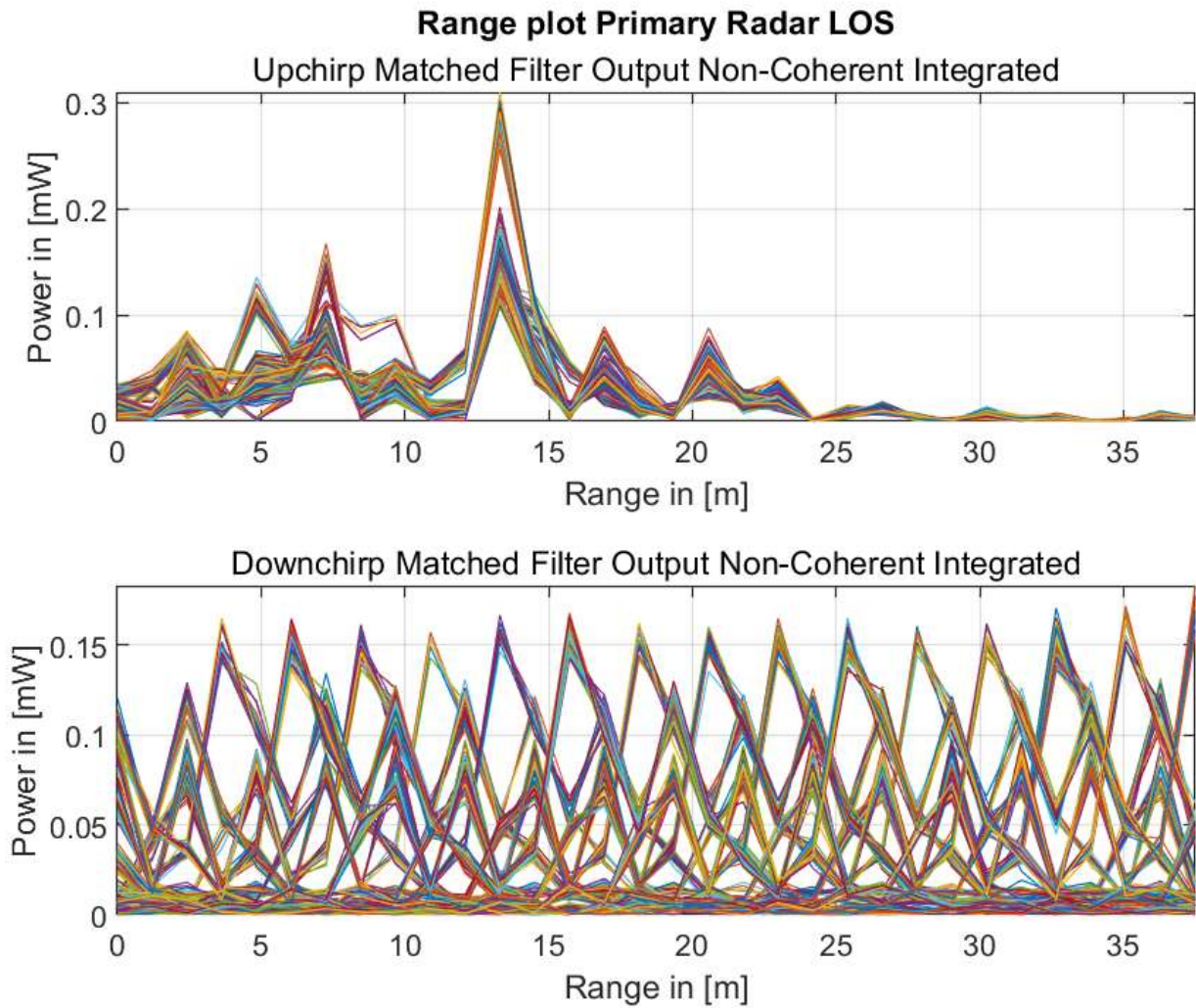


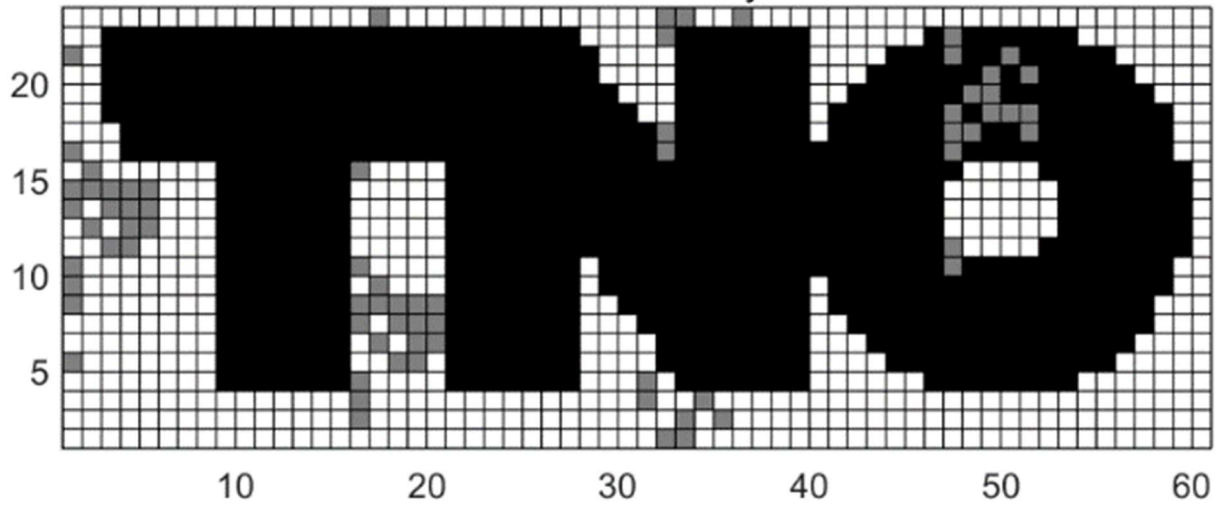
Figure 54 Regular radar performance primary radar with $K = 8$ and Line-of-sight scenario.

6.6. Doubled bit rate

To prove that bit rate is twice as high the recovered data for $K = 4$ are presented in this section. Because the waveform in (49) is used where, after the upchirp downchirp combination, an extra time delay with the duration $T_{PRI} - T_D$ is added. Therefore (46) first the cross-correlation is changed. In the inversed version the downchirp is compared to the following upchirp (K) and the upchirp response one PRI ($K+1$) later. This operation is done by withdrawing the received symbol of 16. For example, in that way the symbol 0 becomes a 15, a 13 becomes a 2 and an 8 will become a 7. In Figure 55 the regular and doubled image for 4 pulses in a burst is shown. The BER looks similar, and the SER is better (+0.029) for the inversed signal.

a.

Figure # 23 K = 4 Bit error rate = 0.051913 Symbol error rate = 0.08399
Mean bit error rate = 0.051348 mean symbol error rate = 0.08456



b.

Figure # 23 K = 4 Bit error rate = 0.051913 Symbol error rate = 0.081365
Mean bit error rate = 0.053635 mean symbol error rate = 0.082164

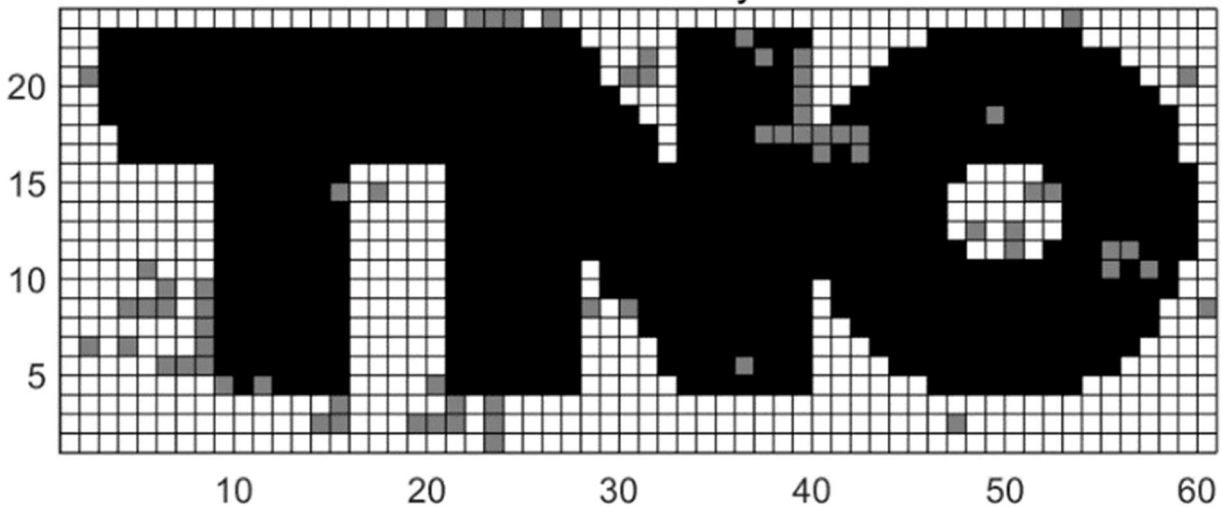


Figure 55 a. Regular figure primary radar line-of-sight retrieved K=4 b. Figure with inversed data.

6.7. BPSK experiment

To compare the TDBRB joint radar and communication waveform with other methods a simple BPSK waveform is chosen. The BPSK signal consists of -1 and 1 multiplications of the carrier (10 GHz). The signal is sampled at the same sampling frequency as TDBRB (128 MHz). For the 32 Mbit/s signal this means an integration gain of 4 (128 MHz/32 Mbit/s). This is the same gain as the matched filtering gain of the TDBRB setup. The signal is a continuous signal while TDBRB uses pulses with 1/4 PRI duration. Therefore, the actual bitrate is 8 Mbit/s when BPSK uses pulses with the same duration. The bit synchronization is performed in MATLAB by shifting the signal and the best BER was found in the data. The BER and SER are stated in Table 12 and Table 13. The corresponding figures are stated in Appendix B. The received signal of the NLOS scenario for both channels contained only 399 of the 418 figures. When we compare these results to TDBRB communication we see that the bit rate is higher for BPSK. However, the BER and SER are higher for BPSK when we compare it to a $K = 64$ or $K = 128$ TDBRB waveform.

	Primary (Y1)	Receive (Y2)
BPSK 32 Mbit/s LOS	0.00097557	0.013656
BPSK 32 Mbit/s NLOS	0.0019362	0.051421

Table 12 BPSK mean bit error rate.

	Primary (Y1)	Receive (Y2)
BPSK 32 Mbit/s LOS	0.0039023	0.052985
BPSK 32 Mbit/s NLOS	0.0077448	0.19374

Table 13 BPSK mean symbol error rate.

6.8. Discussion experiment

It looks that the downchirp had a larger amplitude as the upchirp in the time domain data. In the frequency domain there is a response of the upchirp on the downchirp. The matched filter for the upchirp gives a response on the downchirp. In this case the power of the downchirp looks larger as the upchirp and therefore the response of the matched filter of the upchirp is matched up with the downchirp signal. Also, because the matched filter gain (bandwidth pulse duration product) was low. In this case 4. A higher matched filter output will solve these problems. This higher matched filter gain is therefore recommended for proposed applications. Other measures can be used to prevent this. For instance, both signals should have a similar amplitude and it is better to use more orthogonal signals for the bursts. This can also be solved with another frequency range or phase coding. For the transition from symbols to bits the BCD 8421 scheme is used. With the binary reflected Gray code (BRGC) of Gray [6-01] the bit rate can probably be improved. In BRGC every successive symbol differs one bit. With BRGC only one bit is wrong if the error of the time delay is one range cell. This can be useful in TDBRB because in the simulation of the accuracy it is shown that the absolute error will rise when the SNR decodes.

For the low SNR cases with a low number of pulses in a burst it is better to use a fixed relative PRI comparison. The BER and SER for $K = 2$ were very high when the algorithm makes a choice if it uses the difference of K PRIs or $K+1$ PRIs. For $K = 2$ the best performance was with a fixed difference between the comparison of the upchirp range profile with the downchirp range profile with $K+1$ PRIs difference between them. The bit error rate of the high number of pulses in a burst ($K = 64$ and $K = 128$) is 0. This means no error is detected. The bit error rate is not precisely defined in that case because the number of bits which are transmitted is very low. For $K = 64$ only 1528 bits are transmitted and $K = 128$ only 960 bits. Therefore, the BER for $K = 64$ is less than $1/1528=0.0006545$ and for $K = 128$ less than $1/(2 \times 480) = 0.0010$. Although all the BER of 0 is found 4 times in the different measurements (Y1, Y2 and LOS and NLOS). The experiment has to be repeated more times to find the actual BER.

In Figure 54 the regular radar performance of the primary radar with $K = 8$ for the line-of-sight scenario is presented. In that figure the result for all samples is shown. In Figure 56a the same result is presented where 2 samples per range cell are used. In this plot only 15 peaks for different symbols for the downchirp are shown, while 16 different symbols are transmitted. The first thought is that this is incorrect. This is not the case. In Figure 56b the histogram for the transmitted and decoded symbols is shown. Symbol 11 is not inside the symbols which are transmitted in the TNO image. The peak of the main reflection of the upchirp is at range cell 5. The time delay for symbol 11 is 11 range cells. Therefore, the main reflection is expected at range cell 0. Because this is not detected nor transmitted there is no peak at range cell 0.

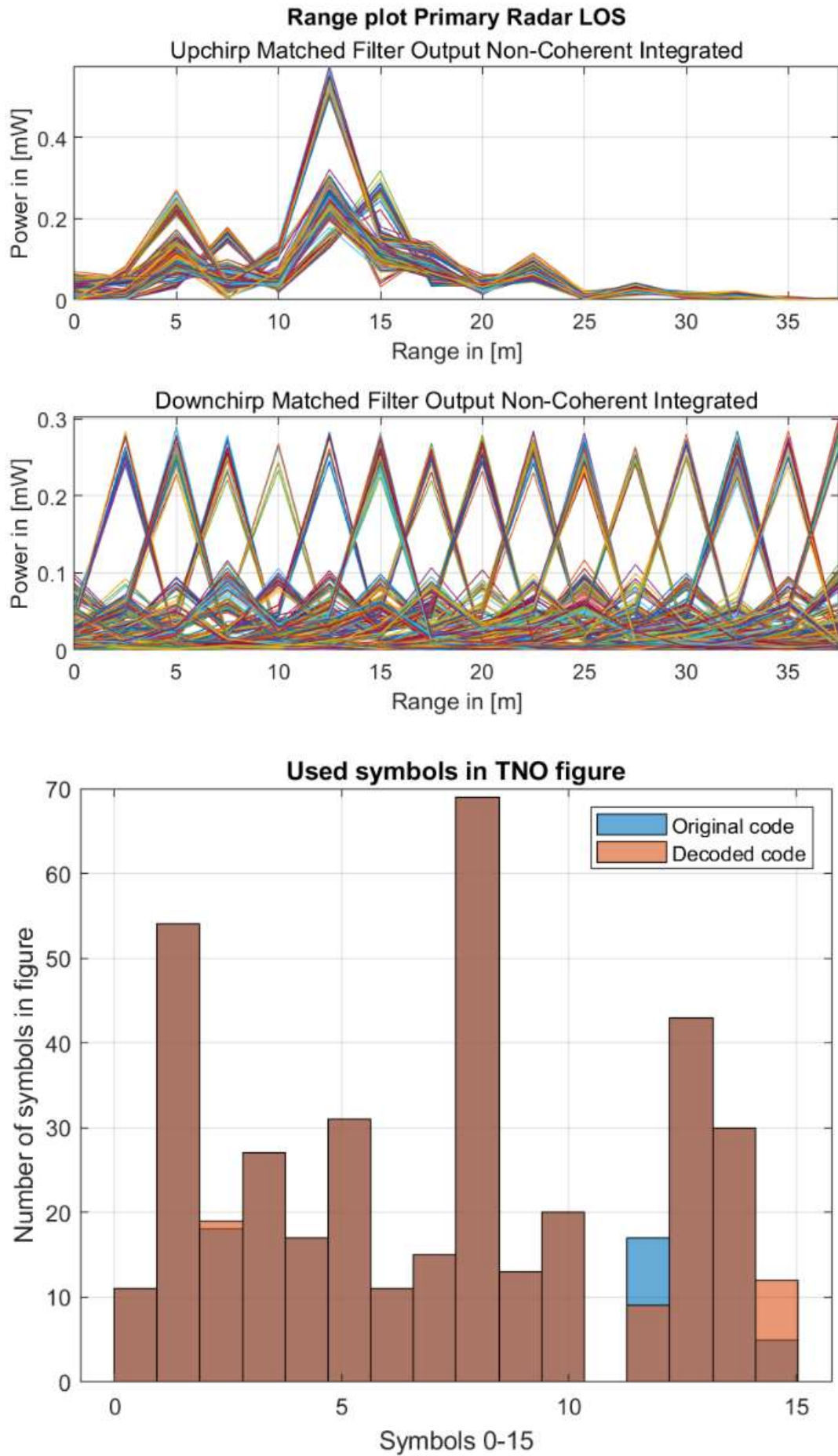


Figure 56 Discussion symbols for Primary Radar. a. Range plot with 2 samples per range cell. B. Histogram decoded and transmitted symbols.

6.9. Comparative analysis

In this section the results of the simulations and the experiment of TDBRB are compared to the other waveforms PC FMCW and LFM-MSK. The proposed TDBRB is compared to the PC FMCW technique as presented by Kumbul in [3-26] and [6-02].

	TDBRB (K = 2)	PC FMCW
<i>Bit rate</i>	6.4 Mbit/s (measured)	<1 Mbit/s [3-26]
<i>Distance</i>	37.5 m	100 m [3-26]
<i>Number of matched filters</i>	2	1 [3-26] up to 1024 [6-02]
<i>Communication hardware</i>	Not necessary	Necessary
<i>Sensing primary radar</i>	Available	Available
<i>Sensing receive radar</i>	Available*	Not available
<i>Bit error rate</i>	0.051 (measured)	Similar as BPSK [3-26]
<i>Communication type</i>	Non-line-of-sight	Line-of-sight

Table 14 Short range TDBRB versus PC FMCW *with more bistatic information and synchronized local oscillators.

Also, TDBRB is compared to the LFM-MSK technique as proposed by Dong in [3-27] for the long distance scenario. For this scenario the variables as PRF and number of pulses for TDBRB are set equal to LFM-MSK.

	TDBRB	LFM-MSK
<i>Number of pulses</i>	128	128 (64 after MSK operation)
<i>Bit rate</i>	62 bit/s	>25 kbit/s
<i>Distance</i>	400 km	400 km
<i>Number of matched filters</i>	2	1
<i>Communication hardware</i>	Not necessary	Necessary
<i>Sensing primary radar</i>	Available	Available
<i>Sensing receive radar</i>	Available*	Available*
<i>Communication type</i>	Non-line-of-sight	Line-of-sight
<i>Communication power</i>	21.1 dB gain (K = 128)	Similar as BPSK
<i>Bit error rate</i>	0 (measured)	Similar as BPSK

Table 15 Long range TDBRB versus LFM-MSK *with more bistatic information and synchronized local oscillators.

The main conclusion is that TDBRB is the only method which is able to have communications without line-of-sight and in low SNR scenarios. If the other methods are not able to transmit data because their energy per bit is too low TDBRB is still able to transmit data, however with a low bit rate (62 bit/s for the setup as presented in Table 5). Compared to the other methods TDBRB communication does not need communication hardware and can be implemented in current radar systems with a software modification.

6.10. Conclusions experiment and comparative analysis

The bitrate is correct calculated and proved with the experiment. To determine the bitrate of TDBRB communication (75) can be used. The BER and SER improves with a higher number of pulses in a burst. For low SNR or non-line-of-sight scenarios the waveform is suited because the BER and SER decreases when more pulses in a burst are used. BPSK or other communication methods which uses the energy of one bit are not suited for low SNR scenarios because the BER and SER cannot be improved. In that case the energy per bit must be higher. On the contrary with coherent integration of multiple pulses of a burst in TDBRB this is possible. The regular radar performance of the primary radar is not degraded with TDBRB. This experiment proves that the primary radar can simultaneously perform communication and ranging tasks without additional hardware or degradation of its performance. TDBRB communication has a better BER and SER than BPSK when the matched filtering gain and number of pulses are increased. The comparative analysis and the experiment show that TDBRB is the most suited method to have communications without line-of-sight and in low SNR scenarios.

7 Applications

7.1. Introduction

In this chapter the applications which are possible with TDBRB, and possible problems are presented. The simplest scenario is with a fixed position of the primary radar and a mobile receive radar. For instance, a radar on top of a lighthouse as presented in Figure 57. From there both radars can start to be mobile. All objects-of-interest are mobile, although they can be standing still.



Figure 57 Lighthouse "de Brandaris" on the isle Terschelling – picture made by the author

7.2. Stationary primary radar scenario

TDBRB is useful in a stationary scenario. For instance, a maritime surveillance radar. When the primary radar is a rotating radar at a fixed and known position. If it transmits the TDBRB waveform as the light of a lighthouse with a known schedule. It can be used as a cooperative hitchhiker radar network. Every lighthouse has its own light characteristics which are known by the mariners and used for navigation. The TDBRB signal of the primary radar is known at the receive radar like the light characteristics of a lighthouse. These characteristics include the frequency, bandwidth, PRI, and number of pulses in a burst.

Every time when the primary radar detects an object-of-interest it sends an inserted time delay which corresponds to the range of this object-of-interest. It does not send an inserted time delay if the primary radar does not detect an object-of-interest. In this way the only degradation of the primary radar is when an object-of-interest is detected. The receive radar is continuously scanning in all directions to detect an upchirp of the primary radar. This is done with its multichannel system which has a 360° coverage. In this way it can detect an upchirp followed by a downchirp at a certain angle. The receive radar can plot this information with the knowledge of the rotating schedule and the first cooperative hitchhiker radar network is a fact. Additional information with the detected bistatic velocity can be processed. Because the primary radar is stationary and the receive radar "knows" its own velocity the bistatic velocity can be processed to a calculated velocity of the object-of-interest.

7.3. Automotive scenario

The automotive scenario is a more complex scenario. Both radars and all objects-of-interest are mobile, although they can be standing still. The range for this scenario is maximal 200 meters. The azimuth is maximal 180° , although practical 150° can be used. The scenario can possibly use a limited elevation angle although this will not exactly contribute to the problem. For instance, the automotive front radar of a car (primary radar) to an automotive back radar (receive radar) of another car or e.g., an automotive front radar of one car to the automotive front radar of an oncoming car.

In the automotive scenario the objects-of-interest include cars, bicycles, and pedestrians. The speed range is respectively 0-200 km/h, 0-40 km/h, and 0-15 km/h. The RCS of pedestrians can be considered as low, the RCS of bicycles is higher, and the RCS of cars is high. The influence of the RCS geometry, with respect to the position of both radars in relation to the object-of-interest, can be considered.

Swerling cases are also used in the automotive scenario. Specifications of the most likely Swerling cases for the automotive scenario are mentioned in the book of Gamba [7-01]. In most cases the vehicles follow Swerling case 1 (a constant RCS within the scan, however different RCS from scan to scan). Additional to this Swerling case 3 is often found where 4 degrees of freedom will influence the probability density function.

In Figure 58 the automotive 2-dimensional (2D) geometry is shown for two cars. Where the car in the middle can be seen as the primary radar and the other car as object-of-interest. The angles can be presented relative to the driving direction of the car or to the North. In the last case both radars should have a compass or Global Positioning System (GPS) available. This can be the receive radar in the line-of-sight scenario. Figure 59 represents an intersection where the primary radar has no direct path connection to the other cars (objects-of-interest). In this case there is a non-line-of-sight connection from a building which can be used for communication.

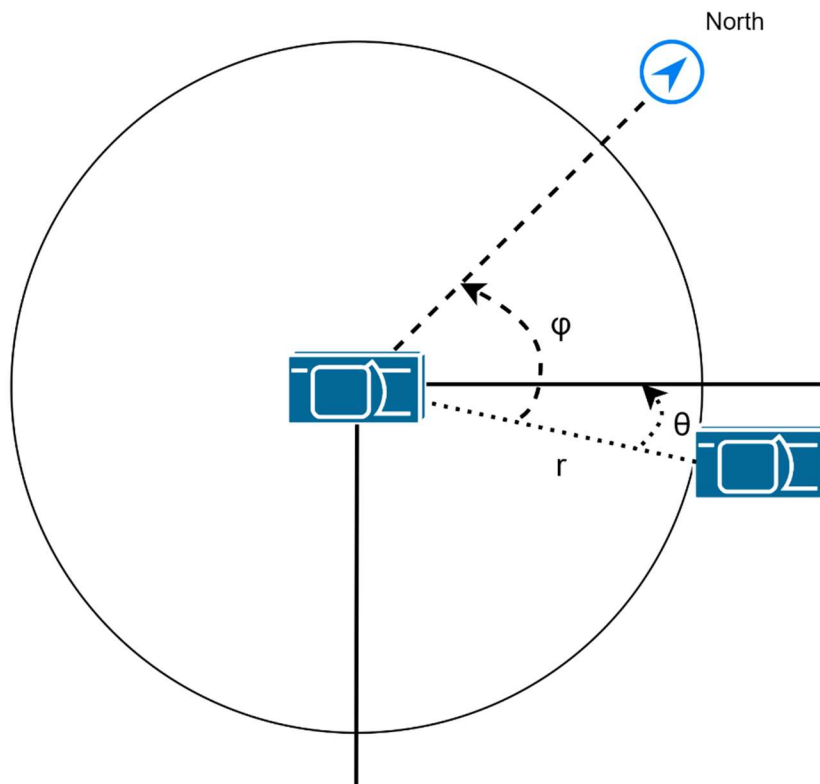


Figure 58 2D automotive geometry with 2 cars. Where r is the range between the car in the middle and the other car. Angle φ is the angle between the cars related to the geographical North and angle θ related to driving direction of the car in the middle.

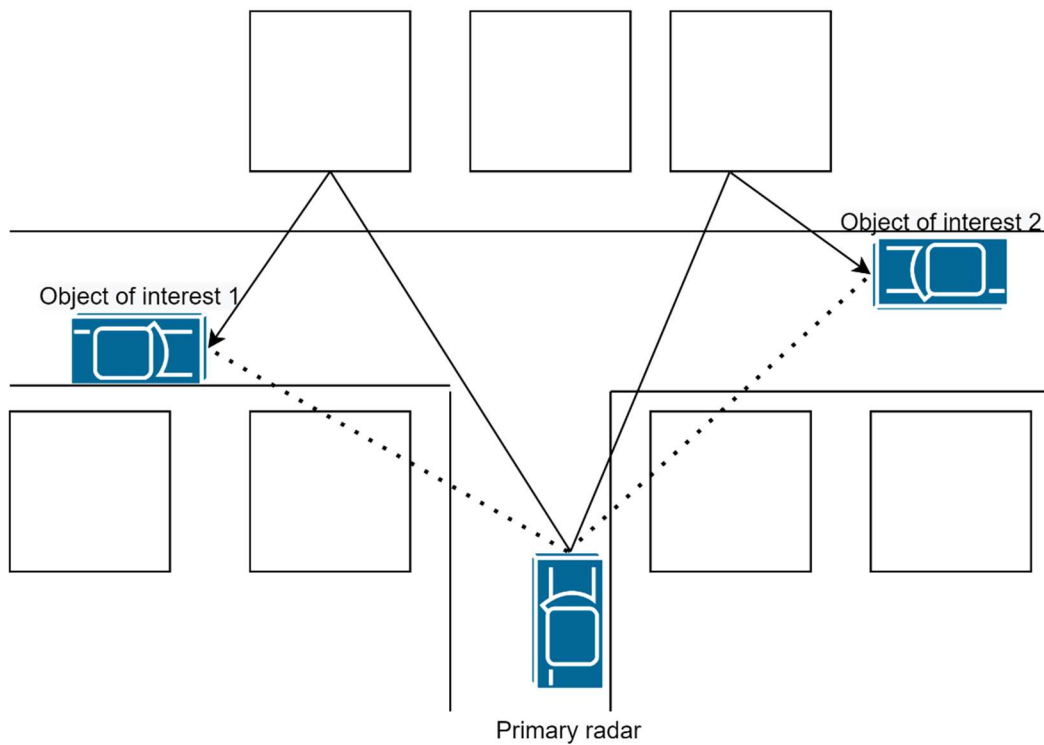


Figure 59 2D automotive geometry with 3 cars. Where one car is the primary radar, and the two other cars are objects-of-interest. In this figure the dotted line represents the line-of-sight connections which are not possible due to the squares which represents buildings. The black line with an arrow represents the non-line-of-sight connection which can occur due to the scattering of the signal on the buildings.

Operating the primary radar with TDBRB in a similar way as for the stationary primary radar scenario is possible however the characteristics of the primary radar are not known at the receive radars. If multiple channels can be used and the different cars switch to unoccupied channels the TDBRB waveform can be useful. In that case the same processing as a hitchhiking radar must be performed. Although it can also be used to send warning or information messages like in the geometry in Figure 59.

7.4. Bistatic operation

The TDBRB waveform can also be used in a mobile scenario where two radars are working together. With other communication methods the bistatic operation can be led. In that way both radars can point their antenna gain on the same point. In this setup the primary radar can use the inserted time delay to transfer information or its detected distance of the object-of-interest.

The bistatic Doppler frequency or bistatic radial velocity can be calculated at the receive radar side. The receive radar can calculate the velocity of the object-of-interest when more (a priori) data are available of the primary radar like heading and velocity. Additional information from the primary radar like the radial measured velocity of the object-of-interest can be used to determine the heading and speed of the object-of-interest.

7.5. Possible problems

Multiple objects in the direction where the primary radar is transmitting will complicate this scenario. All the objects will scatter the information signal. In the scenario where information concerning one object-of-interest (for instance object-of-interest 2 in Figure 60) is transmitted from the primary radar in the direction of object-of-interest 2 an ambiguity, to which object-of-interest the information belongs to (instance object-of-interest 1, 2 or 3), is introduced. This is shown in Figure 60. Ambiguities in information can occur in the system design where information regarding a certain object-of-interest is transmitted via the object-of-interest to the receiver. This happens when this information is scattered by other objects-of-interest or by unwanted reflections of clutter. On the receive side information can be correlated to the wrong objects-of-interest.

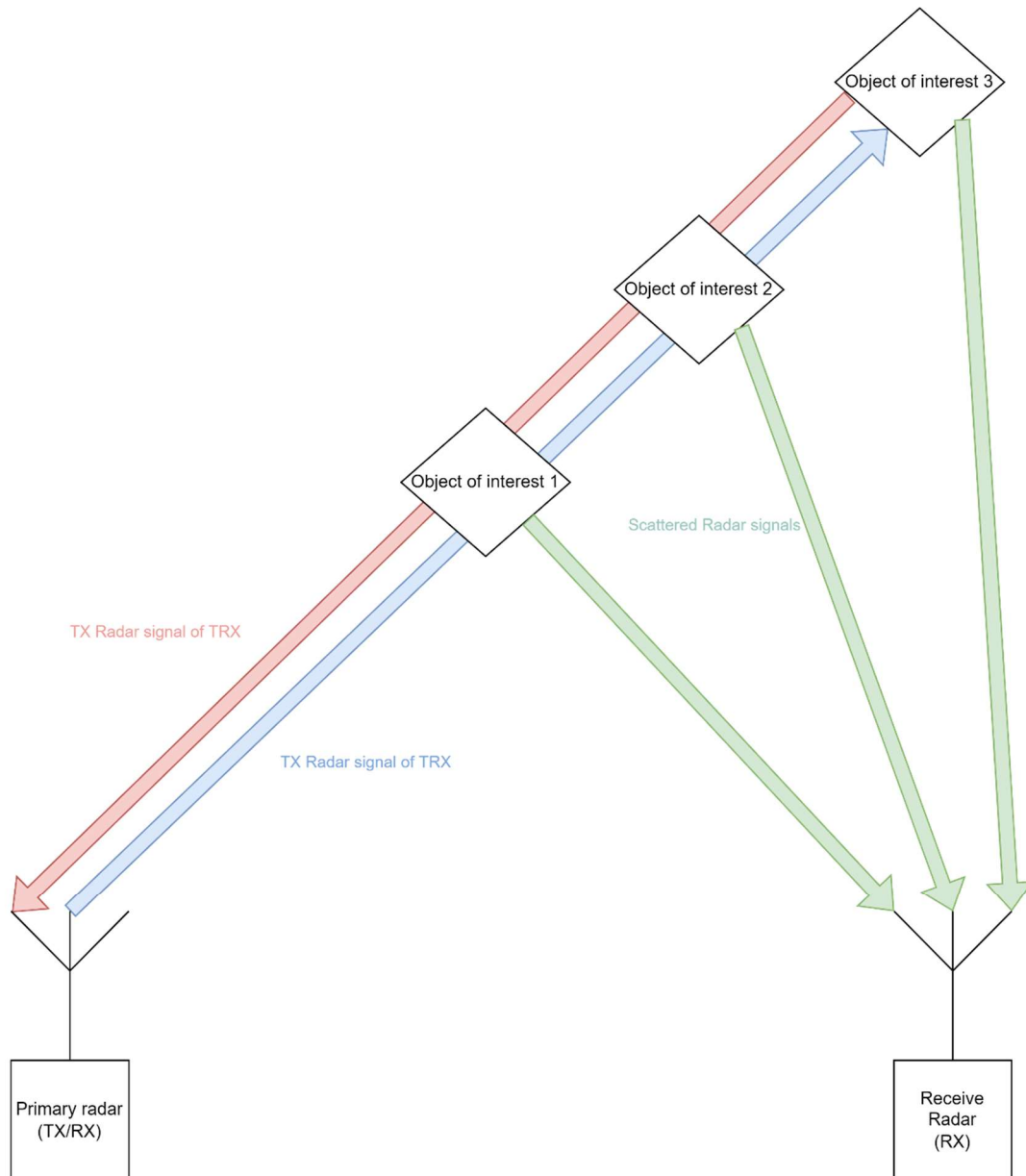


Figure 60 Multiple objects-of-interest with a scattering of the waveform with information towards the receive radar.

It is possible to solve this problem with TDBRB when it operates by sending an inserted time delay which corresponds to the distance of a detected object-of-interest. In the case the primary radar detects two objects-of-interest it transmits first the time delay between the first two bursts of the first object-of-interest. After the second burst it sends a time delay which corresponds to the distance of the second object-of-interest and so on. In that way it should be clear for the receive radar that there are two objects-of-interest,

7.6. Only communication application

The TDBRB can also be used in only communication applications. In that way it is possible to use the high power and the antenna gain of the radar in combination with the coherent integration and matched filtering gain. In this communication setup it is possible to communicate in low SNR environments or with a reflection on a surface.

8 Conclusions

8.1. Introduction

In this chapter, the conclusions are drawn upon the main research questions. Also, the limitations and future work are described. The objective of the thesis is to research techniques for a radar network where one radar transmits and performs its regular operation (primary radar), and one or more radars are only in receive mode (receive radars). The following questions are researched:

1. What techniques can be used to build a radar network, where one radar transmits and another radar only receives, for both radars to build up situation awareness with minimal adjustments to the primary radar task?
2. What radar waveform is suited of performing both radar sensing and communications in low signal-to-noise ratio environments for both radar as communication tasks, and what is the performance of the waveform?

When these questions are answered a new cooperative hitchhiker radar network with communications can be engineered to reduce interference, benefit from dual use of the EM spectrum and profit from bistatic scattering objects. The method of this thesis is firstly, to simulate and evaluate the performance of the proposed waveform and secondly, perform an experiment to verify the results from the simulations, and compare the results to other waveforms found in literature.

8.2. Main conclusions

There are many techniques to modulate communication signals on a sensing waveform. However complex communication hardware is needed or degradation in the performance of the primary radar makes them not useful for the proposed radar network. The current techniques make use of the energy of one bit or one pulse. For similar performance of the primary and receive radars the information should be send without line-of-sight communications and over the object-of-interest.

In this thesis a new waveform is proposed: time delay between radar bursts. This method is based on two similar radar systems where local oscillators are synchronized. The primary radar transmits, and the other radar only receives. By using an upchirp LFM burst of pulses followed by a downchirp LFM burst of pulses, it is possible to insert a time delay between them. This time delay can be used to encode information. When multiple TDBRB waveforms are transmitted after each other a data stream is created.

In the proposed radar network, the receive radar is a multichannel system which has a 360° coverage. The receive radar scans in all directions at all times to determine if there is an upchirp detected. Therefore, all received signals are matched-filtered and Doppler processed. When an upchirp burst is detected, the radar will determine if also the downchirp is detected. The threshold can be similar to the threshold of the primary radar, for instance on 13 dB to create a probability of detection of 0.9 and a probability of false alarms of 1×10^{-6} . The detection probability of the primary radar and the receive radar are similar when other parameters of the radar like antenna gain and radar cross section of the object-of-interest are similar. When both signals are detected for a certain angle of arrival the maximum of their response is compared to each other with a cross-correlation. This operation is performed on a relative interval of one PRI. In this way, the inserted time delay is recovered, and the transmitted symbol is found. With this system setup, it is possible to communicate without a fixed timing schedule.

TDBRB is a communication method where communications with a low SNR can be made where other communication methods (like BPSK) are not suited. Other methods use the power of one pulse or one bit to communicate what leads to a low SNR. With TDBRB communications can be made in a low SNR scenario by increasing the matched-filtering gain and or the number of pulses in a burst. With TDBRB the performance of the primary radar is not degraded, and communications can be performed without degradation of the primary radar. In this way, a cooperative hitchhiker with communications system is possible. Another way to use this waveform is without sensing and only for communication purposes. Reliable communications are possible without line-of-sight with a high matched-filtering gain and coherent integration gain. In this way, it is possible to have communications over an object-of-interest. It is possible to detect a moving object-of-interest and have communications over it. It is also possible to determine the bistatic velocity when more a priori information is known.

8.3. Conclusions on additional research questions

In this section the conclusions of the additional research questions are presented. For a radar network of opportunity, the bistatic radar equation should be solved. Therefore, as much information from the primary radar as possible should be known at the receive side. This information should contain velocity of the primary radar and direction of transmission. To perform coherent integration, the local oscillators of the primary and receive radar must be synchronized for TDBRB. To prevent straddling loss two samples are used per range cell. In that way, it is still possible to detect the inserted time delay when there is an offset at the start of the sampling time. The sampling frequencies of the primary radar and receive radar must be the same. Fluctuations in the timing of the samples, where the start of a new pulse repetition period is kept the same, leads to minor degradation in the bit error rate.

When there is a line-of-sight connection many techniques can be used, and a high data rate and low bit error rate can be achieved. For instance, PARC and LFM-MSK can be used but they require adjustments to the radar and use the energy of one bit or pulse. However, when in the low SNR scenario (especially when there is no line-of-sight connection) only TDBRB is suited. BPSK waveforms influence the detection performance of the primary radar because of its higher sidelobes and is therefore not useful.

The main measures to determine the performance of the information are the bit rate and bit error rate. The radar performance should not degrade. Therefore, the primary radar should be suited to perform its own radar operation with low SNR. Simulations and the experiment with the TDBRB showed that by increasing the number of pulses in a burst and the matched-filtering gain (increase pulse duration or bandwidth) the bit error rate or symbol error rate drops. Due to straddling loss only half of the number of samples can be used as communication symbols. The accuracy of the waveform is proportional to the inversed square root of the signal-to-noise ratio. Simulations showed that by using a threshold the false alarm rate is reduced. The maximal bit rate of the TDBRB waveform is increased by increasing the pulse repetition interval, increasing the number of range cells (higher sampling frequency and bandwidth), and reducing the number of pulses in a burst. In (75) the mean bit rate \overline{R}_B is derived:

$$\overline{R}_B = \frac{N_{bit} \cdot PRF}{(K + \frac{1}{2})}$$

The maximal bit rates were verified with the experiment. One of the results of the experiment is a bit rate of 3.5 Mbit/s and a symbol error rate of 0.05 for 4 pulses in a burst with 16 different symbols and a PRF of 4 MHz. Simulations of the novel TDBRB waveform with and without coherent integration and Doppler processing for the five different Swerling cases resulted in similar results as a regular radar.

The symbol error rate or bit error rate determines the robustness of transferring the information. TDBRB communication uses a similar method as the primary radar to detect an object-of-interest. The matched-filtering gain and coherent integration gain for the communication are similar as for the primary radar to detect an object-of-interest. Therefore, for communications without line-of-sight the communication is as robust as the design of the primary radar to detect the objects-of-interest. The symbol error rate will converge to zero when the number of pulses and or the matched-filtering gain increases. The downside of this is that the bit rate will drop.

With TDBRB the probability of detection of the primary radar is not different as before because the threshold is similar as for the primary radar. This also proved with the influence of different Swerling cases on the algorithm. This is similar as probabilities of detection found in literature for a regular radar.

8.4. Limitations

In the experiment of TDBRB, the waveform with information was scattered on multiple stationary objects. Therefore, the information is well recovered. For the primary radar, it is known in which direction it sends its waveform, and therefore it can use its signal processor to process the signals which are received from that direction. For the receive radar it is unknown, and the signal processing is performed simultaneously for all directions. Therefore, the processing power is higher for the receive radar. The current simulations were performed with white noise and did not include clutter. Certain types of clutter may modify the communication symbols due to incorrect detections after the matched filter. On the other hand, the algorithm is robust and takes the integration of all the information in one PRI of the upchirp burst and cross-correlates this to the same information of the downchirp burst. When certain types of clutter (for example the sea surface waves) remain in the same range cell (at the primary radar) during the upchirp and downchirp burst it is

possible to communicate information over this clutter. In the experiment, all the information of the matched-filtered output of the upchirp and downchirp is used to determine the time delay. If the object-of-interest is detected by the primary radar, there is another probability of detection for the receive radar. Therefore, it is possible communication will not reach the receive radar.

8.5. Recommendations

In this thesis, assumptions are made for the synchronisation of the local oscillators. In future works, research must be done for the synchronisation of the oscillators of the primary and receive radar(s). With a reliable TDBRB communication link, additional way of communication can be exploited. One which fits in the TDBRB framework is an intentional Doppler shift on top of the downchirp burst. The correlation between the upchirp and downchirp can, in that case, contain besides a time delay also a Doppler offset. This Doppler offset will be limited by the number of pulses in a burst because they determine the Doppler resolution. The number of Doppler cells used for communications should be halved to avoid a loss like the straddling loss in the time domain.

More orthogonal signals should be used in future experiments with a low number of pulses in a burst because the matched filter of the upchirp reacts on the downchirp signal. This can also be prevented with a higher matched-filtering gain or use of more pulses in a burst. Another method to reduce the response of the upchirp on the downchirp is to insert an additional fixed and known additional time delay between the upchirp and downchirp and vice versa. However, the strength of TDBRB is using the coherent integration gain of a high number of pulses in a burst.

Bibliography

- [1-01] Blunt, S. D., & Perrins, E. S. (Eds.). (2018). *Radar and communication spectrum sharing*. SciTech Publishing.
- [1-02] Willis, N. J. (2005). *Bistatic radar* (Vol. 2). SciTech Publishing.
- [1-03] Overrein, O., Olsen, K. E., Johnsrud, S., Sornes, P. K., Johnsen, T., Navarro, J., ... & Stemland, R. O. (2005, May). Geometrical and signal processing aspects using a bistatic hitchhiking radar system. In *IEEE International Radar Conference, 2005*. (pp. 332-336). IEEE.
- [2-01] Skolnik, M. (2001). *Introduction to Radar systems*. McGraw Hill, 3rd edition.
- [2-02] Edde, B. (1993). *Radar- Principles, technology, applications*. Englewood Cliffs, Prentice Hall.
- [2-03] Richards, M., Holm, W., & Scheer, J. (2010). *Principles of Modern Radar: Basic Principles*, SciTech Publishing.
- [2-04] Couch, L. W. (1996). *Digital and analog communication systems*. Prentice Hall, 5th edition
- [2-05] Richards, M. A. (2014). *Fundamentals of radar signal processing*. McGraw-Hill Education.
- [2-06] Harrison, L. A. A. (2019). *Introduction to Radar using Python and MATLAB*. Artech House.
- [2-07] Robey, F. C., Fuhrmann, D. R., Kelly, E. J., & Nitzberg, R. (1992). A CFAR adaptive matched filter detector. *IEEE Transactions on aerospace and electronic systems*, 28(1), 208-216.
- [2-08] Swerling, P. (1960). Probability of detection for fluctuating targets. *IRE Transactions on Information theory*, 6(2), 269-308.
- [3-01] Guerri, J. R., Guerri, R. M., Lackpour, A., & Moskowitz, D. (2015, May). Joint design and operation of shared spectrum access for radar and communications. In *2015 IEEE Radar Conference (RadarCon)* (pp. 0761-0766). IEEE.
- [3-02] Hayvaci, H. T., & Tavli, B. (2014, August). Spectrum sharing in radar and wireless communication systems: A review. In *2014 International Conference on Electromagnetics in Advanced Applications (ICEAA)* (pp. 810-813). IEEE.
- [3-03] Zheng, L., Lops, M., Eldar, Y. C., & Wang, X. (2019). Radar and communication co-existence: an overview. *arXiv preprint arXiv:1902.08676*.
- [3-04] Bao, H., Ziemann, A., & He, Z. S. (2021, January). Design and measurements of MSK-LFM RadCom system. In *2020 17th European Radar Conference (EuRAD)* (pp. 9-12). IEEE.
- [3-05] Radio Society of Great Britain. (2023). [RadCom - Radio Society of Great Britain : Radio Society of Great Britain – Main Site \(rsgb.org\)](https://rsgb.org). Assessed: Mar. 9, 2023. [Online]. Available: <https://rsgb.org/main/publications-archives/radcom/>
- [3-06] Zhang, J. A., Liu, F., Masouros, C., Heath, R. W., Feng, Z., Zheng, L., & Petropulu, A. (2021). An overview of signal processing techniques for joint communication and radar sensing. *IEEE Journal of Selected Topics in Signal Processing*, 15(6), 1295-1315.
- [3-07] Zhang, J. A., Rahman, M. L., Wu, K., Huang, X., Guo, Y. J., Chen, S., & Yuan, J. (2021). Enabling joint communication and radar sensing in mobile networks—A survey. *IEEE Communications Surveys & Tutorials*, 24(1), 306-345.
- [3-08] Paul, B., Chiriyath, A. R., & Bliss, D. W. (2016, May). Joint communications and radar performance bounds under continuous waveform optimization: The waveform awakens. In *2016 IEEE Radar Conference (RadarConf)* (pp. 1-6). IEEE.
- [3-09] Feng, Z., Fang, Z., Wei, Z., Chen, X., Quan, Z., & Ji, D. (2020). Joint radar and communication: A survey. *China Communications*, 17(1), 1-27.
- [3-10] Liu, F., Masouros, C., Petropulu, A. P., Griffiths, H., & Hanzo, L. (2020). Joint radar and communication design: Applications, state-of-the-art, and the road ahead. *IEEE Transactions on Communications*, 68(6), 3834-3862.
- [3-11] Sturm, C., Zwick, T., & Wiesbeck, W. (2009, April). An OFDM system concept for joint radar and communications operations. In *VTC Spring 2009-IEEE 69th Vehicular Technology Conference* (pp. 1-5). IEEE.
- [3-12] Hassanien, A., Amin, M. G., Zhang, Y. D., & Ahmad, F. (2015). Dual-function radar-communications: Information embedding using sidelobe control and waveform diversity. *IEEE Transactions on Signal Processing*, 64(8), 2168-2181.
- [3-13] Hassanien, A., Amin, M. G., Zhang, Y. D., & Ahmad, F. (2016). Signaling strategies for dual-function radar communications: An overview. *IEEE Aerospace and Electronic Systems Magazine*, 31(10), 36-45.

- [3-14] Euziere, J., Guinvarc'h, R., Lesturgie, M., Uguen, B., & Gillard, R. (2014, October). Dual function radar communication time-modulated array. In *2014 International Radar Conference* (pp. 1-4). IEEE.
- [3-15] Wild, T., Braun, V., & Viswanathan, H. (2021). Joint design of communication and sensing for beyond 5G and 6G systems. *IEEE Access*, 9, 30845-30857.
- [3-16] Liu, F., Cui, Y., Masouros, C., Xu, J., Han, T. X., Eldar, Y. C., & Buzzi, S. (2022). Integrated sensing and communications: Towards dual-functional wireless networks for 6G and beyond. *IEEE journal on selected areas in communications*.
- [3-17] Yuan, W., Wei, Z., Li, S., Yuan, J., & Ng, D. W. K. (2021). Integrated sensing and communication-assisted orthogonal time frequency space transmission for vehicular networks. *IEEE Journal of Selected Topics in Signal Processing*, 15(6), 1515-1528.
- [3-18] Richards, M. A., Melvin, W. L., Scheer, J. A., & Holm, W. A. (2013). Principles of Modern Radar: Radar Applications, Volume 3, ser. *Electromagnetics and Radar*. Institution of Engineering and Technology.
- [3-19] Quan, S., Qian, W., Guq, J., & Zhang, V. (2014, November). Radar-communication integration: An overview. In *The 7th IEEE/International Conference on Advanced Infocomm Technology* (pp. 98-103). IEEE.
- [3-20] Liu, F., Masouros, C., Li, A., Sun, H., & Hanzo, L. (2018). MU-MIMO communications with MIMO radar: From co-existence to joint transmission. *IEEE Transactions on Wireless Communications*, 17(4), 2755-2770.
- [3-21] Pappu, C. S., Beal, A. N., & Flores, B. C. (2021). Chaos based frequency modulation for joint monostatic and bistatic radar-communication systems. *Remote Sensing*, 13(20), 4113. Online: <https://doi.org/10.3390/rs13204113>
- [3-22] Garmatyuk, D., Giza, P., Condict, N., & Mudaliar, S. (2018, April). Randomized OFDM waveforms for simultaneous radar operation and asynchronous covert communications. In *2018 IEEE Radar Conference (RadarConf18)* (pp. 0975-0980). IEEE.
- [3-23] Xiong, J., Yin, H., Zhu, J., & Tang, Y. (2022, August). An overview of waveform design for integrated sensing and communication. In *2022 IEEE/CIC International Conference on Communications in China (ICCC)* (pp. 991-996). IEEE.
- [3-24] Ciunzolo, D., De Maio, A., Foglia, G., & Piezzo, M. (2015). Intrapulse radar-embedded communications via multiobjective optimization. *IEEE Transactions on Aerospace and Electronic Systems*, 51(4), 2960-2974.
- [3-25] Blunt, S. D., Yatham, P., & Stiles, J. (2010). Intrapulse radar-embedded communications. *IEEE Transactions on Aerospace and Electronic Systems*, 46(3), 1185-1200.
- [3-26] Kumbul, U., Petrov, N., van der Zwan, F., Vaucher, C. S., & Yarovoy, A. (2021, March). Experimental investigation of phase coded FMCW for sensing and communications. In *2021 15th European Conference on Antennas and Propagation (EuCAP)* (pp. 1-5). IEEE.
- [3-27] Dong, C. H. E. N., & Zhang, C. (2018, September). Integrated communication waveform design for bistatic radar. In *2018 IEEE/AIAA 37th Digital Avionics Systems Conference (DASC)* (pp. 1-6). IEEE.
- [3-28] Uysal, F. (2019). Phase-coded FMCW automotive radar: System design and interference mitigation. *IEEE Transactions on Vehicular Technology*, 69(1), 270-281.
- [3-29] Ahmed Y. (2023). BPSK Modulation in AWGN (<https://www.mathworks.com/matlabcentral/fileexchange/33284-bpsk-modulation-in-awgn>), MATLAB Central File Exchange. Retrieved May 8, 2023.
- [4-01] Kay, S. M. (2013). *Fundamentals of statistical signal processing: Practical algorithm development* (Vol. 3). Pearson Education.
- [5-01] Meyer, D. P., & Mayer, H. A. (1973). Radar target detection: handbook of theory and practice (Ser. Electrical science). Academic Press.
- [6-01] Gray, F. (1953). Pulse code communication (1953). *US Patent*, 2.
- [6-02] Kumbul, U. (2023). Phase-Coded FMCW for Automotive Radars.
- [7-01] Gamba, J. (2019). *Radar signal processing for autonomous driving*. Springer.

A. Appendix - Unsynchronized local oscillator

In this appendix the consequences of a not synchronized local oscillator are stated. For the primary radar there is no problem because this radar uses its own local oscillator as showed in Figure 20. Therefore, the equations of the primary radar do not change. However, the equations for the receive radar will change if the local oscillators are not aligned.

The starting point are the two envelopes which are contained in the upchirp $s_{BU}(t)$ and the downchirp burst $s_{BD}(t)$. Only the upchirp will be calculated because the two equations are similar in a mathematical way. The upchirp burst has the following form with the transmitted frequency f_{ct} .

$$s_{BU}(t) = \sum_{k=0}^{K-1} A \cdot e^{j(2\pi f_{ct}(t-k \cdot T_{PRI}) + \pi \gamma (t-k \cdot T_{PRI})^2)} \cdot (u(t-k \cdot T_{PRI}) - u(t-k \cdot T_{PRI} - T_p)) \quad (84)$$

Although this burst is received the signal will be simplified to only the envelope and carrier which are received after the delay τ_r . With:

$$\tau_r = \frac{(R_0 + R_1 + (v_{rop} + v_{ror}) \cdot t)}{c} \quad (85)$$

In this case the received signal is up converted with f_{ct} and is down converted with f_{cr} where both frequencies also contain an additional phase shift (φ_t and φ_r).

$$s_{RRUC}(t) \approx e^{j2\pi f_{ct}t + j2\pi\varphi_t} \cdot e^{-j\frac{2\pi}{\lambda_{ct}}(R_0+R_1)} \cdot e^{+j2\pi\frac{2v_{bit}}{\lambda_{ct}}t} \cdot s_{BU}\left(t - \frac{R_0 + R_1}{c}\right) \cdot e^{-j2\pi f_{cr}t - j2\pi\varphi_r} \quad (86)$$

When this equation is written as equal terms of t this simplifies to:

$$s_{RRUC}(t) \approx e^{-j\frac{2\pi}{\lambda_{ct}}(R_0+R_1) + j2\pi(\varphi_t - \varphi_r)} \cdot e^{j2\pi\frac{2v_{bit}}{\lambda_{ct}}t + j2\pi(f_{ct} - f_{cr})t} \cdot s_{BU}\left(t - \frac{R_0 + R_1}{c}\right) \quad (87)$$

The first term in the equation above is a constant term. The second term introduces a frequency difference on top of the Doppler shift which corresponds to the bistatic velocity. If the difference between the two frequencies f_{ct} and f_{cr} is too large an error is introduced. And without the knowledge of the difference between the frequencies the bistatic velocity can not be calculated. The mathematical explanation for this starts with the Doppler shift:

$$f_d = +\frac{2v}{c}f_c = +\frac{2v}{\lambda_c} \quad (88)$$

When the calculated Doppler shift f_{dc} includes the frequency difference between the two LO frequencies f_e . It looks as follows:

$$f_{dc} = f_d + f_e = \frac{2v_{bit}}{\lambda_{ct}} + (f_{ct} - f_{cr})t \quad (89)$$

To make useful calculations of the bistatic velocity the condition for the difference will be:

$$|f_{ct} - f_{cr}| \ll \frac{2v_{bit}}{\lambda_{ct}} \quad (90)$$

Example 1: The influence of the error can be calculated with the following example: $f_{ct} = 10$ GHz therefore $\lambda_{ct} = 0.03$ m and f_{cr} is the same with an error of 0.01 % what is equal to 1 MHz, in that case $f_{cr} = 10.001$ GHz. In this example (90) leads to:

$$f_{cd} = \frac{2v_{bit}}{0.03} + (1.0 \times 10^6)t \quad (91)$$

The bistatic velocity is 15×10^3 m/s if the measured Doppler frequency is 1 MHz this is for movements on earth too fast. And with $f_{ct} - f_{cr} \gg \frac{2v_{bit}}{\lambda_{ct}}$ similar as in this example the bistatic velocity can not be calculated.

Example 2: In this example the carrier frequency is the same and two LOs are used with an error of ± 10 kHz. The bistatic velocity of the object-of-interest is 500 m/s. Two LOs which have an error can lead to a difference of ± 20 kHz. The Doppler of the bistatic velocity becomes:

$$f_d = \frac{2 \cdot 500 \cdot t}{0.03} = 33.3 \times 10^3 \text{ Hz} \quad (92)$$

The calculated Doppler shift is in that case:

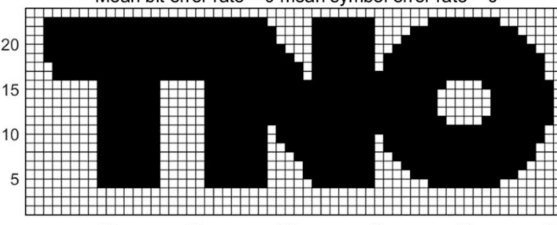
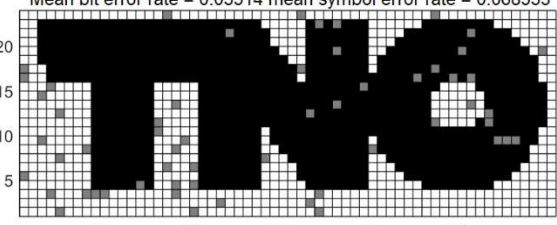
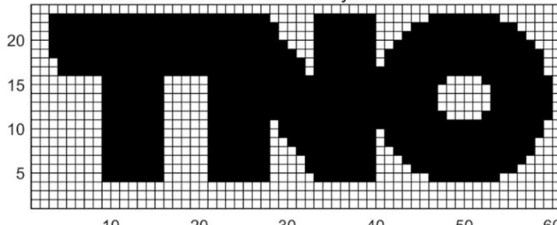
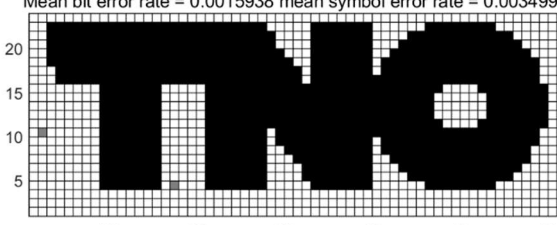
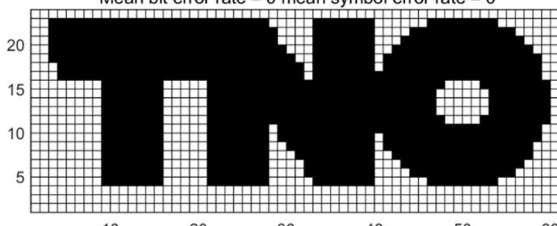
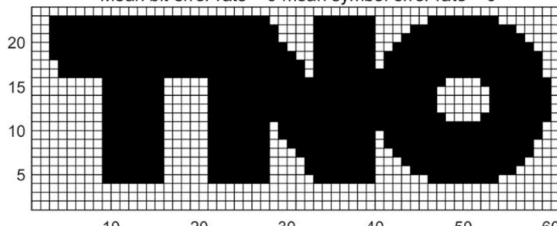
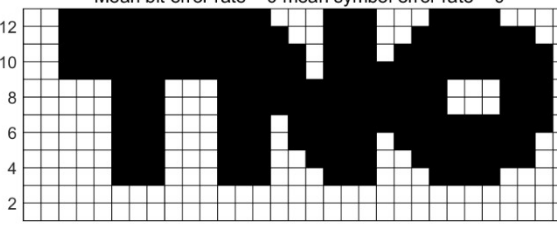
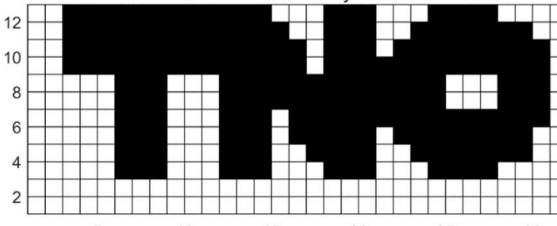
$$f_{cd} = \frac{2 \cdot 500 \cdot t}{0.03} + (20 \times 10^3)t = 53.3 \times 10^3 \text{ Hz} \quad (93)$$

At this point still no correct bistatic velocity can be calculated.

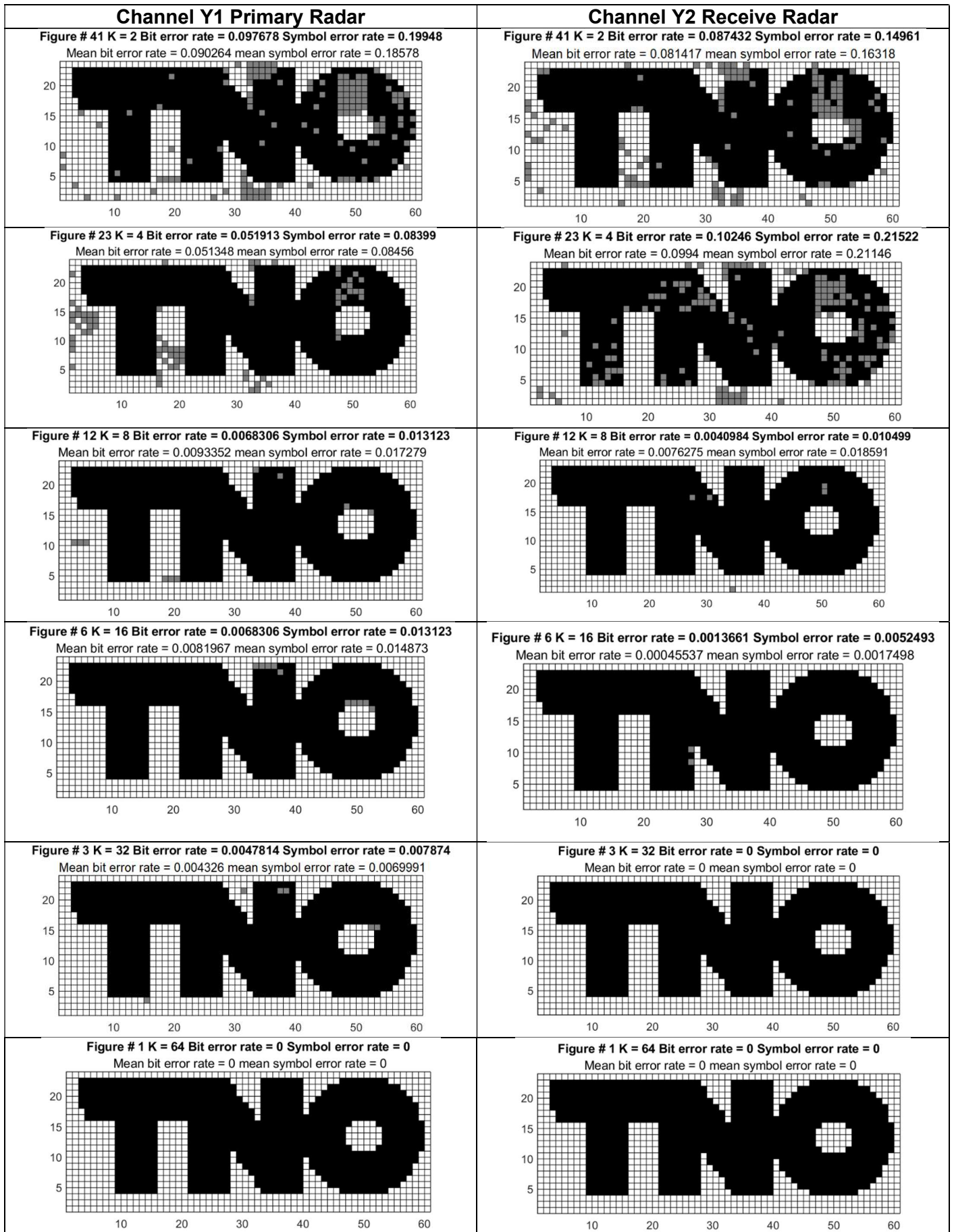
B. Appendix – Figures BER and SER rates

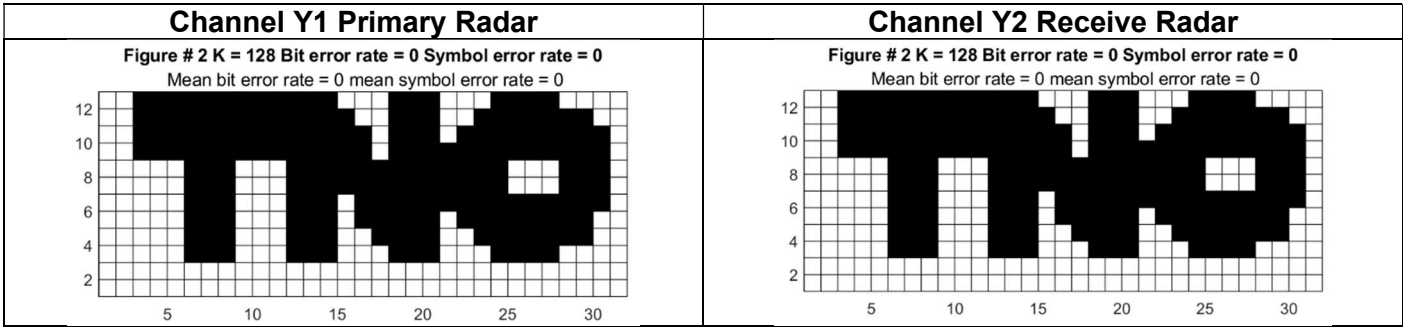
In this appendix the different figures are presented with the calculated mean bit error rate and symbol error rate for the time delay between radar bursts and BPSK waveforms. The first row and last column are not visible because of the MATLAB functions which are used to create the MATLAB figures. The calculations of the BER and SER include the errors in those column and row.

NLOS experiment TDBRB

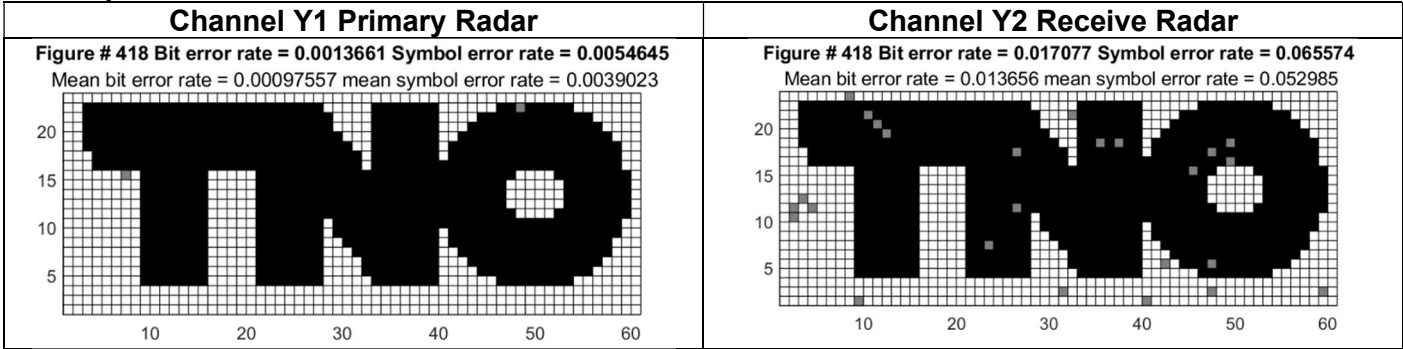
Channel Y1 Primary Radar	Channel Y2 Receive Radar
<p>Figure # 9 K = 8 Bit error rate = 0 Symbol error rate = 0 Mean bit error rate = 0 mean symbol error rate = 0</p> 	<p>Figure # 9 K = 8 Bit error rate = 0.040301 Symbol error rate = 0.070866 Mean bit error rate = 0.03514 mean symbol error rate = 0.068533</p> 
<p>Figure # 3 K = 32 Bit error rate = 0 Symbol error rate = 0 Mean bit error rate = 0 mean symbol error rate = 0</p> 	<p>Figure # 3 K = 32 Bit error rate = 0.0013661 Symbol error rate = 0.0026247 Mean bit error rate = 0.0015938 mean symbol error rate = 0.0034996</p> 
<p>Figure # 1 K = 64 Bit error rate = 0 Symbol error rate = 0 Mean bit error rate = 0 mean symbol error rate = 0</p> 	<p>Figure # 1 K = 64 Bit error rate = 0 Symbol error rate = 0 Mean bit error rate = 0 mean symbol error rate = 0</p> 
<p>Figure # 2 K = 128 Bit error rate = 0 Symbol error rate = 0 Mean bit error rate = 0 mean symbol error rate = 0</p> 	<p>Figure # 2 K = 128 Bit error rate = 0 Symbol error rate = 0 Mean bit error rate = 0 mean symbol error rate = 0</p> 

LOS experiment TDBRB





LOS experiment BPSK



NLOS experiment BPSK

